Research Paper

GEOSPHERE

GEOSPHERE, v. 19, no. 5

https://doi.org/10.1130/GES02593.1

14 figures; 7 tables; 1 set of supplemental files

CORRESPONDENCE: andreisarna@gmail.com

CITATION: Sarna-Wojcicki, A.M., Knott, J.R., Westgate, J.A., Budahn, J.R., Barron, J., Bray, C.J., Ludvigson, G.A., Meyer, C.E., Miller, D.M., Otto, R.E., Pearce, N.J.G., Smith, C.C., Walkup, L.C., Wan, E., and Yount, J., 2023, Ibex Hollow Tuff from ca. 12 Ma supereruption, southern Idaho, identified across North America, eastern Pacific Ocean, and Gulf of Mexico: Geosphere, v. 19, no. 5, p. 1476–1507, https://doi.org/10.1130/GES02593.1.

Science Editor: David E. Fastovsky
Associate Editor: Joel Saylor

Received 7 September 2022
Revision received 22 March 2023
Accepted 26 April 2023

Published online 20 July 2023

Ibex Hollow Tuff from ca. 12 Ma supereruption, southern Idaho, identified across North America, eastern Pacific Ocean, and Gulf of Mexico

Andrei M. Sarna-Wojcicki[1,*], Jefferey R. Knott[2], John A. Westgate[3,*], James R. Budahn[4,*], John Barron[1,*], Colin J. Bray[3], Greg A. Ludvigson[5], Charles E. Meyer[1,*], David M. Miller[1,*], Rick E. Otto[6], Nicholas J.G. Pearce[7], Charles C. Smith[8,*], Laura C. Walkup[1], Elmira Wan[1,†], and James Yount[4,§]

[1]U.S. Geological Survey, 345 Middlefield Road, Menlo Park, California 94025, USA
[2]Department of Geological Sciences, California State University–Fullerton, Fullerton, California 92834-6850, USA
[3]Department of Earth Sciences, University of Toronto, Toronto, Ontario M5S B1, Canada
[4]U.S. Geological Survey, Lakewood, Colorado 80225, USA
[5]Kansas Geological Survey, 1930 Constant Avenue, Lawrence, Kansas 66047-3724, USA
[6]University of Nebraska State Museum, Ashfall Fossil Beds State Historical Park, 86930 517th Avenue, Royal, Nebraska 68773, USA
[7]Department of Geography and Earth Sciences, Aberystwyth University, Aberystwyth SY23 3DB, Wales, UK
[8]Geological Survey of Alabama, 420 Hackberry Lane, P.O. Box O, Tuscaloosa, Alabama 35486-9780, USA

ABSTRACT

The Ibex Hollow Tuff, 12.08 ± 0.03 Ma ($^{40}Ar/^{39}Ar$), is a widespread tephra layer erupted from the Bruneau-Jarbidge volcanic field of southern Idaho. Tephra from this eruption was deposited across much of western and central North America and adjacent ocean areas. We identified the Ibex Hollow Tuff at Trapper Creek, Idaho, near its eruption site, and at 15 distal sites, from the Pacific Ocean to the Gulf of Mexico, by the chemical composition of its glass shards, using electron-microprobe analysis, instrumental neutron activation analysis, and laser-ablation–inductively coupled plasma–mass spectrometry. By these methods, we distinguished the Ibex Hollow Tuff from overlying and underlying tephra layers near its source and at distal sites. Fluvially reworked Ibex Hollow Tuff ash was transported by the ancestral Mississippi River drainage from the interior of the North American continent to the Gulf of Mexico, where it is present within an ~50-m-thick deposit in marine sediments in the subsurface. The minimum fallout area covered by the ash is ~2.7 million km², with a minimum volume of ~800 km³, and potential dispersal farther to the north and northeast. The areal distribution for the Ibex Hollow Tuff is similar to that of the Lava Creek B (0.63 Ma) supereruption. The Ibex Hollow Tuff represents a unique chronostratigraphic marker allowing a synoptic view of paleoenvironments at a virtual moment in time across a large terrestrial and marine region. The Ibex Hollow Tuff is also an important marker bed for North American Land Mammal Ages, and it coincides with climatic cooling in the middle to late Miocene documented in marine cores.

INTRODUCTION

The seven volcanic fields and associated calderas of the Snake River Plain–Yellowstone hotspot (Fig. 1) form a volcanic trend that extends from the Oregon-Idaho-Nevada border to northwestern Wyoming (e.g., Pierce and Morgan, 1992; Perkins and Nash, 2002; Bonnichsen et al., 2008; Knott et al., 2022). These volcanic fields produced many explosive volcanic eruptions over the last ~17 m.y., including a number of supereruptions (e.g., Perkins et al., 1995, 1998; Mason et al., 2004; Knott et al., 2020). The source calderas of these volcanic fields progress from the oldest in the southwest to youngest in the northeast (Perkins et al., 1995, 1998; Perkins and Nash, 2002; and references above; Fig. 1). They are considered to be the result of the passage of North American continental crust over a mantle hotspot or plume at depth (e.g., Pierce and Morgan, 1992; Christiansen, 2001). Two of the youngest supereruptions are the Huckleberry Ridge (ca. 2.1 Ma; Ellis et al., 2012) and Lava Creek B (ca. 0.63 Ma; Matthews et al., 2015) (Fig. 1), which were erupted from the Yellowstone Plateau volcanic field in Wyoming and have estimated proximal volumes of 2500 km³ and ~1000 km³, respectively (Christiansen and Blank, 1972; Christiansen, 2001). Snake River Plain–Yellowstone hotspot tephra layers are found at many sites in western and central North America, the Gulf of

*Emeritus
†Emerita
§Retired

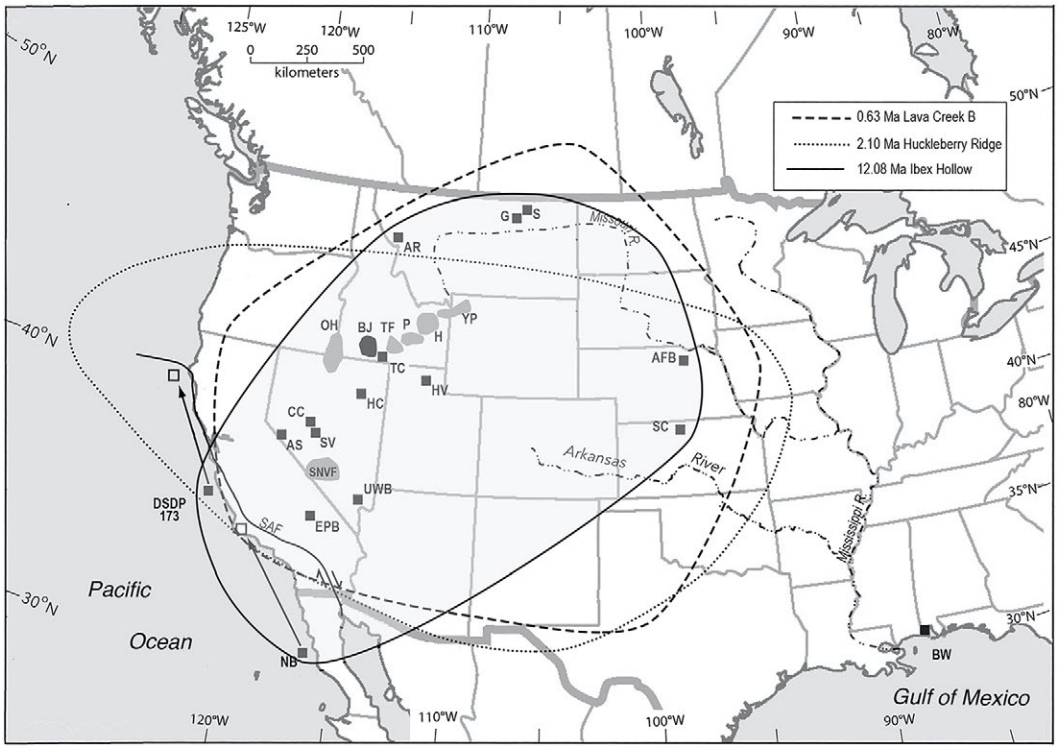

Figure 1. Map of western North America showing the volcanic fields of the Snake River Plain–Yellowstone hotspot and sampling sites of the Ibex Hollow Tuff. The source of the Ibex Hollow Tuff is the Bruneau-Jarbidge volcanic field (BJ; black) with older (Owyhee-Humboldt [OH]) and younger (Twin Falls [TF], Picabo [P], Heise [H], and Yellowstone Plateau [YP]) volcanic fields shown in gray (after Perkins et al., 1998). The Southern Nevada volcanic field (SNVF) is also shown in gray. Ibex Hollow Tuff locations are shown as black squares: Trapper Creek (TC, type locality of the Ibex Hollow Tuff), Hansel Valley (HV), Ambrose Road (AR), Glentana (G), Scobey (S), Ashfall Fossil Beds (AFB), Smith County (SC), Boswell (BW), Huntington Creek (HC), Stewart Valley (SV), Cobble Cuesta (CC), Aldrich Station (AS), Upper White Basin (UWB), El Paso basin (EPB), Deep Sea Drilling Project Site 173 (DSDP 173), and Naples Beach (NB; a.k.a. Dos Pueblos Beach). Black squares for NB and DSDP-173 are sites on the Pacific plate where, based on our calculations, deposition occurred at ca. 12 Ma. Open squares for NB and DSDP-173 indicate where these sites are today after right-lateral movement of the Pacific plate along the San Andreas fault system (SAF) relative to the North American plate. We infer that the ash at the Boswell site (BW) is beyond the ash-fall limits of the Ibex Hollow Tuff, and it was transported by the ancestral Mississippi-Missouri River system to the Gulf of Mexico (see text). The approximate minimum areal distribution of the Ibex Hollow Tuff is enclosed by the solid line. Shown for comparison are the approximate minimum ash-fall distributions of the Huckleberry Ridge (ca. 2.10 Ma) and Lava Creek B (ca. 0.63 Ma) ash falls from these supereruptions (after Sarna-Wojcicki, 2000), shown by dotted and dashed lines, respectively.

Mexico, and northeastern Pacific Ocean (e.g., Izett and Wilcox, 1982; Westgate et al., 1977; Sarna-Wojcicki et al., 1987; Sarna-Wojcicki, 2000; Ostergren, 1991; Perkins et al., 1998; Knott et al., 2022).

Bruneau-Jarbidge Volcanic Field and the Cougar Point Tuff

The Upper Miocene Bruneau-Jarbidge volcanic field in Idaho was the active caldera of the Snake River Plain–Yellowstone hotspot from ca. 12.7 to ca. 10.4 Ma (Fig. 1; Perkins and Nash, 2002; Bonnichsen et al., 2008). Tephra derived from this source is found as distal tephra layers at many sites in central and western North America (Perkins et al., 1995, 1998; Perkins and Nash, 2002; Smith et al., 2018; Knott et al., 2022; this report). This volcanic field was the source of the voluminous supereruptions collectively named the Cougar Point Tuff (Bonnichsen, 1982; Bonnichsen and Citron, 1982; Bonnichsen et al., 2008; Perkins et al., 1995, 1998; Mason et al., 2004; Knott et al., 2022).

Tuff of Ibex Peak and Ibex Hollow Tuff

At Ibex Hollow in Trapper Creek and vicinity in southern Idaho, ~130 km southeast of the center of the Bruneau-Jarbidge volcanic field in Idaho (TC, Fig. 1) and ~80 km southeast of the caldera margin, there is an ~600-m-thick section consisting of rhyolitic tephra beds, collectively named the Tuff of Ibex Peak (Fig. 2; Perkins et al., 1995), which is a local subset of the Cougar Point Tuff. Within the Tuff of Ibex Peak, there is a 4-m-thick, vitric, ash-flow tuff, the tephra of which was erupted from the Bruneau-Jarbidge volcanic field (stratigraphic number 30 of Perkins et al., 1995; see Fig. 2 here). This ash flow is overlain by a 1-m-thick, coignimbritic(?) ash-fall or late-stage Plinian ash fall. Glass shards from the ash flow of the Ibex Hollow Tuff have been characterized by electron microprobe and wavelength-dispersive X-ray fluorescence analyses (Perkins et al., 1995, 1998). Sanidines from the Ibex Hollow Tuff yielded a $^{40}Ar/^{39}Ar$ date of 11.80 ± 0.03 Ma (Perkins et al., 1995). This date was subsequently revised to 11.93 ± 0.03 Ma (Perkins et al., 1998), and it is further revised here to 12.08 ± 0.03 Ma.

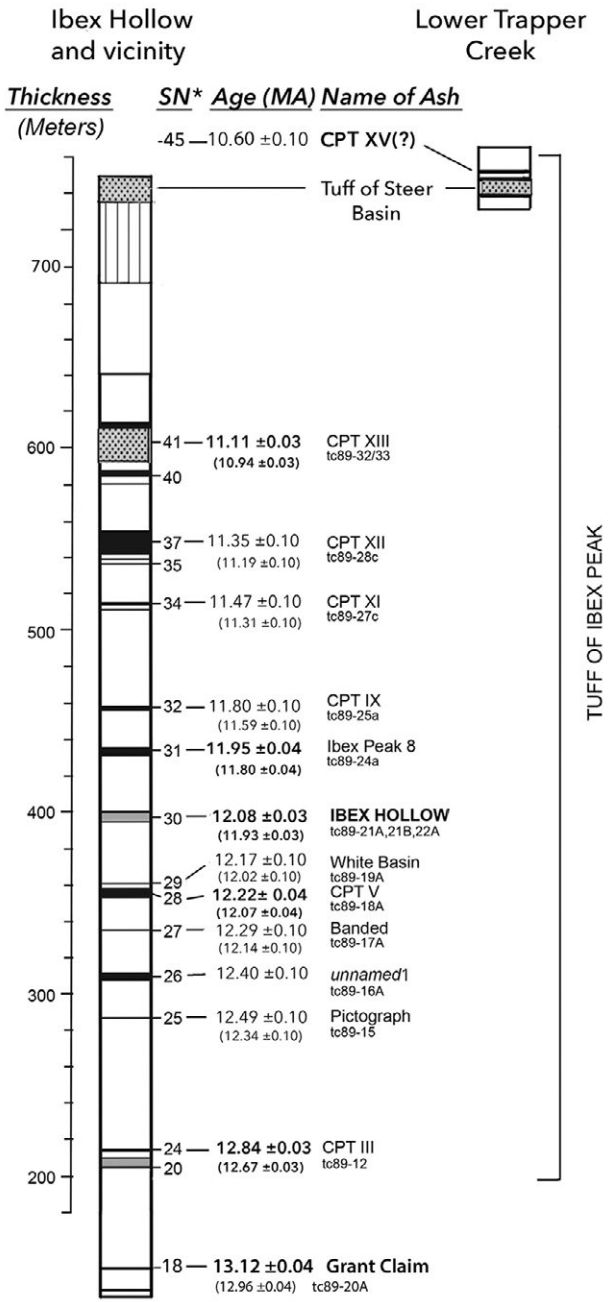

This latter, revised age is presented in the abstract and used throughout this report. This last date, and all other $^{40}Ar/^{39}Ar$ dates presented here, as well as estimated ages from previous studies, are corrected here to the new Fish Creek Tuff age and reference standard of Kuiper et al. (2008) and new decay constant of Min et al. (2000). Perkins et al. (1998) named this ash-flow tuff and associated fall ash as the Ibex Hollow Tuff.

At distal sites farther from the volcanic center, Perkins et al. (1998) correlated tuffs in Nevada at Huntington Creek (sample htc93–461), Stewart Valley (sample sv92–54), Aldrich Station (sample as89–42), and in California at El Paso Basin (sample epb94–580) with the Ibex Hollow Tuff (Fig. 1). Perkins and Nash (2002) also identified the Ibex Hollow Tuff in the Great Plains (Nebraska/Kansas) and the Upper White River Basin of southern Nevada. Perkins et al. (1998) and Perkins and Nash (2002), however, did not present geochemical data for correlation of these distal locations. We present the evidence for these correlations in this report.

The present study extends the work of Perkins et al. (1995, 1998) by focusing on the 12.08 Ma Ibex Hollow Tuff. The Ibex Hollow Tuff coincides in time with a Clarendonian subinterval boundary (Cl1/Cl2) of the North American Land Mammal Age (NALMA; Whistler et al., 2009; Tedford et al., 2004) and immediately precedes a late Miocene cooling period (Westerhold et al., 2020), a paleomagnetic transition (C5r.2n/C5An.1n; Ogg, 2012), and widespread micropaleontological transitions in the northern Pacific Ocean (Barron and Isaacs, 2001). Thus, the Ibex Hollow Tuff erupted at a time of significant paleoclimatic and possibly related paleontologic changes, and it represents an important stratigraphic marker bed, if not evidence of a direct or indirect cause of these changes. For example, a massive death assemblage of a herd of fossil rhinoceroses (*Teleoceras major*) is present in the basal part of the Ibex Hollow Tuff at Ashfall Fossil Beds State Historical Park, Nebraska, showing one of the impacts of this eruption on the regional fauna (Fig. 3). Many other animal species have been found buried in this ash bed.

Here, we present data on the composition, age, and occurrence of the Ibex Hollow Tuff across western North America and adjacent ocean margins. These data indicate that the Ibex Hollow Tuff is one of the most extensive tephra beds in North America (Fig. 1), a supereruption that had widespread

Figure 2. Stratigraphic section at Trapper Creek, Idaho, showing the position of the Ibex Hollow Tuff relative to other tephra layers within the composite Tuff of Ibex Peak, the relative thicknesses (meters) of the tephra layers, stratigraphic numbers assigned to each tephra layer (SN), $^{40}Ar/^{39}Ar$ ages (bold type), and interpolated ages (regular type). The Tuff of Ibex Peak is a local subset of the regionally broader Cougar Point Tuff (CPT) recognized in the Bruneau-Jarbidge area ~80 km NW (to the margin of field) to ~150 km NW (center of field) of Trapper Creek. Ages in bold type are $^{40}Ar/^{39}Ar$ dates, corrected for current Fish Canyon Tuff monitor age of Kuiper et al. (2008) and decay constant of Min et al. (2000). Ages in regular type are the corrected interpolated ages from the dated tephra layers stratigraphically above and below the undated layers. Ages in parentheses are the original $^{40}Ar/^{39}Ar$ and interpolated ages given in Perkins et al. (1998). Tephra layers in black—tephra falls; tephra layers in gray—ash flows. Figure is modified from Perkins et al. (1995).

Figure 3. Photograph of Konservat-Lagerstätte (exceptionally well-preserved and abundant fossil assemblage) of juvenile barrel-chested rhinoceroses (*Teleoceras major*) encased in the basal part of the Ibex Hollow Tuff at Ashfall Fossil Beds State Historical Park, Nebraska. Skull in the foreground is 33 cm long. Numerous skeletons of both adult and juvenile male and female rhinoceroses were found within the basal part of this tuff, including one female with an unborn fetus. In addition, there were five genera of horses, three of camelids, three canids, a musk deer, an extinct crowned crane (*Balearica exigua*), a hawk resembling the living secretary bird (*Apatosagittarius*), a scavenger related to Old World vultures (*Anchigyps*), and three species of turtle. In short, this represents a broad death assemblage resulting from an event of relatively short duration. The presence of such a broad spectrum of taxa within the basal Ibex Hollow Tuff is a *res ipso loquitur* (the thing speaks for itself) for the cause of the associated death assemblage. Excavations are continuing at this and nearby sites (University of Nebraska State Museum, 2023). Photograph is courtesy of the University of Nebraska State Museum, Lincoln, Nebraska.

environmental impact. With regard to correlation and chronostratigraphy, the Ibex Hollow Tuff represents a virtual "moment" in time, allowing a synoptic view over western North America and its ocean boundary areas and, perhaps, the Northern Hemisphere, at ca. 12 Ma.

METHODS

A brief summary of the analytical methods is provided below. A detailed description of the analytical methods, together with standards used, is presented in the Supplemental Material (Item S1).[1]

[1]Supplemental Material. Item S1 (MS Word document): Detailed methods for major, minor, and trace-element analysis; electron-microprobe analysis (EMA); instrumental neutron activation analysis (INAA); laser ablation–inductively coupled–mass spectrometry (LA-ICP-MS); isothermal-plateau fission-track method of age determination; correlation methods; references cited for methods section. Item S2: Table of major– and minor–EMA analyses of individual glass shards of tephra beds correlated to Ibex Hollow Tuff; contains plots of Fe_2O_3 versus CaO for samples (University of Toronto, Toronto, Canada). Item S3: Table of major– and minor–EMA analyses of individual glass shards of tephra beds of the Ibex Hollow Tuff (U.S. Geological Survey, Menlo Park, California). Initial compositions and totals on analysis are presented, with plots of Fe_2O_3 versus CaO. Item S4: Table of major– and minor–EMA analyses of individual glass shards of tephra beds that correlate with the Ibex Hollow Tuff. Initial compositions and totals on analysis are presented, with plots of Fe_2O_3 versus CaO (University of Utah, Salt Lake City, Utah). Item S5: Binary graphic plots of major oxides and elements of the Ibex Hollow Tuff and overlying and underlying tephra layers at Trapper Creek, Idaho, USA. Please visit https://doi.org/10.1130/GEOS.S.22965632 to access the supplemental material, and contact editing@geosociety.org with any questions.

Field Methods

Samples were collected at multiple locations by several investigators over a number of years (Table 1). Whenever possible, the basal or ash-fall component of a compound deposit was sampled, and at some sites, multiple samples were collected to test for compositional variations within the tephra layer. All samples were located on U.S. Geological Survey (USGS) topographic maps, and latitude and longitude were determined using a global positioning system (GPS) device or a geobrowser (e.g., Google Earth).

Preparation of Tephra Samples for Analysis

Samples were disaggregated in a mullite mortar, or gently crushed if indurated, and wet-sieved into size fractions to retain the ~65 to ~150 µm and the ~150 to ~250 µm fractions, using nylon-mesh screens to avoid contamination with metals. The larger size range was preferred for analysis, but the smaller size range was used when only finer material was present, as for distal samples. For instrumental neutron activation analysis (INAA) and laser-ablation–inductively coupled plasma–mass spectrometry (LA-ICP-MS) analysis, sieved samples were treated with a 10% solution of HCl, to remove any postdepositional calcium carbonate that may have been precipitated in the tephra layer by groundwater, followed by an 8% HF solution, to remove any weathered or altered rinds on the surfaces of glass shards. This latter treatment

TABLE 1. LOCATION OF IBEX HOLLOW TUFF (IHT) AT ITS TYPE LOCALITY AND AT DISTAL SITES WHERE IT HAS BEEN IDENTIFIED*

Location and map abbreviation on Figure 1	Latitude (°N)	Longitude (°W)	U.S. Geological Survey 7.5' quadrangle	Collector, reference	Geologic unit	Description
Naples (Dos Pueblos) Beach, CA (NB)	34.43944	119.96222	Dos Pueblos Canyon	A.M. Sarna-Wojcicki; C.E. Meyer (this report)	Monterey Formation	15-cm-thick, water-laid air-fall ash
Deep Sea Drilling Project Hole 173 (DSDP 173)	39.96194	125.45194	n/a	D.A. McManus (McManus et al., 1970)	Deep-ocean sediments	1- to 3-cm-thick, water-laid, air-fall ash
El Paso Basin, CA (EPB)	35.42791	117.93483	Saltdale NW	M.E. Perkins (Perkins et al., 1995)	Member 2 of Dove Spring Formation	Air-fall and reworked tephra; near section F of Whistler and Burbank (1992)
Upper White Basin, NV (UWB)	36.33361	114.66611	Muddy Peak	J.C. Yount; C.E. Meyer (this report)	Red sandstone member of Horse Spring Formation	30-cm-thick, light-gray, air-fall tephra
Aldrich Station, NV (AS)	38.48556	118.89861	Ninemile Ranch	W.C. Eastwood (Eastwood, 1969); M.E. Perkins (Perkins et al., 1995)	Aldrich Station Formation	1-m-thick, light-silvery-gray, massive, indurated, air-fall and reworked tephra
Stewart Valley, NV (SV)	38.66349	117.97113	Granny Goose Well	M.E. Perkins (Perkins et al., 1995)	Stewart Valley Group	Air-fall and reworked tephra
Cobble Cuesta, NV (CC)	38.88250	118.89861	Hussman Spring	J.H. Stewart (Stewart et al., 1999)	Miocene sedimentary deposits	1-m-thick, very-light-gray, thinly bedded, air-fall and reworked tephra; tephra layer C-3 (Stewart et al., 1999)
Huntington Creek, NV (HC)	40.58481	115.71559	W of Lee	M.E. Perkins (Perkins et al., 1995)	Humboldt Formation	Air-fall and reworked tephra
Trapper Creek, ID (TC)	**42.12583**	**114.06806**	**Severe Spring**	**M.E. Perkins (Perkins et al., 1995)**	**Tuff of Ibex Peak**	**Type locality: 4-m-thick, dark brown, massive, tephra flow and coignimbrite air-fall ash**
Hansel Valley, UT (HV)	41.63805	112.61694	Sunset Pass	D.M. Miller (Miller and Schneyer, 1994)	Salt Lake Formation	Air-fall and reworked tephra
Ambrose Road, MT (AR)	46.54889	113.93250	Grayhorse Creek	J.A. Westgate (Westgate et al., 2011)	Unnamed	1-m-thick, tan, massive, air-fall and reworked tephra
Glentana, MT (G)	48.76444	106.11833	Richland	J.A. Westgate (Westgate et al., 2011)	Unnamed	5-m-thick, white, air-fall and reworked tephra; Sample CT-1 of Collier and Thom (1918)
Scobey, MT (S)	48.88056	105.90972	Flaherty Coulee	J.A. Westgate (Westgate et al., 2011)	Flaxville Formation	Up to 7-m-thick, massive, white, air-fall and reworked tephra; Fouhy ash bed
Ashfall Fossil Beds, NE (AFB)	42.42111	98.15722	Orchard NW	R. Otto (this report)	Ash Hollow Formation of Ogallala Group	2.5–3-m-thick, gray, bedded to massive, air-fall and reworked tephra
Smith County, KS (SC)	39.95667	98.73398	Cora	G.A. Ludvigson (Ludvigson et al., 2009)	Ogallala Group	In sandstones and siltstones
Boswell, AL (BW)	30.42139	88.31444	Grand Bay	C.C. Smith (Smith, 1991)	Pensacola Formation	50-m-thick tuffaceous interval in marine sediments, in core

Notes: Bold text indicates type locality. CA—California; NV—Nevada; ID—Idaho; UT—Utah; MT—Montana; NE—Nebraska; KS—Kansas; AL—Alabama.
*Also see Figures 1, 11, and 13C.

was quenched with distilled water after ~30 s or less to prevent excessive dissolution of the glass, particularly of small glass shards. The above treatment with acids was not necessary for electron-microprobe analysis (EMA), because polished internal surfaces of individual glass shards, mounted in epoxy in small-diameter holes in glass slides, were analyzed.

The sized separates were passed through a Frantz magnetic separator at low- and high-amperage settings to separate the volcanic glass shards from other particles in the tephra samples. Magnetic minerals such as magnetite and ilmenite were removed with a hand magnet before being passed through the magnetic separator. The glass shards were usually concentrated in the fraction that was intermediate in magnetic susceptibility. Mafic minerals (e.g., pyroxene and amphibole) were concentrated in the high-magnetic-susceptibility fraction, and nonmagnetic minerals (e.g., feldspars, zircon, and apatite) were concentrated in the low-susceptibility fraction. If necessary, the glass shards were further separated in a vertical glass tube that contained methylene-iodide (specific gravity of 3.2), to which the sized tephra sample was added, followed by slow addition of acetone at the top of the tube; the solution was gently stirred. The density gradient thus formed by the methylene-iodide and acetone solution allowed the sample to spread out vertically in the tube, according to particle density, and the sample was then drained from the tube in successive increments at the bottom of the tube. The purest glass shard separate obtained was selected for analysis.

EMA of Individual Volcanic Glass Shards

At the USGS, field samples were prepared and analyzed by EMA (Table 2; Item S1) following the procedures described by Sarna-Wojcicki et al. (2005) and by INAA (Table 3; Item S1) following procedures described by Budahn and Wandless (2002). Many of the samples in Table 2 are splits of samples collected

TABLE 2. (A) ELECTRON-MICROPROBE ANALYSIS OF GLASS SHARDS FROM TEPHRA LAYERS, TRAPPER CREEK SECTION, IDAHO, INCLUDING IBEX HOLLOW TUFF (IHT; IN BOLD TYPE); (B) IBEX HOLLOW TUFF AND TEPHRA LAYERS AT DISTAL SITES CORRELATED WITH THE IBEX HOLLOW TUFF (SEE MAP, FIG. 1)

USGS comp. no.	Name and age of tephra (Ma)	Site, Fig. 1	Sample no.	Laboratory	SNO	SiO_2	Al_2O_3	Fe_2O_3	MgO	MnO	CaO	TiO_2	Na_2O	K_2O	Total recalc.	Notes
(A) Tephra Layers within the Trapper Creek section, including the Ibex Hollow Tuff, in stratigraphic order, youngest at top (site TC; see Figs. 1, 2, and 13C). Ibex Hollow Tuff, stratigraphic number (SNO) 30, is in bold type																
3560	Tuff of McMullen Creek, 8.84 ± 0.04	TC	TC92-71	U. of Utah	51	75.35	12.09	2.64	0.11	0.03	0.92	0.31	2.92	5.63	100.00	
4136	Section 26 ash, 9.70 ± 0.20	TC	tc90-22(Perkins)	U. of Utah	49 (?)	75.44	12.22	2.43	0.18	0.04	0.93	0.36	2.87	5.52	99.99	SNO?
3561	Tuff of Wooden Shoe Butte, 10.13 ± 0.03	TC	TC90-20	U. of Utah	47	75.39	12.06	2.35	0.10	0.03	0.81	0.31	2.70	6.24	99.99	
3562	CPT XV ash, 10.45 ± 0.10	TC	TC90-17	U. of Utah	45	76.02	12.11	2.33	0.13	0.03	0.77	0.31	2.53	5.79	100.02	
3563	Tuff of Steer Basin (A)	TC	TC92-15c	U. of Utah	44	75.39	12.01	2.39	0.10	0.03	0.87	0.33	2.71	6.16	99.99	
3564	Tuff of Steer Basin (B)	TC	TC89-36a	U. of Utah	44	76.67	12.31	1.04	0.01	0.02	0.31	0.35	2.71	6.57	99.99	Diff. source?
3565	Ibex Peak 19 ash, 10.74 ± 0.10	TC	TC89-34a	U. of Utah	42	76.04	11.97	2.60	0.09	0.04	0.84	0.33	2.31	5.78	100.00	
3566	CPT XIII ash, 11.11 ± 0.03	TC	TC89-33b	U. of Utah	41	76.64	11.98	2.16	0.03	0.03	0.65	0.20	2.52	5.78	99.99	
3567	CPT XIII ash, 11.11 ± 0.03	TC	TC89-31a	U. of Utah	41	76.45	12.06	2.18	0.03	0.03	0.66	0.20	2.52	5.87	100.00	
3568	CPT XII ash, 11.34 ± 0.10	TC	TC89-28a	U. of Utah	37	75.83	12.09	2.24	0.12	0.04	0.77	0.32	2.65	5.94	100.00	
3569	CPT XI ash, 11.46 ± 0.10	TC	TC89-27c	U. of Utah	34	76.61	11.96	2.02	0.05	0.03	0.61	0.21	2.31	6.19	99.99	
3570	CPT IX ash, 11.74 ± 0.10	TC	TC89-25a	U. of Utah	32	76.61	11.96	1.91	0.07	0.03	0.58	0.24	2.20	6.40	100.00	
3571	Ibex Peak 8 ash, 11.95 ± 0.10	TC	TC89-24a	U. of Utah	31	75.85	12.08	2.15	0.12	0.03	0.74	0.34	2.44	6.25	100.00	
3507	**Ibex Hollow Tuff, coignimbritic ash?, 12.08 ± 0.03**	**TC**	**TC89-22A**	**USGS, Menlo**	**30**	**76.09**	**12.10**	**2.12**	**0.06**	**0.03**	**0.64**	**0.23**	**2.43**	**6.30**	**100.00**	Type loc. IHT
3506	**Ibex Hollow Tuff, ash flow**	**TC**	**TC89-21A**	**USGS, Menlo**	**30**	**75.82**	**12.22**	**2.16**	**0.06**	**0.04**	**0.66**	**0.24**	**2.37**	**6.44**	**100.01**	Type loc. IHT
3572	**Ibex Hollow Tuff, ash flow**	**TC**	**TC89-21b**	**U. of Utah**	**30**	**75.71**	**11.89**	**2.21**	**0.07**	**0.04**	**0.73**	**0.27**	**2.29**	**6.78**	**99.99**	Type loc. IHT
3573	White Basin ash, 12.17 ± 0.10	TC	TC89-19b	**U. of Utah**	29	76.72	12.00	1.64	0.09	0.02	0.55	0.25	1.89	6.84	100.00	
3574	CPT V ash, 12.07 ± 0.04	TC	TC89-18a	**U. of Utah**	28	76.31	11.97	1.96	0.06	0.03	0.61	0.21	2.39	6.45	99.99	
3575	Banded ash, 12.14 ± 0.10	TC	TC89-17a	**U. of Utah**	27	75.99	12.30	1.86	0.13	0.03	0.69	0.28	2.00	6.73	100.01	
3576	Unnamed (?) ash	TC	TC89-16a	**U. of Utah**	26	76.76	11.99	1.64	0.08	0.02	0.55	0.23	1.79	6.94	100.00	
3577	Pictograph ash, 12.34 ± 0.10	TC	TC89-15	**U. of Utah**	25	76.80	12.03	1.71	0.08	0.02	0.58	0.23	1.48	7.07	100.00	
3578	CPT III ash, 12.67 ± 0.03	TC	TC89-12	**U. of Utah**	24	76.23	12.20	1.55	0.06	0.03	0.54	0.18	1.93	7.28	100.00	
3579	Grant Claim ash, 12.96 ± 0.04	TC	TC89-20a	**U. of Utah**	18	76.36	11.95	1.77	0.04	0.03	0.56	0.18	1.69	7.40	99.98	
3580	Unnamed (?) ash bed, 13.89 ± 0.04	TC	TC90-40	**U. of Utah**	5	76.34	11.98	1.72	0.02	0.02	0.58	0.11	1.59	7.63	99.99	
3581	Road-cut ash (?)	TC	TC92-135	**U. of Utah**	1(?)	76.08	11.74	2.32	0.05	0.03	0.67	0.25	1.49	7.36	99.99	

(B) Ibex Hollow Tuff (IHT) at the Trapper Creek section (TC, bold type) and at distal correlative localities of the Ibex Hollow Tuff (sites with letter abbreviations, e.g., HV, AR, etc.; see Fig. 1)

	Locality (Ibex Hollow Tuff, type, and correlatives)	Site, Fig. 1	Sample no.	Laboratory	State	SiO_2	Al_2O_3	Fe_2O_3	MgO	MnO	CaO	TiO_2	Na_2O	K_2O	Total recalc.	Notes
3507	**Ibex Hollow Tuff, coignimbritic ash?**	**TC**	**TC89-22A**	**USGS, Menlo**	**Idaho**	**76.09**	**12.10**	**2.12**	**0.06**	**0.03**	**0.64**	**0.23**	**2.43**	**6.30**	**100.00**	Type loc. IHT
3506	**Ibex Hollow Tuff, ash flow**	**TC**	**TC89-21A**	**USGS, Menlo**	**Idaho**	**75.82**	**12.22**	**2.16**	**0.06**	**0.04**	**0.66**	**0.24**	**2.37**	**6.44**	**100.01**	Type loc. IHT
3572	**Ibex Hollow Tuff, ash-flow**	**TC**	**TC89-21b**	**USGS, Menlo**	**Idaho**	**75.71**	**11.89**	**2.21**	**0.07**	**0.04**	**0.73**	**0.27**	**2.29**	**6.78**	**99.99**	Type loc. IHT
2393	Hansel Valley,	HV	M89TH-23	USGS, Menlo	Utah	76.43	12.03	2.06	0.06	0.04	0.64	0.27	2.63	5.83	99.99	
N/A	Ambrose Road	AR	UT2283-20	U. of Toronto	Montana	76.43	11.95	2.08	0.05	0.03	0.67	0.31	2.64	5.82	99.98	
N/A	Scobey (Fouhy tephra; CT-1)	S	UT2289	U. of Toronto	Montana	76.58	12.08	2.02	0.02	0.05	0.64	0.18	3.00	5.44	100.00	Low TiO_2
N/A	Scobey (Fouhy tephra; CT-1)	S	UT2286	U. of Toronto	Montana	76.58	12.03	2.17	0.03	0.01	0.69	0.14	2.60	5.76	100.00	Low TiO_2
6327	Ashfall Fossil Beds State Park, NE	AFP	Orchard-N1 T615-2	USGS, Menlo	Nebraska	76.29	12.42	2.18	0.06	0.06	0.69	0.25	1.12	6.93	100.00	
N/A	Ashfall Fossil Beds State Park, NE	AFP	UT2425-30	U. of Toronto	Nebraska	76.34	11.94	1.97	0.04	0.03	0.64	0.31	2.04	6.67	99.98	
5594	Smith Co., Kansas	SC	GL-SCS-KMI T559-9	USGS, Menlo	Kansas	76.44	12.30	1.97	0.06	0.04	0.65	0.21	1.90	6.42	99.99	Low TiO_2
3500	Boswell oil industry well, Mobile Bay	BW	BOSWELL 1810-1990 ALL T320-t32	USGS, Menlo	Alabama	76.77	12.50	2.13	0.07	0.03	0.66	0.25	4.14	3.44	99.99	
3501	Boswell oil industry well, Mobile Bay	BW	BOSWELL SELECT T320,T324	USGS, Menlo	Alabama	76.73	12.49	2.18	0.06	0.03	0.67	0.25	4.13	3.45	99.99	
2338	Boswell oil industry well, Mobile Bay	BW	BOSWELL-1840 T194-7	USGS, Menlo	Alabama	76.91	12.39	2.19	0.06	0.05	0.68	0.25	4.02	3.46	100.01	

(*Continued*)

TABLE 2. (A) ELECTRON-MICROPROBE ANALYSIS OF GLASS SHARDS FROM TEPHRA LAYERS, TRAPPER CREEK SECTION, IDAHO, INCLUDING IBEX HOLLOW TUFF (IHT; IN BOLD TYPE); (B) IBEX HOLLOW TUFF AND TEPHRA LAYERS AT DISTAL SITES CORRELATED WITH THE IBEX HOLLOW TUFF (SEE MAP, FIG. 1) (*Continued*)

	Locality (Ibex Hollow Tuff, type, and correlatives) (*continued*)	Site, Fig. 1	Sample no.	Laboratory	State	SiO_2	Al_2O_3	Fe_2O_3	MgO	MnO	CaO	TiO_2	Na_2O	K_2O	Total recalc.	Notes
2339	Boswell oil industry well, Mobile Bay	BW	BOSWELL-1870 T194-8	USGS, Menlo	Alabama	76.81	12.28	2.18	0.06	0.04	0.68	0.27	4.06	3.61	99.99	
N/A	Huntington Creek	HC	htc93-461	U. of Utah	NE Nevada	76.02	11.85	2.27	0.06	0.03	0.68	0.25	2.43	6.38	100.00	
N/A	Stewart Valley	SV	sv92-054	U. of Utah	Cent. Nevada	75.90	11.93	2.31	0.07	0.04	0.69	0.27	2.36	6.44	100.00	
2904	Cobble Cuesta	CC	2379-17JB T268-4	USGS, Menlo	Cent. Nevada	76.74	12.25	2.12	0.07	0.04	0.67	0.25	3.61	4.25	100.00	
2790	Aldrich Station	AS	BE-16A T254-4	USGS, Menlo	W. Nevada	76.45	12.23	2.13	0.07	0.04	0.65	0.25	1.80	6.63	100.00	
2792	Aldrich Station	AS	BE-16A T254-4(2)	USGS, Menlo	W. Nevada	76.99	12.32	2.16	0.07	0.05	0.68	0.27	1.51	6.48	99.99	
5942	Aldrich Station	AS	BE-16A T589-6	USGS, Menlo	W. Nevada	76.99	12.53	2.22	0.07	0.04	0.69	0.27	1.25	5.93	99.99	
2653	Upper White Basin	UWB	UWB-17 T238-1	USGS, Menlo	SE Nevada	76.80	12.16	2.15	0.04	0.03	0.67	0.23	3.60	4.33	100.01	
N/A	El Paso Basin	EPB	epb94-580	U. of Utah	S California	76.96	12.45	2.37	0.07	0.04	0.70	0.27	1.73	5.89	100.00	
1060	Deep Sea Drilling Site 173	DSDP-173	DSDP 173-21-4 (27-28 cm)	USGS, Menlo	Pacific Ocean	76.40	12.16	2.14	0.06	0.03	0.69	0.26	3.12	5.14	100.00	
1061	Deep Sea Drilling Site 173	DSDP-173	DSDP 173-21-4 (32-35 cm)	USGS, Menlo	Pacific Ocean	76.47	12.08	2.08	0.06	0.05	0.69	0.23	2.99	5.36	100.01	
2443	Dos Pueblos Beach (Naples Beach)	NB	DPB-12 T211-3	USGS, Menlo	SW California	77.22	12.33	2.05	0.07	0.04	0.64	0.26	2.93	4.45	99.99	
5148	Dos Pueblos Beach (Naples Beach)	NB	DPB-12 T211-3(2)	USGS, Menlo	SW California	77.85	12.35	2.15	0.07	0.04	0.67	0.26	2.63	3.99	100.01	
					Average of B	76.593	12.187	2.144	0.058	0.038	0.672	0.255	2.684	5.418	99.998	
					Std. dev, 1σ	0.450	0.212	0.095	0.014	0.010	0.023	0.036	0.886	1.191	0.010	
	Homogeneous obsidian used as internal standard															
	(*n* = 18), ~20 shards per *n*	Puebla, Mex.	RSL-132	USGS, Menlo	Mexico	75.4	11.3	2.12†	0.06	0.16	0.11	0.19	4.9	4.4	98.6	
	±1σ					0.1	0.2	0.04	0.01	0.01	0.01	0.01	0.1	0.1		
	% σ					0.2	1.4	1.9	17	6.3	9	5.3	2.7	1.4		

Notes: Samples of glass shards from tephra layers were analyzed at three laboratories. Distal samples and some samples from the Trapper Creek section were analyzed at the U.S. Geological Survey (USGS), Menlo Park, California, laboratory using ARL, SEMQ, and JEOL8900 instruments, sequentially, over a period of ~50 yr (see text); analysts were Lewis Caulk, Charles E. Meyer, James W. Walker, Elmira Wan, and Laura Walkup. Some samples from the Trapper Creek section (site TC) and three of the distal sites were analyzed at the University (U.) of Utah, Salt Lake City, using a Cameca SX-50 electron microprobe (Perkins et al., 1995, 1998); analysts were Barbara P. Nash and Michael E. Perkins. Analyses at the University of Toronto were by John A. Westgate, using a JEOL JXA-8230 electron microprobe. At all laboratories, oxide totals on analysis for the nine oxides were summed, and a total was calculated; then, the oxides were recalculated to a 100% basis. The difference between the two totals is mainly water (hydration) in the glass, with less than 1% of other oxides and elements (e.g., CO_2, S, P, Cl, Ba, and Zr). Comp. no—computer number (USGS Tephra Laboratory); SNO—stratigraphic number (Perkins et al., 1998); Cent.—central; Mex.—Mexico; Diff.—different source than the Bruneau-Jarbidge volcanic area?; Type loc.—type locality; N/A—not applicable; Std. dev—standard deviation; CPT—Cougar Point Tuff. See Supplemental Item S1, section A, for additional information on analytical methods.

†FeO for obsidian standard RSL-132.

and analyzed by Perkins et al. (1995, 1998) from Trapper Creek, Idaho, provided to the USGS by M.E. Perkins, and many of the distal samples were provided to Perkins by the USGS Tephrochronology Laboratory in Menlo Park, California, representing cooperative exchanges that had been going on for several decades.

Glass shards were separated from these samples and were analyzed by EMA. Data from individual shards of six samples analyzed on the JEOL 8900 microprobe are given in Item S3. The remaining samples were analyzed on earlier instruments that did not provide individual shard data.

At the University of Toronto, major-element concentrations in the glass were determined using a JEOL JXA-8230 electron probe micro-analyzer (Table 2; Item S2). At the University of Utah, EMA analyses were conducted on a Cameca electron probe, using methods described in Perkins et al. (1995, 1998) (see Table 2; Item S4).

INAA of Separated Bulk Glass Samples

The INAA was conducted at the USGS facility in Lakewood, Colorado (Table 3). Abundances of 33 major, minor, and trace elements, including 11 rare earth elements (REEs), were determined on ~0.5–1 g separates of cleaned glass shards. In this procedure, two irradiations were performed. The samples were first irradiated in the USGS-TRIGA reactor at a neutron flux of 2.5×10^{10} n/cm²/s for 30 min, followed by a long irradiation at a flux of 2.5×10^{12} n/cm²/s for 6 h. The absorption of neutrons causes these elements to emit characteristic gamma rays, which also decay at unique rates. Gamma-ray radiation emitted by a radionuclide is converted to an electrical signal by a semiconductor detector. The electrical signal is analyzed by a multichannel analyzer. A gamma spectrum is produced, and the intensities of each gamma-ray photopeak are

TABLE 3. INSTRUMENTAL NEUTRON ACTIVATION ANALYSIS (INAA) OF VOLCANIC GLASSES OF TEPHRA LAYERS: (A) TEPHRA LAYERS OF THE TRAPPER CREEK, IDAHO, SECTION CONTAINING THE IBEX HOLLOW TUFF; (B) THE IBEX HOLLOW TUFF AT TRAPPER CREEK, IDAHO, SITE TC, COMPARED TO DISTAL SAMPLES; (C) COMPARISON OF IBEX HOLLOW TUFF COMPOSITION BY INAA AND LASER ABLATION–INDUCTIVELY COUPLED PLASMA–MASS SPECTROMETRY (LA-ICP-MS)

Name of tephra bed, Ar/Ar age (Ma)	Field no.	SN* or site	Elements analyzed using INAA																	
			Sc	Mn	Fe%	Rb	Cs	La	Ce	Nd	Sm	Eu	Tb	Dy	Yb	Lu	Hf	Ta	Th	U
(A) Tephra layers within the Trapper Creek, Idaho, section, in stratigraphic order, youngest at top																				
CPT XV ash, 10.60 ± 0.10	TC90-17	45	3.27	249	1.55	192	3.48	82.2	154	58.1	12.00	1.16	1.59	10.50	5.97	0.85	13.00	3.50	31.60	8.38
CPT XIII ash, 11.11 ± 0.03	TC89-31A	41	2.42	215	1.42	198	3.73	97.6	184	74.5	15.10	1.18	2.13	14.20	7.66	1.07	10.70	3.55	33.40	8.55
CPT XII ash, 11.34 ± 0.10	TC89-28A	37	3.91	240	1.50	195	3.27	81.9	151	59.8	12.00	1.09	1.61	10.50	5.71	0.81	11.50	3.16	31.70	8.32
CPT XI ash, 11.47 ± 0.10	TC89-27C	34	2.64	205	1.33	202	3.84	89.8	166	65.6	12.90	0.74	1.72	11.10	6.15	0.86	9.97	3.30	34.50	8.90
CPT IX ash, 11.80 ± 0.10	TC89-25A	32	2.80	198	1.21	208	3.88	82.8	155	61.9	11.90	0.73	1.56	10.40	5.58	0.79	9.91	3.36	34.20	8.83
Ibex Peak 8 ash, 11.95 ± 0.04	TC89-24A	31	4.12	240	1.45	201	3.68	79.2	148	57.4	11.50	1.04	1.52	9.94	5.41	0.78	11.20	3.27	31.80	8.17
Ibex Hollow Tuff, coignimbrite fall	**TC89-22A**	**30**	**3.31**	**251**	**1.39**	**202**	**3.75**	**86.6**	**164**	**65.6**	**13.50**	**0.98**	**1.79**	**11.30**	**6.38**	**0.89**	**10.50**	**3.67**	**32.60**	**8.53**
Ibex Hollow Tuff, ash flow, 12.08 ± 0.03	**TC89-21A**	**30**	**3.43**	**259**	**1.45**	**206**	**3.75**	**87.8**	**166**	**68.3**	**13.60**	**1.04**	**1.82**	**11.80**	**6.40**	**0.91**	**10.50**	**3.66**	**33.10**	**8.49**
White Basin ash, 12.17 ± 0.10	TC89-19A	29	3.35	174	1.11	221	3.83	79.3	148	57.0	11.00	0.65	1.41	9.11	5.18	0.72	9.26	3.15	35.20	8.95
CPT V ash, 12.22 ± 0.04	TC89-18A	28	2.19	214	1.23	213	3.85	92.0	174	69.3	13.80	0.94	1.86	12.20	6.71	0.92	9.47	3.74	34.00	8.89
Banded ash, 12.29 ± 0.10	TC89-17A	27	3.31	193	1.24	210	3.79	75.6	141	53.0	10.20	0.70	1.28	8.08	4.73	0.67	9.74	3.01	33.90	8.68
Unnamed ash 1, 12.40 ± 0.10	TC89-16A	26	3.27	190	1.10	231	3.83	86.6	163	63.2	12.00	0.53	1.59	9.98	5.71	0.80	9.48	3.46	36.40	8.96
Pictograph ash, 12.49 ± 0.10	TC89-15	25	3.15	169	1.10	230	3.93	86.0	162	63.0	11.90	0.50	1.55	9.80	5.73	0.81	9.18	3.43	37.50	9.11
Grant Claim ash, 13.11 ± 0.04	TC89-20A	18	1.49	222	1.14	211	3.52	99.7	186	74.9	14.60	0.49	1.90	12.60	6.72	0.97	8.65	4.16	33.70	8.27
(B) Tephra layers at distal sites correlated with the Ibex Hollow Tuff (bold type)																				
Ibex Hollow Tuff, coignimbrite fall	**TC89-22A**	**TC (30)**	**3.31**	**251**	**1.39**	**202**	**3.75**	**86.6**	**164**	**65.6**	**13.50**	**0.98**	**1.79**	**11.30**	**6.38**	**0.89**	**10.50**	**3.67**	**32.60**	**8.53**
Ibex Hollow Tuff, ash flow, 11.93 ± 0.03	**TC89-21A**	**TC (30)**	**3.43**	**259**	**1.45**	**206**	**3.75**	**87.8**	**166**	**68.3**	**13.60**	**1.04**	**1.82**	**11.80**	**6.40**	**0.91**	**10.50**	**3.66**	**33.10**	**8.49**
Hansel Valley, Nebraska/Utah	M89TH-23	HV	3.36	255	1.43	207	3.80	86.7	167	68.0	13.60	0.99	1.86	11.80	6.49	0.94	10.40	3.74	33.1	8.60
Boswell, oil industry well, Mobile Bay, Alabama	BOSWELL	BW	3.62	267	1.53	212	3.90	89.0	169	71.0	14.30	1.04	1.79	12.10	6.51	0.88	10.70	3.83	33.8	8.82
Aldrich Station, west-central Nevada	BE-16-A	AS	3.62	281	1.54	207	3.80	88.9	175	71.0	14.20	1.09	1.83	12.30	6.44	0.91	11.20	3.82	33.2	8.79
White Basin, S. Nevada	UWB-17	UWB	3.59	275	1.50	225	4.10	86.7	167	68.0	13.60	1.10	1.81	11.50	6.48	0.93	10.90	3.72	32.6	8.61
DSDP-173 SW of Mendocino, California	DSDP-173	DSDP-173	3.57	265	1.50	202	3.80	86.7	165	68.0	13.90	1.01	1.82	11.80	6.44	0.91	10.70	3.69	32.5	8.52
Dos Pueblos Beach (Naples Beach), SW California	DPB-12	NB	3.37	259	1.48	206	3.90	88.9	175	71.0	14.10	1.04	1.84	12.00	6.49	0.92	10.70	3.84	34.2	8.85
Ash similar in composition to the Ibex Hollow ash, but with Mn much higher and Rb lower than in the IHT, possibly a consequence of postdepositional alteration (see text)																				
Cobble Cuesta (Gabbs Valley), Nevada	2397-17	CC	3.51	554	1.46	182	3.7	86.3	162	69.0	13.80	1.05	1.80	11.90	6.31	0.91	10.70	3.63	32.1	8.39
Analytical error for INAA expressed as CV(%) multiplied by the concentration in ppm (for Fe, multiplied by the concentration in percent), for selected samples as examples of typical analytical error																				
Ibex Peak 8 ash, 11.80 ± 0.10	TC89-24A	31	0.04	2	0.01	2	0.07	0.5	1	1.0	0.07	0.03	0.32	0.08	0.07	0.01	0.11	0.03	0.32	0.08
Ibex Hollow ash, coignimbritic (?) air fall	**TC89-22A**	**30**	**0.03**	**3**	**0.01**	**2**	**0.04**	**0.9**	**2**	**1.4**	**0.14**	**0.04**	**0.33**	**0.17**	**0.06**	**0.01**	**0.11**	**0.04**	**0.33**	**0.17**
Ibex Hollow ash, ash flow, 11.93 ± 0.03	**TC89-21A**	**30**	**0.03**	**3**	**0.01**	**2**	**0.04**	**0.9**	**2**	**1.4**	**0.14**	**0.04**	**0.33**	**0.17**	**0.06**	**0.01**	**0.11**	**0.04**	**0.33**	**0.17**
White Basin ash, 12.02 ± 0.10	TC89-19A	29	0.02	2	0.07	3	0.06	0.3	1	1.0	0.06	0.02	0.21	0.13	0.06	0.01	0.07	0.02	0.21	0.13

(C) Comparison of INAA and LA-ICP-MS analyses of glass of Ibex Hollow Tuff (IHT), at Trapper Creek section (TC) and distal IHT sites AR, G, S, and AFP (Figs. 1 and 2), for elements analyzed by both methods

Name of tephra bed or unit	Field no.	Site	Rb	Zr	Ba	Cs	La	Ce	Nd	Sm	Eu	Gd	Tb	Dy	Tm	Yb	Lu	Hf	Th	U
Samples analyzed by INAA																				
Ibex Hollow ash, air fall	**TC89-22A**	**TC, 30**	**202**	**398**	**696**	**3.75**	**86.6**	**164**	**65.6**	**13.50**	**0.98**	**11.50**	**1.79**	**11.30**	**1.08**	**6.38**	**0.89**	**10.50**	**32.60**	**8.53**
Ibex Hollow ash, ash flow, 11.93 ± 0.03	**TC89-21A**	**TC, 30**	**206**	**366**	**801**	**3.75**	**87.8**	**166**	**68.3**	**13.60**	**1.04**	**12.00**	**1.82**	**11.80**	**1.03**	**6.40**	**0.91**	**10.50**	**33.10**	**8.49**
Samples analyzed by LA-ICP-MS																				
Ambrose Road, Stevensville, Montana	UT2282	AR	221	368	832	3.85	90.9	167	64.9	12.31	1.15	10.30	1.72	10.44	0.87	6.09	0.84	10.26	32.10	8.11
Glentana, Montana	UT2289	G	220	351	595	4.14	101.7	182	73.8	14.18	1.11	11.94	2.05	12.77	1.11	7.66	1.05	10.69	34.10	8.52
Scobey, Montana, 2286,	UT2286	S	216	333	608	4.01	96.5	175	70.0	13.39	1.11	11.34	1.94	11.79	1.03	7.17	0.98	9.94	31.50	8.43
Ashfall Fossil State Park, Orchard, Nebraska	UT2425	AFP	237	363	766	4.00	102.4	192	73.2	13.55	1.18	10.95	1.87	11.19	0.95	6.69	0.99	10.59	38.70	8.88

Notes: (A) Tephra layers are listed in stratigraphic order, youngest at top. Ibex Hollow Tuff is in bold type, near lower middle part of section (see Fig. 2). (B) For distal tephra layers of the IHT, see Figures 1, 11, and 13C, and Table 1 for locations. (C) Comparison of four distal samples of the IHT analyzed by LA-ICP-MS compared to the IHT at Trapper Creek type locality. Concentrations in table are in parts per million except for Fe, which is in weight percent. Elements are arranged according to increasing atomic number. Analytical error is given for several of the samples at the bottom of section B. The error is expressed as the coefficient of variation [CV(%)], the actual or "reduced" counting statistics error, based on multiple determinations, multiplied by the concentration. Samples were analyzed at the U.S. Geological Survey (USGS), Lakewood, Colorado, by J.R. Budahn (INAA), except for samples prefixed by UT, which were analyzed by J.A. Westgate at the University of Toronto, Toronto, Canada (LA-ICP-MS). CPT—Cougar Point Tuff; DSDP—Deep Sea Drilling Project.

*SN—stratigraphic number at Trapper Creek Section, Idaho, as given in Perkins et al. (1998).

measured. The counts accumulated for each elemental photopeak are corrected for background, elemental interferences, and decay, and the count rates are directly proportional to the concentration. Details of analytical methods and standards used in INAA are given in Item S1.

LA-ICP-MS Analysis

Trace, minor, and major elements were analyzed using the LA-ICP-MS system at the Department of Earth Sciences, University of Toronto (Table 4), following the methods outlined below. We used a New Wave UP-213 (solid-state frequency quintupled Nd:YAG) laser-ablation microscope connected to a VG PQ-Excell quadrupole ICP-MS. Helium was used as the transfer gas at a rate of 1000 cm^3/min, and the plasma was tuned to achieve oxide production of <2% by monitoring ThO^+/Th^+ (masses 248/232) and U^+/Th^+ (masses 238/232) as close as possible to unity. Samples were analyzed for 80 s, of which the first 20 s consisted of background. The sample cell was flushed for a minimum of 60 s between each analysis. Glass shards from each sample were analyzed in batches, with standard NIST 610 being analyzed at the beginning and end of each batch. ATHO-G was also analyzed in each batch as a reference standard. Additional information and data used in LA-ICP-MS analysis are given in Item S1.

TABLE 4. AVERAGE MINOR- AND TRACE-ELEMENT COMPOSITION OF INDIVIDUAL GLASS SHARDS FROM TEPHRA BEDS CORRELATED TO THE IBEX HOLLOW TUFF, AS DETERMINED BY LASER ABLATION–INDUCTIVELY COUPLED PLASMA–MASS SPECTROMETRY (LA-ICP-MS)

Site (Fig. 1):	Ashfall Fossil Beds (AFB) Nebraska	Ambrose Road (AR) Montana	Glentana (G) Montana	Scobey (S) Montana	ATHO-G	Average/ GeoRem
UT no:	UT2425	UT2282	UT2289	UT2286		
Rb	237 ± 11	221 ± 9	220 ± 9	216 ± 8	65 ± 4	0.99
Sr	34.2 ± 5.0	33.1 ± 3.5	23.6 ± 3.3	23.6 ± 2.6	91.2 ± 5.4	0.97
Y	66.3 ± 4.7	57.1 ± 2.9	72.2 ± 2.5	67.8 ± 2.4	91.9 ± 4.5	0.97
Zr	363 ± 26	368 ± 22	351 ± 15	333 ± 15	500 ± 21	0.98
Cs	4.00 ± 0.25	3.85 ± 0.24	4.14 ± 0.28	4.01 ± 0.29	1.15 ± 0.14	1.06
Ba	766 ± 100	832 ± 69	595 ± 108	608 ± 82	504 ± 35	0.92
La	102.4 ± 9.0	90.9 ± 4.0	101.7 ± 3.0	96.5 ± 3.9	57.6 ± 2.8	1.04
Ce	192.1 ± 15.8	167.4 ± 6.7	182.3 ± 5.6	175.2 ± 6.7	116.6 ± 6.8	0.96
Pr	19.93 ± 1.75	17.55 ± 0.80	19.64 ± 0.61	18.66 ± 0.77	14.12 ± 0.83	0.97
Nd	73.2 ± 5.4	64.9 ± 3.6	73.8 ± 1.9	70.0 ± 3.1	61.1 ± 3.1	1.00
Sm	13.55 ± 0.93	12.31 ± 0.81	14.18 ± 0.49	13.39 ± 0.63	14.07 ± 0.60	0.99
Eu	1.18 ± 0.12	1.15 ± 0.11	1.11 ± 0.08	1.11 ± 0.11	2.83 ± 0.20	1.03
Gd	10.95 ± 0.58	10.30 ± 0.72	11.94 ± 0.46	11.34 ± 0.53	14.08 ± 0.78	0.92
Tb	1.87 ± 0.12	1.72 ± 0.14	2.05 ± 0.07	1.94 ± 0.09	2.50 ± 0.11	0.99
Dy	11.19 ± 0.66	10.44 ± 0.91	12.77 ± 0.38	11.79 ± 0.51	15.83 ± 0.83	0.98
Ho	2.34 ± 0.15	2.14 ± 0.16	2.68 ± 0.08	2.48 ± 0.13	3.38 ± 0.13	0.99
Er	6.55 ± 0.28	5.90 ± 0.46	7.49 ± 0.22	6.88 ± 0.32	9.55 ± 0.44	0.93
Tm	0.95 ± 0.04	0.87 ± 0.07	1.11 ± 0.04	1.03 ± 0.04	1.39 ± 0.06	0.92
Yb	6.69 ± 0.45	6.09 ± 0.42	7.66 ± 0.14	7.17 ± 0.34	10.40 ± 0.59	0.99
Lu	0.99 ± 0.11	0.84 ± 0.05	1.05 ± 0.05	0.98 ± 0.05	1.45 ± 0.09	0.94
Hf	10.59 ± 0.72	10.26 ± 0.69	10.69 ± 0.37	9.94 ± 0.40	13.17 ± 0.45	0.96
Th	38.7 ± 5.1	32.1 ± 1.1	34.1 ± 1.0	31.5 ± 1.5	7.2 ± 0.2	0.98
U	8.88 ± 0.72	8.11 ± 0.43	8.52 ± 0.27	8.43 ± 0.56	2.07 ± 0.37	0.88
La/Ce	0.53	0.54	0.56	0.55		
Zr/Hf	34.23	35.86	32.87	33.46		
n	11	13	9	14	6	

Notes: Analyses were done at the Department of Earth Sciences, University of Toronto, by J.A. Westgate, analyst. Description of LA-ICP-MS analytical methods is given in text and in Supplemental Item S1 (see text footnote 1). See text for analytical methods. Accuracy was monitored against analyses of the ATHO-G glass standard. Average and standard deviation (1σ) are given in table; concentrations are in ppm. Sample sites are shown in Figure 1. See Figures 1, 11, and 13C for locations of samples. UT—prefix for University of Toronto, Canada, sample numbers; *n*—number of analyses for each sample.

Isothermal Plateau Fission-Track Analyses of Glass Shards

Isothermal-plateau fission-track ages (Table 5) were determined at the University of Toronto following methods described in Sandhu et al. (1993). The glass fission-track method used to determine the age of tephra beds in Montana—beds that are correlated to the Ibex Hollow Tuff—is the zeta calibration method, which is based on analysis of age standards (Hurford and Green, 1983; Wagner and Van den Haute, 1992). The age standard used is the Moldavite tektite glass (Lhenice locality) with a $^{40}Ar/^{39}Ar$ age of 14.808 ± 0.021 Ma (2σ) (Schmieder et al., 2018). The population-subtraction variant was used (Westgate, 2015), and correction for partial track fading was carried out using the isothermal-plateau method (Westgate, 1989) or the diameter-correction method (Sandhu and Westgate, 1995). Additional information on methods used in fission-track dating is given in Item S1.

Data Evaluation and Presentation

We correlated tephra layers using a combination of graphical and statistical methods (e.g., Sarna-Wojcicki, 2000; Lowe, 2011). We used the similarity coefficient of Borchardt et al. (1972) to search for geochemically similar glass shard compositions from over 7000 EMA results from volcanic glass shards analyzed in the USGS Tephrochronology Laboratory database. The pool of closest matches was then further examined using binary diagrams for selected elements, and REEs were ratioed and graphed using the chondrite values of Boynton (1992).

Our correlations, however, were not solely determined by glass shard composition. Robust correlations were supplemented with geochemical data from homotaxial successions (unidirectional sequences, from lower to higher layers within stratigraphic sections; Huxley, 1862), as well as paleontology, paleomagnetic, or direct-dating methods.

TABLE 5. GLASS FISSION-TRACK AGES OF TEPHRA BEDS FROM MONTANA CORRELATED TO THE IBEX HOLLOW TUFF*

Sample number	Method for determination of area track density	Method for correction of partial track fading	Spontaneous track density (10^4 t/cm^2)	Corrected spontaneous track density (10^4 t/cm^2)	Induced track density (10^4 t/cm^2)	Track density on muscovite detector over dosimeter glass (10^5 t/cm^2)	Etching conditions HF:temp:time (%: °C: s)	D_s (μm)	D_i (μm)	D_s/D_i or D_i/D_s	Age ± 1σ (Ma)
Ambrose Road tephra (AR)											
UT2282 near top	Point-counting	DCFT	2.23 ± 0.04 (3671)	2.77 ± 0.05 (3671)	28.00 ± 0.15 (35034)	3.75 ± 0.03 (14,393)	24: 22: 100	5.62 ± 0.12 [101]	6.96 ± 0.11 [401]	1.24 ± 0.03†	11.50 ± 1.01
UT2283 near base	Graticule	DCFT	2.93 ± 0.14 (472)	3.90 ± 0.18 (472)	76.90 ± 1.14 (4577)	7.30 ± 0.06 (14,017)	24: 19: 180	6.85 ± 0.11 [281]	9.12 ± 0.11 [631]	1.33 ± 0.03†	11.51 ± 0.57
Glentana tephra (G) (CT-1)											
UT2289	Point-counting	ITPFT	2.15 ± 0.05 (1838)		22.00 ± 0.14 (24,517)	3.75 ±0.03 (14,393)	24: 23: 150	6.05 ± 0.17 [103]	6.26 ± 0.10 [359]	0.97 ± 0.03	11.39 ± 1.22
Scobey tephra (Fouhy) (S)											
UT2286	Point-counting	ITPFT	2.09 ± 0.06 (1329)		21.30 ± 0.14 (14,393)	3.75 ± 0.03 (14,393)	24: 23: 150	6.74 ± 0.13 [101]	6.94 ± 0.09 [316]	0.97 ± 0.02	11.45 ± 1.37
Age reference standard											
UT2354	Graticule	DCFT	1.85 ± 0.05 (2085)	2.17 ± 0.05 (2085)	78.50 ± 0.86 (8301)	7.30 ± 0.06 (14,017)	24: 19: 260	7.60 ± 0.11 [224]	8.92 ± 0.11 [615]	1.17 ± 0.02†	6.27 ± 0.16

Notes: The population-subtraction method was used (Westgate, 2015). Ages were calculated using the zeta approach and $\lambda_D = 1.551 \times 10^{-10}$ yr^{-1}. Zeta value is 311 ± 4 based on 7 irradiations at the McMaster Nuclear Reactor, Hamilton, Ontario, Canada, using the NIST SRM 612 glass dosimeter and the Moldavite tektite glass with a $^{40}Ar/^{39}Ar$ age of 14.808 ± 0.021 Ma (2σ) (Schmieder et al., 2018). Number of tracks counted is given in parentheses; number of tracks measured is given in square brackets. The fluence was obtained by multiplying the muscovite track density by 0.53×10^{10} based on nine determinations. Age determinations were corrected for partial track fading using the isothermal plateau method (ITPFT) (Westgate, 1989) or the diameter correction (DCFT) method (Sandhu and Westgate, 1995). D_s—mean long axis of spontaneous tracks; D_i—mean long axis of induced tracks. The weighted mean age and error on the four determinations is 11.49 ± 0.44 Ma. The $^{40}Ar/^{39}Ar$ age of Walcott Tuff (UT2354) is 6.27 ± 0.04 Ma (2σ) (Morgan and McIntosh, 2005). This standard was included in the irradiation can with UT2283. J.A. Westgate, analyst.

*See Figures 1, 11, and 13C for location.

Previously published (legacy) $^{40}Ar/^{39}Ar$ ages of tephra layers were recalculated using the updated reference age of 28.201 ± 0.046 Ma for the Fish Canyon Tuff (Kuiper et al., 2008) and a decay constant for ^{40}Ar of 5.37×10^{-10} yr^{-1} (Min et al., 2000). Perkins et al. (1998) estimated the age of undated tephra layers using interpolation between dated overlying and underlying tephra layers. We consider these to be approximate ages and show them using "~" or "ca." (for example, ca. 12.3 Ma). These estimated ages were recalculated using the updated $^{40}Ar/^{39}Ar$ ages of the dated underlying and overlying tephra layers in Perkins et al. (1998). For a comprehensive summary of analytical data and metadata presented in this report, see Walkup et al. (2023).

RESULTS

Petrographic and Chemical Characterization of the Ibex Hollow Tuff

As noted by Perkins et al. (1995), the volcanic layers at Trapper Creek, including the Tuff of Ibex Peak (Fig. 2), are all rhyolitic (Table 2). The Ibex Hollow Tuff within the Tuff of Ibex Peak is an unwelded, massive, 4-m-thick, ash-flow tuff in the middle to lower part of the section (Fig. 2). Note that this unit is ~80 km distant from the margin of the Bruneau-Jarbidge eruptive source and ~150 km from its center. The Ibex Hollow Tuff is covered by a 1-m-thick ash-fall tuff likely of coignimbritic origin. A characteristic petrographic feature of the Ibex Hollow Tuff is the presence of abundant, highly elongated, rod-like glass shards, although bubble-wall and bubble-wall-junction shards typical of the Snake River Plain–Yellowstone hotspot tephra are abundant as well (Figs. 4A–4C). The fine fall ash overlying the ash flow has nearly the same composition as the Ibex Hollow Tuff ash flow, but it is somewhat less evolved than the latter. This fall ash is probably the elutriate derived from the ash flow, as well as some late fallout or reworked ash from the earlier Plinian eruption. The Ibex Hollow Tuff at Trapper Creek is underlain by over 20 m of redeposited tephra, which may be the early Plinian component of the Ibex Hollow Tuff eruption.

The glass shard composition of the three samples from the 4-m-thick bed of the Ibex Hollow Tuff at Trapper Creek and, of the overlying 1-m-thick coignimbritic(?) and fall ash, is relatively homogeneous as determined by EMA (Table 2). The similarity coefficients (Borchardt et al., 1972) for the five elements used in the sample comparison range from ~0.93 to ~0.98, with a mean of ~0.96 (Table 6A). The highest relative standard deviation for the oxides used for the similarity coefficient calculations is 6.3%.

Comparison of the Ibex Hollow Tuff to Other Tephra Layers in the Trapper Creek Section (the Composite Tuff of Ibex Peak, and Layers above and below the Tuff)

EMA and INAA Comparisons

Comparison of the Ibex Hollow Tuff to other tuffs within the Trapper Creek section by EMA major- and minor-element concentrations yielded a number of potential correlative tuffs with similarity coefficients greater than 0.93 (Table 6B). This is attributable to the high chemical similarity of the tephra layers in the Tuff of Ibex Peak. Perkins et al. (1995), however, described an overall compositional gradient for major and trace elements of the Tuff of Ibex Peak group over time (Table 6A; Fig. 5). This trend begins at ca. 12.5 Ma, when, as Perkins et al. (1995) suggested, the volcanic source of the rhyolite eruptions changed from the Owyhee-Humboldt volcanic field to the Bruneau-Jarbidge volcanic field. The 12.08 Ma Ibex Hollow Tuff must have erupted ~0.4 m.y. after the time of initiation of Bruneau-Jarbidge volcanic field activity.

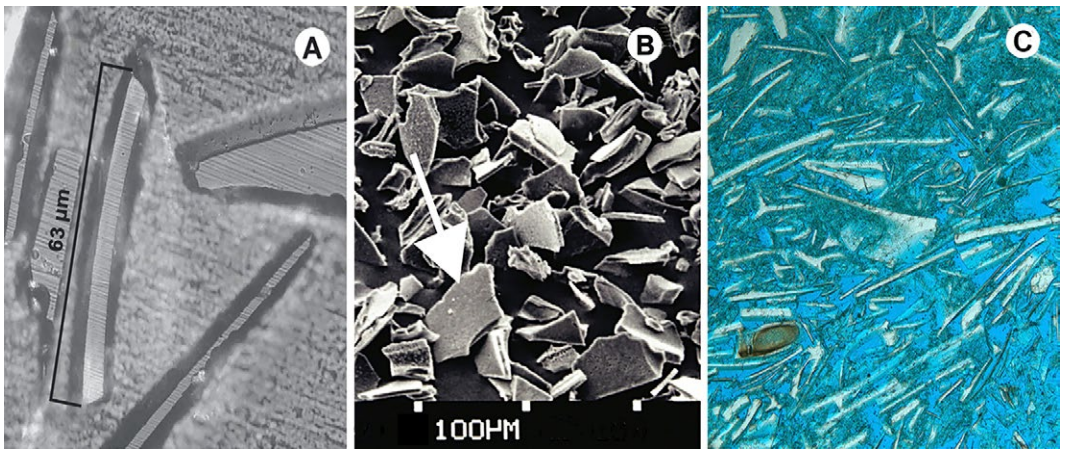

Figure 4. (A) Backscattered electron image of elongate, rod-shaped glass shards of the Ibex Hollow Tuff (sample UT2425; Ashfall Fossil Beds State Park, Nebraska), on polished, epoxy-mounted slide. Photo by John Westgate. (B) Scanning electron microscope (SEM) microphotograph of slightly curved, platy, bubble-wall shards (arrow) typical of tephra erupted from the Snake River Plain–Yellowstone hotspot eruption sources. The lens-like shapes reflect in sunlight, giving these ashes a glittering, light bluish to silver gray color. White ticks at bottom are 100 µm apart. Photo by Janet Slate, U.S. Geological Survey. (C) Thin-section photomicrograph of isotropic glass shards embedded in blue-dyed resin. Plane-polarized light. Field of view is 1.25 mm. Sample SCS-KMI, at locality SC, near Cora, Kansas (Figs. 1 and 13C). Rod-shaped, bubble-wall junction and bubble-wall shards can be seen in this photomicrograph by Greg Ludvigson.

TABLE 6A. COMPARISON OF COMPOSITIONS OF GLASS SHARDS IN TEPHRA LAYERS IN THE TRAPPER CREEK AREA, IDAHO, USING THE SIMILARITY COEFFICIENT (SC) OF BORCHARDT ET AL. (1972)

Name of ash bed or tuff*	Sample no.	Age (Ma)	Concentration of oxides (wt%)									SC†
			SiO_2	Al_2O_3	Fe_2O_3	MgO	MnO	CaO	TiO_2	Na_2O	K_2O	
McMullen Creek	TC92-71	8.99	75.35	12.09	2.64	0.11	0.03	0.92	0.31	2.92	5.63	0.8675
Section 26	TC90-22	9.20	75.44	12.22	2.43	0.18	0.04	0.93	0.36	2.87	5.52	0.8552
Wooden Shoe Butte	TC90-20	10.26	75.39	12.06	2.35	0.10	0.03	0.81	0.31	2.70	6.24	0.9074
CPT XV	TC90-17	10.45	76.02	12.11	2.33	0.13	0.03	0.77	0.31	2.53	5.79	0.9180
Steer Basin	TC92-15c	10.60	75.39	12.01	2.39	0.10	0.03	0.87	0.33	2.71	6.16	0.8841
Steer Basin	TC89-36a	10.60	76.67	12.31	1.04	0.01	0.02	0.31	0.35	2.71	6.57	0.7331
Ibex Peak 19	TC89-34a	10.74	76.04	11.97	2.60	0.09	0.04	0.84	0.33	2.31	5.78	0.8770
CPT XIII	TC89-33b	10.94	76.64	11.98	2.16	0.03	0.03	0.65	0.20	2.52	5.78	0.9466
CPT XIII	TC89-31a	10.94	76.45	12.06	2.18	0.03	0.03	0.66	0.20	2.52	5.87	0.9446
CPT XII	TC89-28a	11.34	75.83	12.09	2.24	0.12	0.04	0.77	0.32	2.65	5.94	0.9202
CPT XI	TC89-27c	11.46	76.61	11.96	2.02	0.05	0.03	0.61	0.21	2.31	6.19	0.9355
CPT IX	TC89-25a	11.74	76.61	11.96	1.91	0.07	0.03	0.58	0.24	2.20	6.40	0.9391
Ibex Peak 8	TC89-24a	11.80	75.85	12.08	2.15	0.12	0.03	0.74	0.34	2.44	6.25	0.9202
Ibex Hollow Tuff (IHT)	**TC89-21a**	**11.93**	**76.05**	**11.93**	**2.18**	**0.06**	**0.04**	**0.64**	**0.26**	**2.34**	**6.50**	**1.0000**
White Basin	TC89-19b	12.17	76.72	12.00	1.64	0.09	0.02	0.55	0.25	1.89	6.84	0.9117
CPT V	TC89-18a	12.22	76.31	11.97	1.96	0.06	0.03	0.61	0.21	2.39	6.45	0.9306
Banded	TC89-17a	12.29	75.99	12.30	1.86	0.13	0.03	0.69	0.28	2.00	6.73	0.9357
Unnamed ash 1	TC89-16a	12.30	76.76	11.99	1.64	0.08	0.02	0.55	0.23	1.79	6.94	0.8964
Pictograph	TC89-15	12.49	76.80	12.03	1.71	0.08	0.02	0.58	0.23	1.48	7.07	0.9114
CPT III	TC89-12	12.84	76.23	12.20	1.55	0.06	0.03	0.54	0.18	1.93	7.28	0.8445
Grant Claim	TC89-20a	13.13	76.36	11.95	1.77	0.04	0.03	0.56	0.18	1.69	7.40	0.8747
Unnamed ash 2	TC90-40	13.89	76.34	11.98	1.72	0.02	0.02	0.58	0.11	1.59	7.63	0.8221
Road cut	TC92-135	13.90	76.08	11.74	2.32	0.05	0.03	0.67	0.25	1.49	7.36	0.9680

Notes: Data are from electron-microprobe analysis (EMA; Table 2). Tephra layers are listed in stratigraphic order, oldest at bottom. Ibex Hollow Tuff (IHT) is highlighted in bold type. Tuffs of Ibex Peak of Perkins et al. (1995) are in gray shading (see Perkins, 1998; Perkins et al., 1995, 1998). See Figure 2, stratigraphic section. CPT—Cougar Point Tuff.

*Names of tephra units are from Perkins et al. (1995, 1998).

†Similarity coefficient (SC) of Borchardt et al. (1972) was used to compare the samples quantitatively, where 1.0000 represents a perfect match. All similarity coefficients were calculated using concentrations of Si, Al, Fe, Ca, and Ti oxides.

TABLE 6B. SIMILARITY MATRIX COEFFICIENTS FOR PUTATIVE IBEX HOLLOW TUFFS USING INAA AND LA-ICP-MS (ELEMENTS Rb, Cs, Ba, La, Ce, Nd, Sm, Eu, Gd, Tb, Dy, Yb, Lu, AND Hf) FROM TABLE 3

	TC89-21A	M89TH-23	DSDP-173	BE-16-A	UWB-17	DPB-12	BOSWELL	UT2282	UT2289	UT2286	UT2425
TC89-21A	1	0.9807	0.9877	0.9772	0.9742	0.9789	0.9762	0.9395	0.9057	0.9329	0.9289
M89TH-23		1	0.9776	0.9614	0.9633	0.9735	0.9671	0.9263	0.9118	0.9423	0.9295
DSDP-173			1	0.9723	0.9682	0.9757	0.9357	0.9357	0.9011	0.9291	0.9264
BE-16-A				1	0.9663	0.9830	0.9774	0.9283	0.9205	0.9324	0.9307
UWB-17					1	0.9636	0.9640	0.9390	0.9153	0.9348	0.9401
DPB-12						1	0.9868	0.9262	0.9234	0.9410	0.9404
BOSWELL							1	0.9324	0.9201	0.9339	0.9328
UT2282								1	0.8736	0.9088	0.9183
UT2289									1	0.9536	0.9296
UT2286										1	0.9416
UT2425											1

Notes: INAA—instrumental neutron activation analysis; LA-ICP-MS—laser ablation–inductively coupled plasma–mass spectrometry. Locality/samples numbers: TC—Trapper Creek, Idaho (TC89-21A); HV—Hansell Valley, Utah (M89TH-23); DSDP-173—Deep Sea Drilling Project Site 173 (DSDP-173); AS—Aldrich Station, Nevada (BE-16-A); UWN—Upper White Basin, Nevada (UWB-17); DPB—Dos Pueblos Beach, California (DPB-12); BW—Boswell oil well, Alabama (BOSWELL); AR—Ambrose Road, Montana (UT2282); G—Glentana, Montana (UT2289); S—Scobey, Montana (UT2286); AFB—Ashfall Fossil Beds, Nebraska (UT2425). UT—analyses by LA-ICP-MS; other samples by INAA.

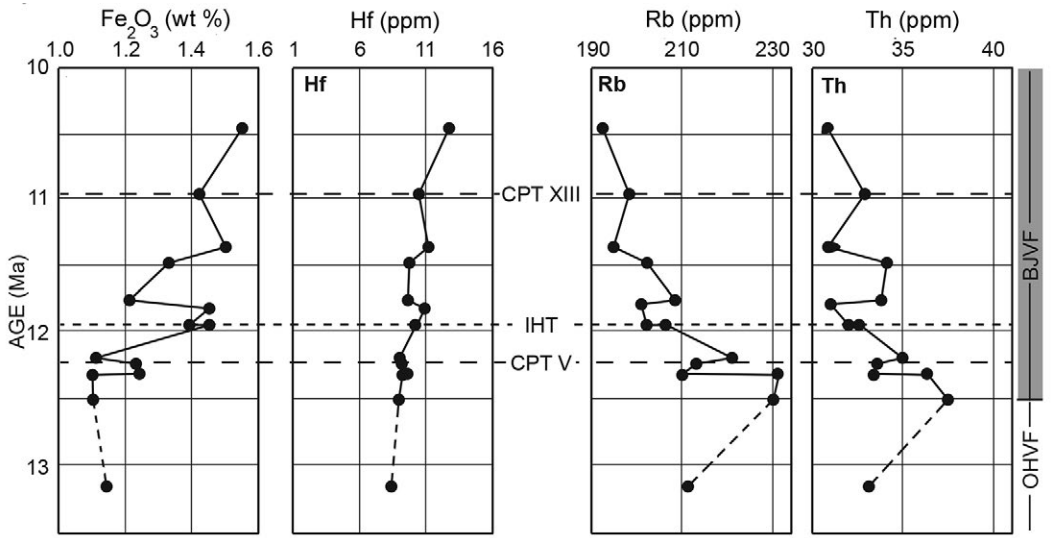

Figure 5. Plots of concentrations of Fe_2O_3, Hf, Rb, and Th vs. age for glass shards from tephra layers at the Trapper Creek section, Idaho. Sequence of tuffs is from Table 6A. The positions of the Ibex Hollow Tuff (IHT), Cougar Point Tuff V (CPT V), and Cougar Point Tuff XIII (CPT XIII) are shown by the dashed lines. The Cougar Point Tuff V and Cougar Point Tuff XIII are the bounding tuffs of the Tuff of Ibex Peak of Perkins et al. (1995). The two points for the Ibex Hollow Tuff show the difference between the coignimbritic(?) and ash-flow phases of this unit. The change in volcanic field from Owyhee-Humboldt (OHVF) to the Bruneau-Jarbidge (BJVF) is indicated by a dashed line and at the right side of the figure.

The lower tuff beds of the Tuff of Ibex Peak are generally more evolved than those near the top of the section (Tables 2 and 3; Fig. 5). Specifically, TiO_2, Fe_2O_3, CaO, Ba, Sr, Zr, and Hf all increase in concentration toward the top of the Trapper Creek section (Fig. 5). Conversely, the highly incompatible Rb, Th, and Cs, and, to some extent, the REEs, decrease in concentration with time. These compositional trends can be explained by fractionation of the phenocryst phases, with the more evolved part of the magma being erupted first. Hence, to a certain extent, the stratigraphic position of any tuff bed in the Tuff of Ibex Peak sequence can be approximated by its glass composition. Moreover, these compositional trends make each tuff distinctive when compared using trace-element concentrations (Table 3). Thus, the trace-element composition of the Ibex Hollow Tuff is distinctive even among tuffs immediately above and below each other in the Tuff of Ibex Peak (Figs. 2 and 6A–6F), and they can be identified using glass shard composition. For example, the similarity coefficients for trace elements (Table 3) show a strong similarity between the Ibex Hollow Tuff and the 12.22 Ma Cougar Point Tuff V. This similarity is shown in the REE compositions as well (Fig. 6A). Despite this similarity, we are able to distinguish between the Ibex Hollow Tuff and Cougar Point Tuff V by differences in Fe_2O_3, Hf, Rb, and Th concentrations, as well as by the REEs (Figs. 5 and 6A–6F; Table 3).

In several instances, these two tuffs may be further distinguished by their associated tephrostratigraphic sequence and paleomagnetic orientation. The Ibex Hollow Tuff overlies the White Basin ash bed, whereas the Cougar Point Tuff V underlies the White Basin ash bed. The Ibex Hollow Tuff is within a reverse polarity interval, but the Cougar Point Tuff V is within a normal polarity interval (Ogg, 2012). We refer to these characteristic sequences as homotaxial successions (Huxley, 1862; see discussion below).

The chemical trend described above, from a highly evolved to less evolved composition in these tephra layers with time (Fig. 5), however, is not monotonic. Several smaller reversals in the overall trend occur going stratigraphically upward within this section. To further eliminate any ambiguity in correlation of the Ibex Hollow Tuff and its correlatives at distal locations, we have drawn up a sequence of binary scatter diagrams that show the compositions of tephra layers within the proximal Trapper Creek locality (the Tuff of Ibex Peak), including the Ibex Hollow Tuff, within this source-proximal section, as well as the proposed correlations of the Ibex Hollow Tuff to distal sites. By going through a sequence of these binary scatter plots, we indicate the samples in this section that compositionally overlap consistently with the Ibex Hollow Tuff samples for each pair of elements or oxides, and we eliminate those samples that do not (Figs. 7–10).

A plot of CaO against Fe_2O_3 (Fig. 7; data in Table 2), based on EMA of the glass shards, defines a roughly linear trend for the Trapper Creek section, as well as for some tephra units in the underlying and overlying beds. This trend is not systematically related to age of eruption. The Ibex Hollow Tuff occupies a restricted, central part of the trend obtained for the Trapper Creek section, and there is apparent compositional overlap only with the Cougar Point Tuff XIII tephra layer (11.11 ± 0.03 Ma). Other tephra layers close to the Ibex Hollow Tuff in this plot are the Ibex Peak 8 (11.95 ± 0.10 Ma), Cougar

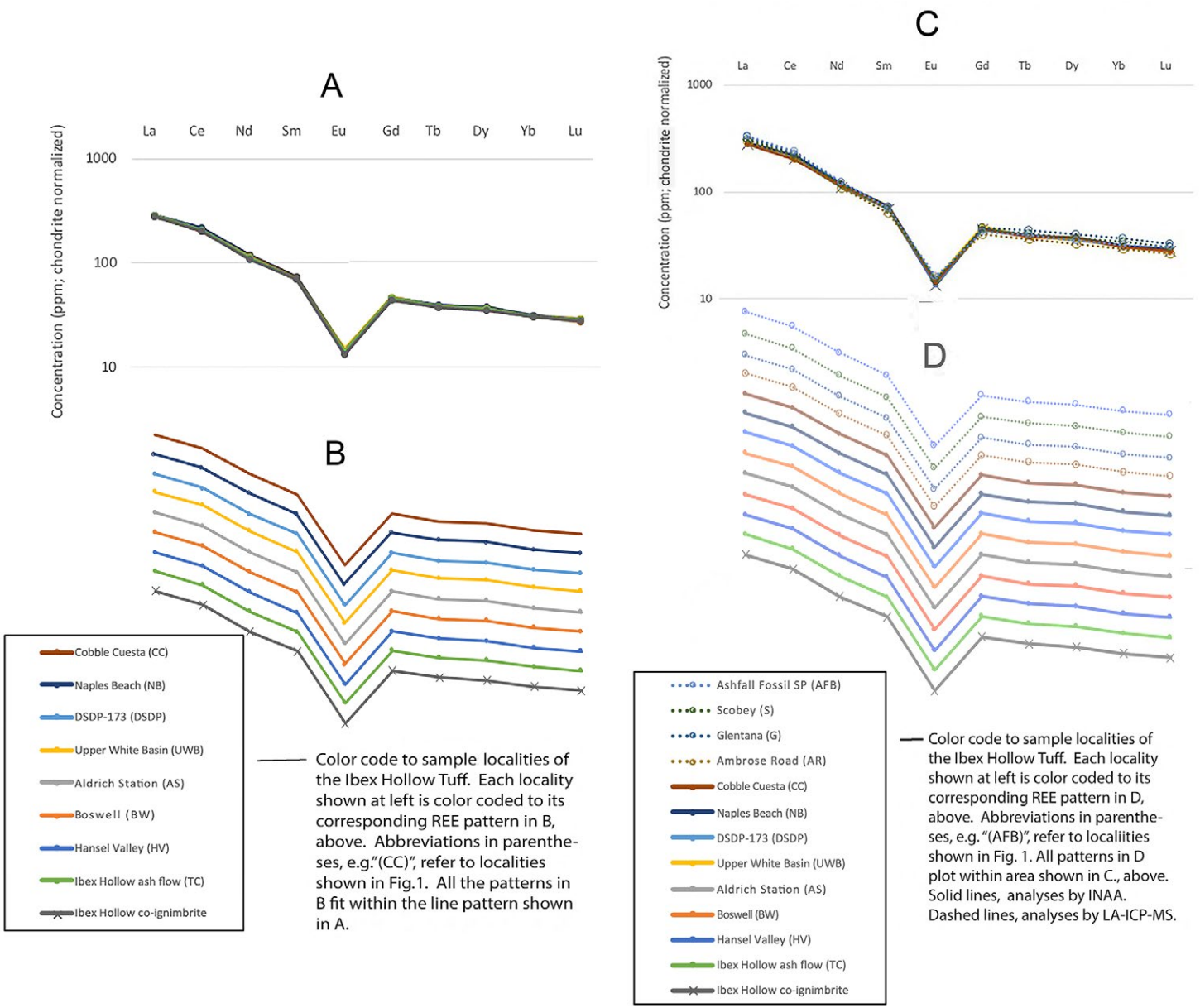

Figure 6. (A, B) Plots of rare earth element (REE) concentrations in glass shards for the Ibex Hollow Tuff (IHT) in the Trapper Creek, Idaho, section as ratios to those in a chondrite (Boynton, 1992), where analyses were by instrumental neutron activation analysis (INAA) of glass shard separates: (A) Ibex Hollow Tuff (IHT) samples at Trapper Creek, Idaho (both ash flow and ash fall) compared to distal samples that we correlate here with the Ibex Hollow Tuff. Values are ratios of the REEs in the volcanic glass divided by the concentration of the same elements in a chondrite meteorite (Boynton, 1992). The patterns here stack almost exactly one on top of the other. (B) REE patterns from A, above, separated out to illustrate the similarity of the Ibex Hollow Tuff at proximal and distal locations. Tephra localities are color coded, with the key to the localities shown in the box. See Figure 1 for locations. (C, D) Plots of REE concentrations for the IHT in the Trapper Creek, Idaho, section, as ratios to a chondrite (Boynton, 1992), where glass shards were analyzed by INAA of bulk glass shard separates, and by laser-ablation–inductively coupled plasma–mass spectrometry (LA-ICP-MS) of individual shards: (C) INAA (solid lines) analyses of glass shard separates and LA-ICP-MS (dashed lines) analyses of individual glass shards. The patterns are stacked here, with those for the INAA almost one on top of the other, and those for the LA-ICP-MS showing somewhat greater scatter. (D) REE patterns from C, above, separated out to illustrate the similarity of the Ibex Hollow Tuff at proximal and distal locations. INAA analyses, in solid lines, show less scatter than the LA-ICP-MS analyses, shown in dashed lines. Tephra localities are color coded, with the key to the localities shown in the box. Abbreviations at end of sample name correspond with locations on Figure 1. DSDP—Deep Sea Drilling Project; TC—Trapper Creek type section. (*Continued.*)

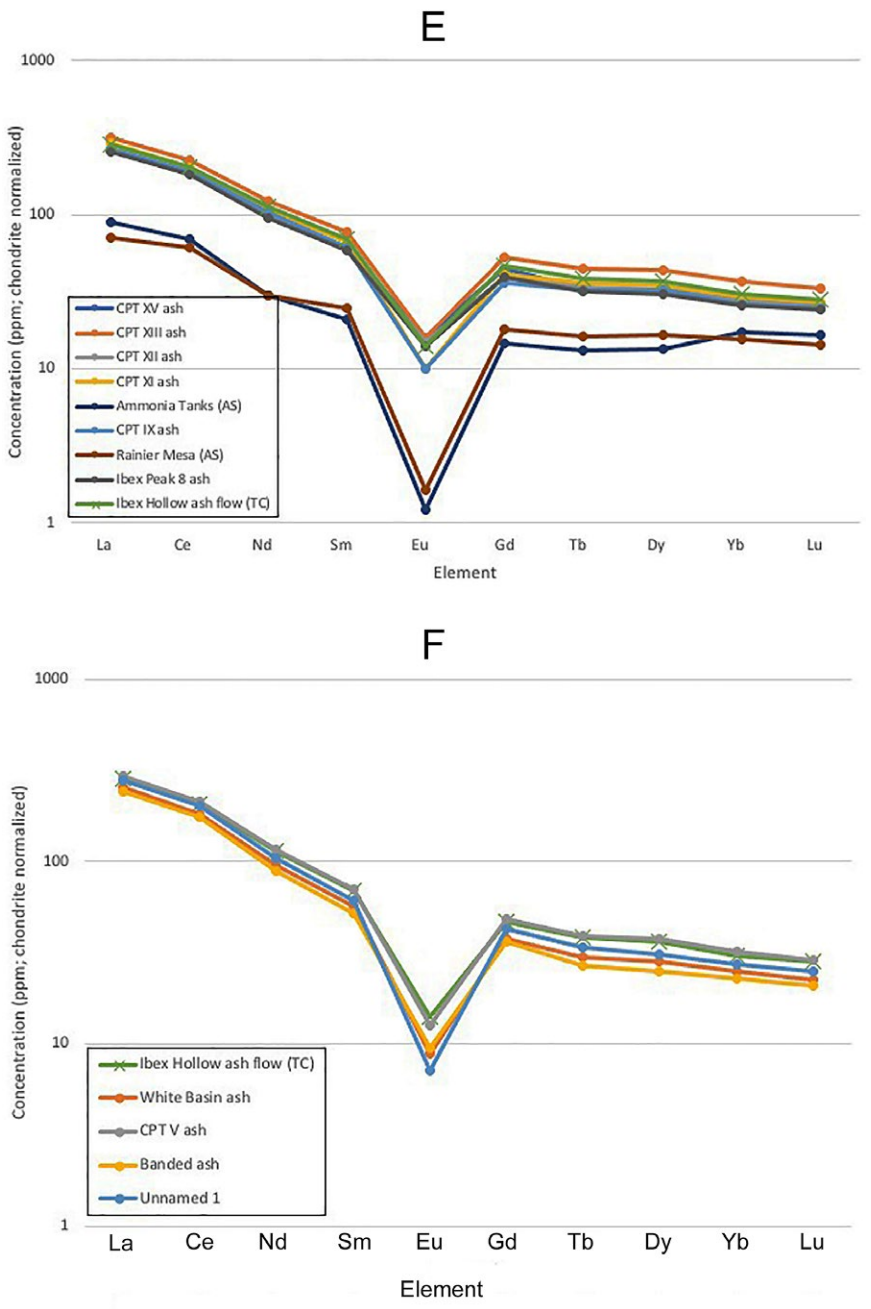

Figure 6 (*Continued*). (E) Rare earth element (REE) diagram of Ibex Hollow Tuff (IHT) at Trapper Creek section, Idaho (both ash flow and ash fall, averaged), compared with tephra layers situated stratigraphically above the Ibex Hollow Tuff in the section (see Figs. 1 and 2). Analyses of glass shard separate by instrumental neutron activation analysis (INAA). Analyses of the Ammonia Tanks and Rainier Mesa, erupted from the Southern Nevada volcanic field, are included here to show the large differences in the REE/chondrite ratios between tephra layers erupted from different volcanic fields. Values are ratios of the REEs in the volcanic glass divided by the concentration of the same elements in a chondrite meteorite (Boynton, 1992). (F) REE diagram of IHT at Trapper Creek section, Idaho (both ash flow and ash fall, averaged), compared with tephra layers situated below the Ibex Hollow Tuff in the section (see Fig. 2). Analyses by INAA of glass shard separate. TC—Trapper Creek type section.

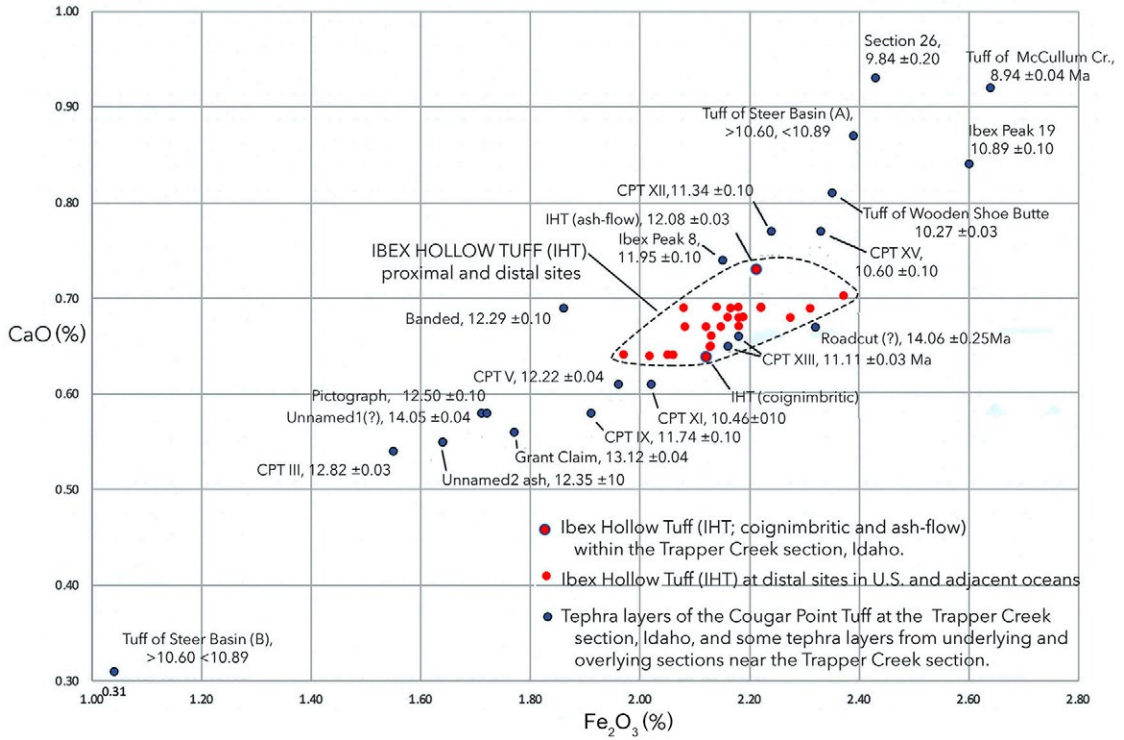

Figure 7. Plot of CaO vs. Fe_2O_3 (in oxide weight percent) for glass shards from tephra layers of the Trapper Creek section, Idaho, including the Ibex Hollow Tuff within the section, and distal tephra layers correlated to the Ibex Hollow Tuff (see Fig. 1 for locations; see Fig. 2 for stratigraphy of Trapper Creek section). Analyses by electron microprobe (EMA). Samples of the Trapper Creek section were analyzed at the University of Utah, Salt Lake City, Utah, and at the U.S. Geological Survey, Menlo Park, California. Distal samples of the Ibex Hollow Tuff were analyzed at the latter laboratories and at the University of Toronto, Canada. CPT—Cougar Point Tuff. See text and Table 2.

Point Tuff V (11.07 ± 0.04 Ma), Cougar Point Tuff XI (11.74 ± 0.10 Ma), and the Roadcut (?) (>13.89 Ma) tephra layers. The two proximal samples of the Ibex Hollow Tuff at Trapper Creek, the ash-flow tuff and the coignimbritic(?) ash overlying the latter, define the CaO range for all samples we correlate here with the Ibex Hollow Tuff (for an enlargement of the central part of Figure 7, see Item S5). From this and other binary plots, it also appears that the ash-flow phase of the Ibex Hollow Tuff was less evolved than the overlying fall ash, a phenomenon observed in other large eruptions having both a Plinian and ash-flow component (Bacon, 1983; Bacon and Druitt, 1988; Hildreth and Wilson, 2007). The data for the Ibex Hollow Tuff suggest, however, that the ash-fall unit overlying the ash flow may contain Plinian fallout or reworked early Plinian tephra of the Ibex Hollow Tuff, as well as a component of the later coignimbritic ash fall. Figure 7 supports correlation of all distal sites with the proximal Ibex Hollow Tuff tephra layer; Cougar Point Tuff XIII, however, is a possible marginal alternative—one which we eliminated using minor- and trace-element data (see below). For additional detailed data for individual samples analyzed by EMA in this study, such as the composition of individual shards analyzed by EMA, original averages, and average totals before recalculation to a 100% basis, and additional binary scatter plots of samples, see Items S2–S5.

INAA data are available for the Trapper Creek section, Idaho, for 14 samples, which includes 12 tephra beds stratigraphically below and above the Ibex Hollow Tuff in the Trapper Creek section, and two samples of the Ibex Hollow Tuff, the 4-m-thick ash-flow tuff and the 1-m-thick overlying coignimbritic and reworked Plinian (?) ash-fall bed (Fig. 2), as well as for seven distal sites correlated here with the Ibex Hollow Tuff (Figs. 1, 6A, and 6B).

Minor- and Trace-Element LA-ICP-MS Analysis for Correlation of the Ibex Hollow Tuff

Minor- and trace-element LA-ICP-MS analyses were performed on individual glass shards of samples from three distal sites in Montana (Fig. 1, sites AR, G, and S), and one distal site from Nebraska (Fig. 1, site AFB). The LA-ICP-MS data show greater scatter than the INAA data for most elements, probably because the LA-ICP-MS analyses represent compositions of individual glass shards, but the INAA analyses represent average compositions of multiple glass shards (Figs. 6C and 6D). The scatter plots for the two sets of minor- and trace-element data plot in somewhat different fields. For example, in a plot of Hf versus Eu (Fig. 8), one in which the LA-ICP-MS data show the least scatter, the midpoint of the scatter field for Ibex Hollow Tuff is offset by ~0.5 ppm for Hf and by ~0.1 ppm for Eu from the INAA scatter field; the two plots, however, do not overlap. If we interpret that the distal site AFB, the Ash Fall Park site in Nebraska (Fig. 1), is the Ibex Hollow Tuff, as we infer from the EMA data (Fig. 7) and the U-Pb age obtained on zircons from this site of 11.86 ± 0.13 Ma (Smith et al., 2018), then the two fields should be superposed in the diagram. We do not know what the reason is for these differences: instrumentation, standards, or something else. The University of Toronto study was initially a separate one from that conducted by the USGS and the University of Utah until we recently compared data from all three laboratories. We initially attempted to analyze several samples previously analyzed by INAA using LA-ICP-MS at the University of Aberystwyth, Wales. That run was flawed due to technical problems, so we were not able to derive a direct transfer calibration from the one method to the other in this study. Nevertheless, the EMA data provide correlations for all the samples, the INAA data provide correlations for most samples, and the LA-ICP-MS data provide correlation for four sites: the samples from the three Montana samples (G, AR, and S) and the one site from Nebraska (AFB). The four samples analyzed by LA-ICP-MS are chemically the most similar to the

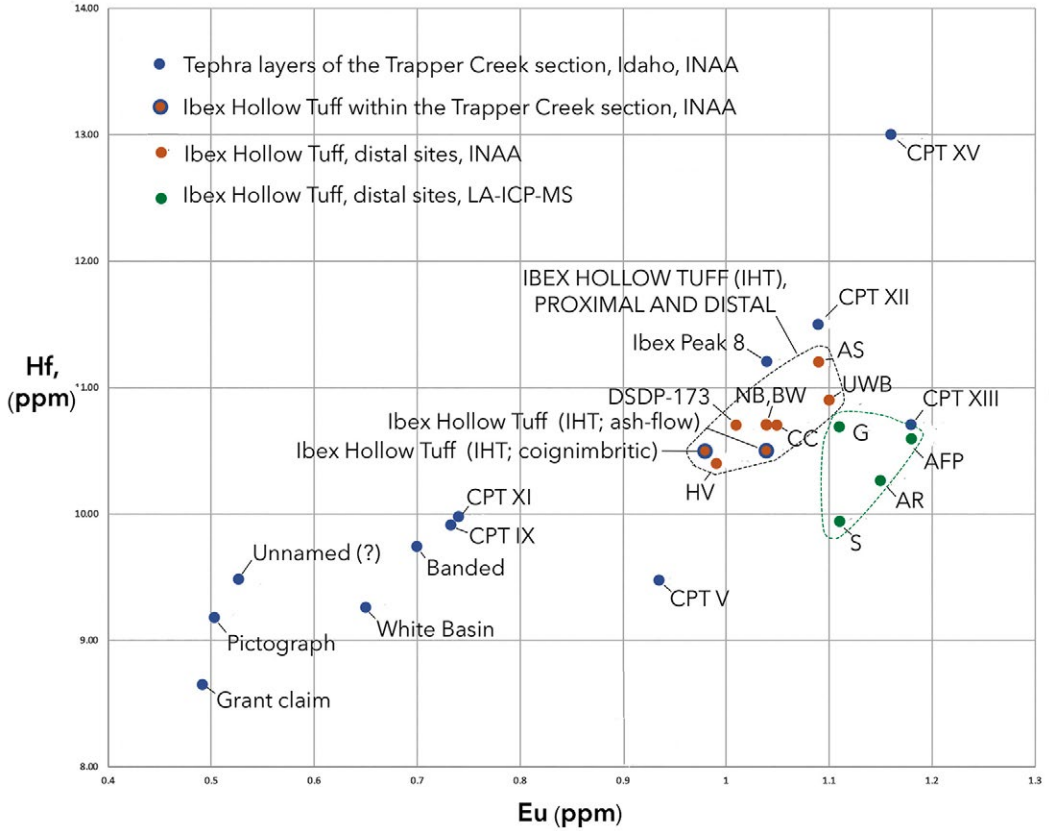

Figure 8. Plot of Hf vs. Eu for glass shards from tephra layers of the Trapper Creek section, Idaho, the proximal Ibex Hollow Tuff within this section, and the Ibex Hollow Tuff at distal sites (see Fig. 1 for locations and abbreviations; see Fig. 2 for stratigraphy of the Trapper Creek section). CPT—Cougar Point Tuff; INAA—instrumental neutron activation analysis; LA-ICP-MS—laser-ablation–inductively coupled plasma–mass spectrometry.

Ibex Hollow Tuff, compared to the rest of the Trapper Creek section, based on an overall assessment of the data (Figs. 6A–6F) and sequential exclusion of other possible correlations in comparisons using binary diagrams (Figs. 7–10).

A plot of Sm versus Dy based on INAA data (Fig. 9) indicates a nearly linear relationship for samples of the Trapper Creek section and the Ibex Hollow Tuff, with samples of the latter, both proximal and distal, forming a tight group within this trend. Only Cougar Point Tuff V (12.22 ± 0.04 Ma) lies close to the Ibex Hollow Tuff field. Note here also that Cougar Point Tuff XIII, which was at the margin of the Ibex Hollow Tuff in the Fe_2O_3 versus CaO plot of the EMA data (Fig. 7), is far outside the scatter fields of the Ibex Hollow Tuff INAA and LA-ICP-MS data sets in Figure 9. Although the scatter fields for INAA and LA-ICP-MS points overlap for the Ibex Hollow Tuff, the scatter in the latter is about twice that of the INAA, and data overlap for the Cougar Point Tuff XI and Cougar Point Tuff V ash beds of the Trapper Creek section. The center points of the scatter fields for INAA and LA-ICP-MS data are offset ~0.05 ppm for both Sm and Dy, which indicate small but, in the present case, important differences.

A plot of Lu versus Tb for the Trapper Creek section based on INAA defines a nearly straight-line relationship for these REEs in the samples (Fig. 10). Samples of the Ibex Hollow Tuff, both proximal and distal, form a tight cluster within this trend, with only Cougar Point Tuff V (12.22 ± 0.04 Ma) close at the margin of this field. The other tephra layers of Trapper Creek are compositionally far from the Ibex Hollow Tuff field. The LA-ICP-MS data, however, encompass the latter sample as well as Cougar Point Tuff XI and the Grant Claim ash bed (Fig. 10), with scatter in this instance being about three times that of the INAA, and with the center points of the scatter fields displaced ~0.05 ppm for both Lu and Tb.

Additional binary plots, such as those of Ce versus La, Fe versus Sc, Ta versus Hf, U versus Th, and Rb versus Cs, have been made, but they do not add appreciably to the discussion here. These plots are available in Item S5.

In conclusion, using various combinations of major, minor, and trace elements, and the REEs in particular (Figs. 6A–6F), as well as the binary plots (Figs. 7–10), we can distinguish among the 12 tephra layers within the Trapper Creek section on the basis of the chemical composition of their volcanic glasses, as well as distinguish the Ibex Hollow Tuff within this section and correlate

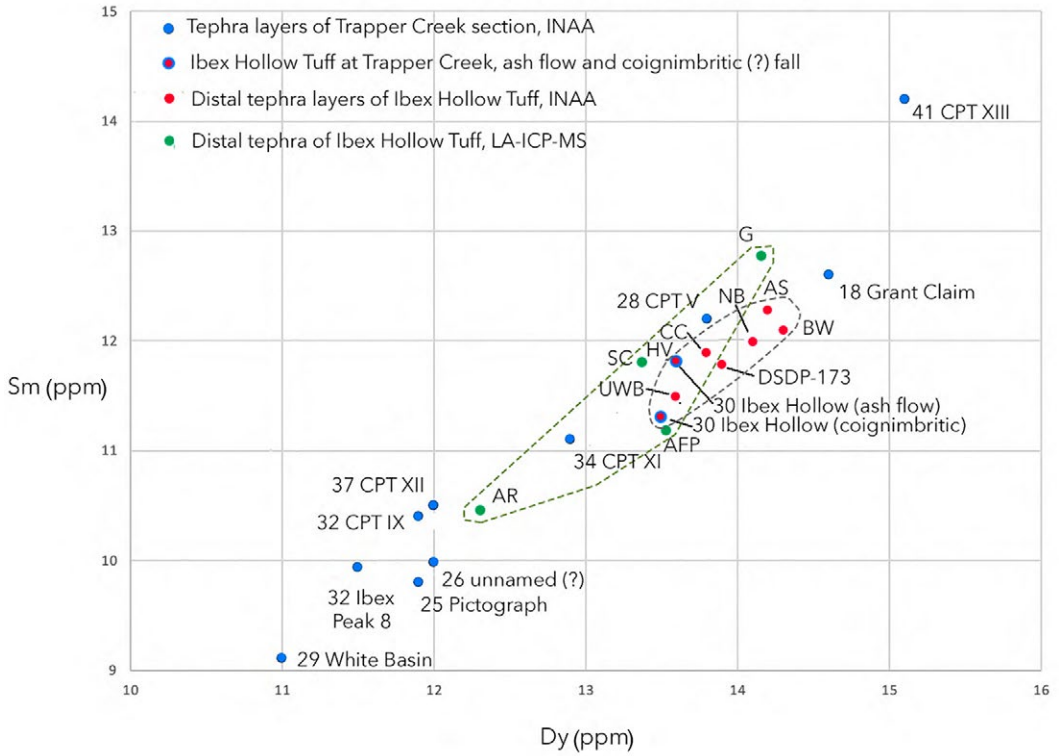

Figure 9. Plot of Sm vs. Dy for samples of the Trapper Creek section, Idaho, the Ibex Hollow Tuff within the section, and the Ibex Hollow Tuff at distal sites (see Fig. 1 for locations and abbreviations; see Fig. 2 for stratigraphy of the Trapper Creek section). CPT—Cougar Point Tuff; INAA—instrumental neutron activation analysis; LA-ICP-MS—laser-ablation–inductively coupled plasma–mass spectrometry.

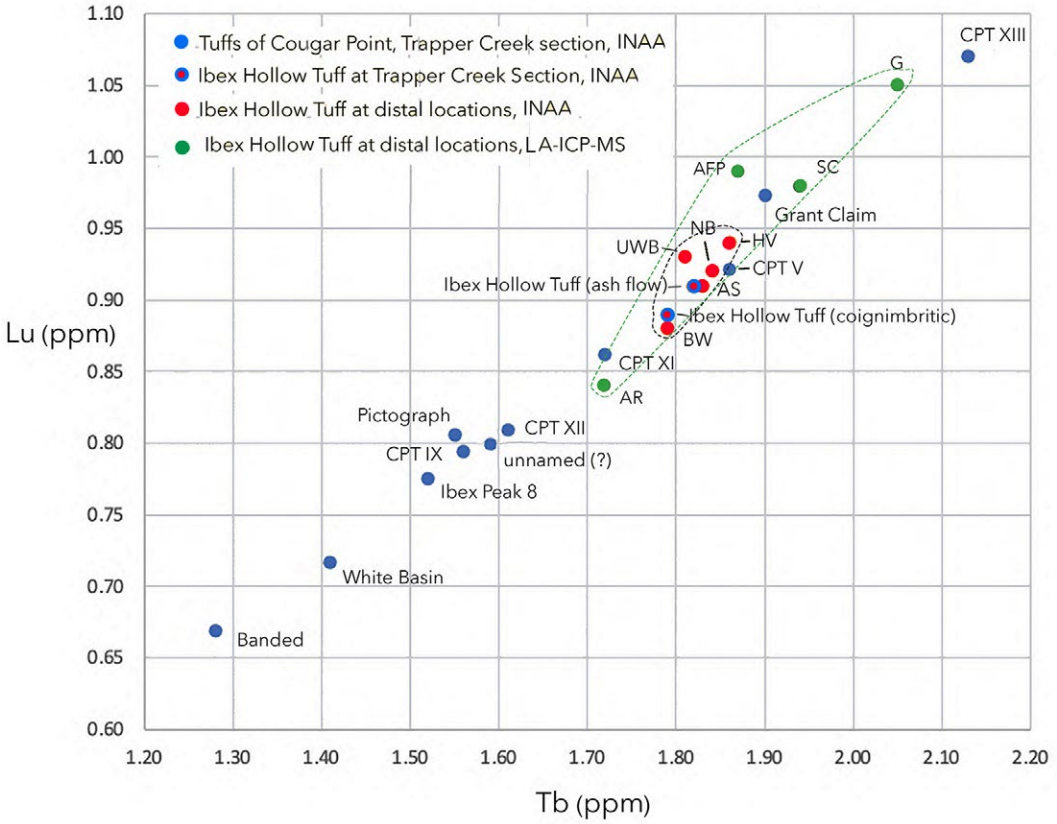

Figure 10. Plot of Lu vs. Tb for samples of the Trapper Creek section, Idaho, the Ibex Hollow Tuff within the section, and the Ibex Hollow Tuff at distal sites (see Fig. 1 for locations and abbreviations; see Fig. 2 for stratigraphy). CPT—Cougar Point Tuff; INAA—instrumental neutron activation analysis; LA-ICP-MS—laser-ablation–inductively coupled plasma–mass spectrometry.

it to distal sites in North America and the nearby ocean areas, based on the chemical compositions of the glass shards. The REE patterns (Figs. 6A–6F) show the similarities and differences among the tephra layers most clearly, but there is compositional overlap in some of the binary plots of elements. Sequential elimination of matching possibilities using the binary diagrams makes it possible to match the proximal Ibex Hollow Tuff to distal correlative localities. INAA data for the shard compositions show less scatter than that of LA-ICP-MS data.

Correlation of the Ibex Hollow Tuff from the Trapper Creek Section to Distal Localities

We correlated the proximal Ibex Hollow Tuff and, in a number of instances, underlying and overlying tephra layers of the Trapper Creek section and tephra layers erupted from other sources to 15 distal localities (Figs. 1 and 11). We use the term "tuff" for proximal exposures where the units have been named by others as such, or are indurated, but we use the term "ash layers" or, preferably, the more general "tephra layers" for the Ibex Hollow tephra identified at distal sites and underlying and overlying tephra beds.

In most instances, our correlation of a specific distal tephra layer to the Ibex Hollow Tuff depends on multiple lines of evidence (e.g., shard chemical composition, stratigraphic sequence of tephra layers, paleontology, and independent dating). Where multiple tephra layers are present, a key line of evidence in our correlations is homotaxial succession (Huxley, 1862), a unique and distinct succession of compositional types, in the present case as characterized by the chemical composition of the volcanic glasses in tephra layers at different sites, among multiple stratigraphic sections (Fig. 11). Although not all tephra layers are present at every site where the Ibex Hollow Tuff is found, the stratigraphic sequence of compositional types is not violated when

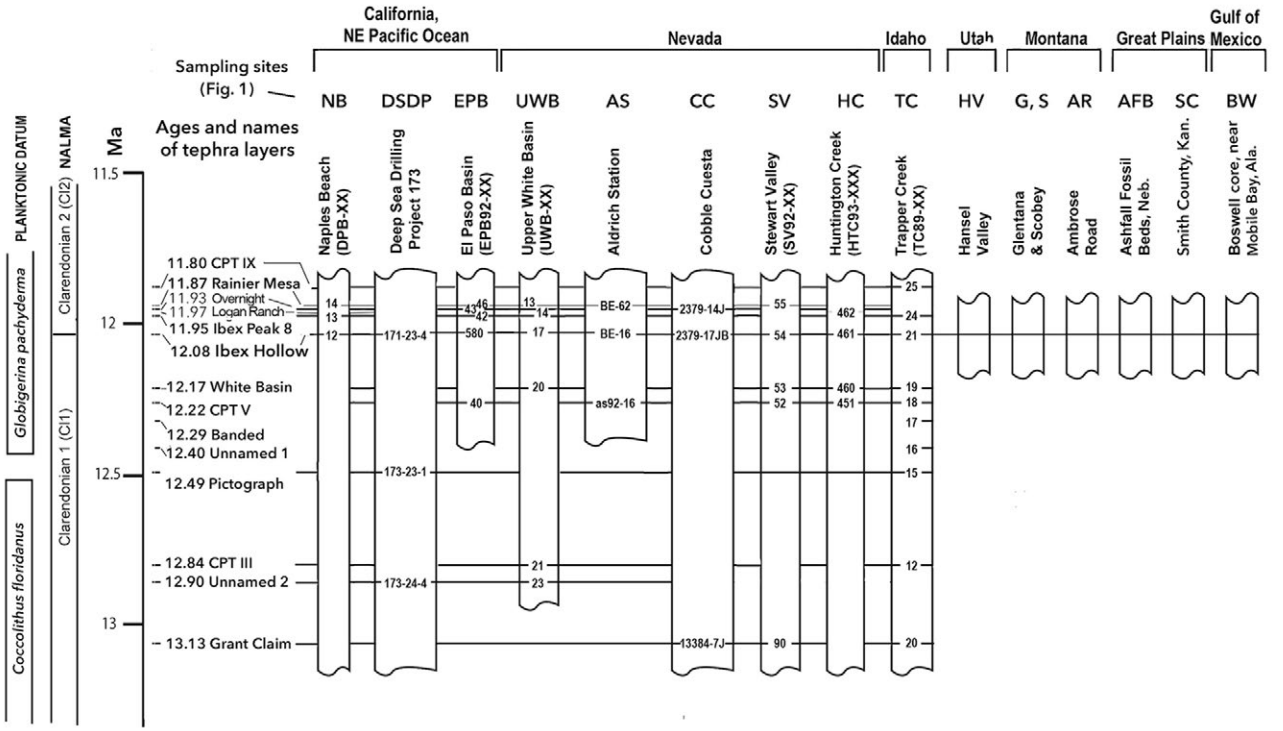

Figure 11. Correlation of the Ibex Hollow Tuff and underlying and overlying tuffs at sites across the conterminous United States and adjoining ocean areas. Planktonic datum and North American Land Mammal Ages (NALMA) are shown for reference. Solid line through column indicates presences of a particular tephra layer at that site, and associated sample number. The prefix for the location of sites (e.g., NB) is given above each stratigraphic column. Specific sample numbers are given within the columns. For example: EPB-40 is a sample within El Paso Basin, California, that correlates with the 12.22 Ma Cougar Point Tuff (CPT) V ash bed, SN 18, at Trapper Creek, Idaho.

multiple tephra layers are present within a stratigraphic section. In the case of stratigraphic tephra sequences, unlike other lithologic sequences (e.g., Bouma sequences), there is no mechanism known that would exactly replicate volcanic compositional sequences at different times. In other words, when found at multiple sites, such sequences must represent the same temporal sequence of eruptive events (Sarna-Wojcicki, 2000). For example, the tephrostratigraphic sequence of White Basin ash, Ibex Hollow Tuff, Ibex Peak 8 ash, and Rainier Mesa Tuff, going from base upward, is a stratigraphically unique sequence and is not replicated at a different time. When this sequence is found at other sites, it must represent the same eruptive units and thus is bounded by these layers within the same interval of time (Sarna-Wojcicki, 2000).

Below, we list the distal sites at which the Ibex Hollow Tuff has been identified, in addition to the proximal Trapper Creek section in Idaho, which we have described and discussed above. Descriptions of the stratigraphy and stratigraphic position of the Ibex Hollow Tuff within the sections, identities of tephra layers above and below the Ibex Hollow Tuff, and any age information available are given in the Appendix (see below). Photographs of several outcrops of the Ibex Hollow Tuff are shown in Figure 12. The locations of these sites are shown in Figures 1 and 13C; a stratigraphic correlation diagram of the localities for these sites is given in Figure 11.

Distal Sites (see Descriptions in Appendix)

- Hansel Valley, northeastern Utah (HV)
- Ambrose Road, western Montana (AR)
- Glentana, northeastern Montana (G)
- Scobey, northeastern Montana (S)

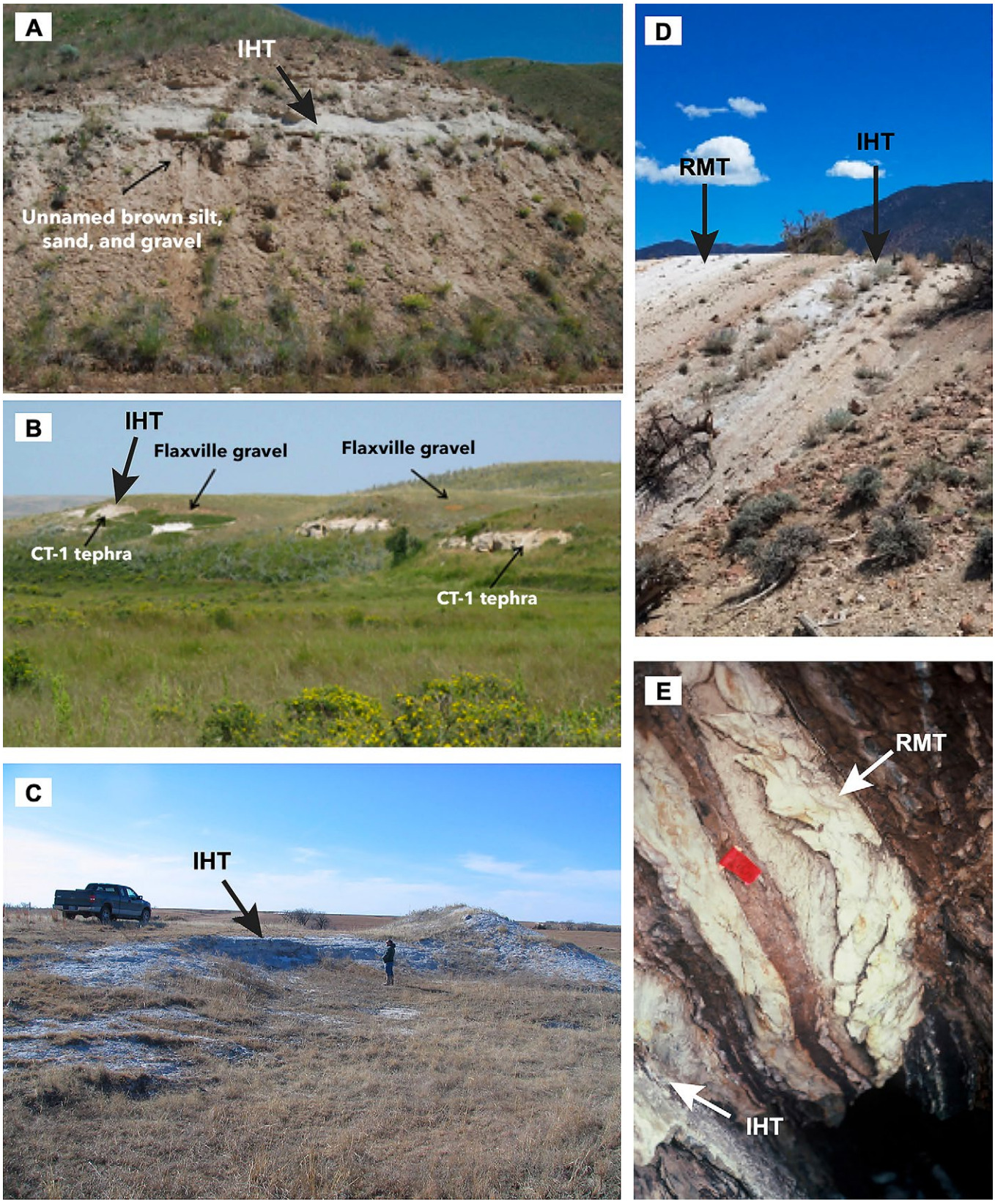

Figure 12. Photographs of the Ibex Hollow Tuff (IHT). (A) Ambrose Road, Montana (site A; photo by John Westgate); tephra layer here is about 1 m thick. (B) Glentana, Montana (site G; photo by John Westgate); tephra layer here is about 2 m thick. (C) South County, Kansas (site SC; photo by Greg Ludvigson, Kansas Geological Survey). (D) Aldrich Station, Nevada (site AS; photo by Jeffrey Knott); tephra layer here is about 1 m thick, and light bluish-gray. (E) Naples Beach, California (NB; photo by Andrei Sarna-Wojcicki); Ibex Hollow Tuff (IHT) here is 2–15 cm thick (thickened and repeated here by shearing), and underlies the Rainier Mesa Tuff (RMT). The RMT is also shown where present (D and E). See Figures 1 and 13C for locations, and see Figure A1 for the Aldrich Station stratigraphic section.

- Ashfall Fossil Beds State Park, northern Nebraska (AFB)
- Smith County, northern Kansas (SC)
- Boswell, southern Alabama/Gulf of Mexico (BW)
- Huntington Creek, northeastern Nevada (HC)
- Stewart Valley, west-central Nevada (SV)
- Cobble Cuesta, west-central Nevada (CC)
- Aldrich Station, western Nevada (AS)
- Upper White Basin, southeastern Nevada (UWB)
- El Paso Basin, southeastern California (EPB)
- Deep-Sea Drilling Program Hole 173, eastern Pacific Ocean (DSDP Hole 173)
- Naples Beach (Dos Pueblos Beach), southwestern California (NB)

The sample from Cobble Cuesta in west-central Nevada (CC in Fig. 1) appears to match well with the Ibex Hollow Tuff (Tables 2 and 3), except for Mn, which is highly enriched, and Rb, which is depleted, relative to concentrations of these elements in other proximal and distal samples of the Ibex Hollow Tuff (Table 3). There may have been some element mobility within the glass shards over time, however, that has selectively leached Rb and enriched Mn. The alkalis Na and K also appear to be mobile for many of the samples analyzed here and in other studies—becoming depleted or enriched with time after deposition—so identification of tephra samples on the basis of the alkalis is often less definitive than with some of the other higher-valence elements, which are more strongly bonded within volcanic glass (Sarna-Wojcicki, 2000). We consider that, in the case of U, Th, Cs, ands Rb, some postdepositional movement may have occurred over time. The amount of movement in and out of the glass probably depends on the natural depositional ("storage") environment of the tephra and how it changed with time. Most likely, repeated hydration and dehydration of sediments above the groundwater table occurred in arid areas such as that of the Cobble Cuesta, Nevada, leading to leaching or enrichment.

DISCUSSION

Age and Correlation of the Ibex Hollow Tuff

The $^{40}Ar/^{39}Ar$ age of the Ibex Hollow Tuff has been revised twice owing to successively newer determinations of decay constants, monitors, and standards. Perkins et al. (1995) determined a laser fusion $^{40}Ar/^{39}Ar$ date of 11.80 ± 0.03 Ma (1σ) on sanidine crystals from the ash-flow tuff of the Ibex Hollow Tuff at Trapper Creek (named at the time by them as the Tuff of Ibex Hollow). They used the 27.92 Ma age of the Taylor Creek Rhyolite and cited Lanphere et al. (1990) for other standards used. Perkins et al. (1998) revised the age of the Ibex Hollow Tuff to 11.93 ± 0.03 Ma, using the 27.84 Ma age of the Fish Creek Tuff, and cited Sampson and Alexander (1987) for other standards and decay constants. Corrected for the latest $^{40}Ar/^{39}Ar$ standards and decay constant (Kuiper et al., 2008; Min et al., 2000), we recalculated the age to 12.08 ± 0.03 Ma, i.e., somewhat older than the previous age given in Perkins et al. (1998), and older yet than that in Perkins et al. (1995). The U-Pb date on zircons from Ashfall Fossil Bed State Park, Nebraska, is 11.86 ± 0.13 Ma (Smith et al., 2018), i.e., not quite the same at 1σ, but overlapping at 2σ with the most recent revision of the $^{40}Ar/^{39}Ar$ age of the Ibex Hollow Tuff. The weighted mean of the four glass fission-track dates from Montana (Table 5) is 11.49 ± 0.44 Ma (1σ). This is also not the same date at 1σ, but it overlaps at 2σ. Thus, all three dating methods overlap at the 2σ error with the most recently corrected $^{40}Ar/^{39}Ar$ age of 12.08 ± 0.03 Ma for the Ibex Hollow Tuff, but not at 1σ. We do not know the cause for these small differences in age between the $^{40}Ar/^{39}Ar$, glass fission-track, and U-Pb methods. The U-Pb and isothermal-plateau fission-track ages match much better, within 1σ, with the original $^{40}Ar/^{39}Ar$ age of 11.80 ± 0.03 Ma (Perkins et al., 1995), than they do with the (twice) recalculated age of 12.08 ± 0.03 Ma we give here.

The consistent stratigraphic sequence provided by the succession of glass chemical types in these tephra layers (homotaxial succession; Huxley, 1862), however, provides an independent confirmation of the correlations in many instances. A 12.08 ± 0.03 Ma age for the Ibex Hollow Tuff is stratigraphically consistent with the $^{40}Ar/^{39}Ar$ date of 11.87 ± 0.03 Ma for the overlying Rainier Mesa Tuff in Upper White Basin (Fig. 11), Naples Beach (Fig. 12E), and Aldrich Station (Figs. 12D and A1). In addition, the 12.08 Ma Ibex Hollow Tuff is underlain by the 12.22 ± 0.04 Ma Cougar Point Tuff V ash bed at Trapper Creek, Huntington Creek, Stewart Valley, Aldrich Station, and El Paso Basin (Fig. 11; see Figs. 1 and 13C for locations).

The age of 12.08 Ma for the Ibex Hollow Tuff agrees with the broader 12.5–10 Ma age range of activity from the Bruneau-Jarbidge volcanic field eruptive source area (Perkins and Nash, 2002). The age of the Ibex Hollow Tuff is also consistent with the broad 13.6–10.3 Ma Clarendonian NALMA stage assigned to mammals found at Ashfall Fossil Beds, Nebraska (Voorhies and Thomasson, 1979), and El Paso Basin (Whistler and Burbank, 1992; Tedford et al., 2004; Whistler et al., 2009). The 12.08 Ma age of the Ibex Hollow Tuff is within the 12.3–10 Ma North Pacific diatom zone *Denticulopsis hustedii-Denticulopsis lauta* subzone c at both DSDP Hole 173, and at Naples Beach, California (Knott et al., 2022).

Sites in the Great Plains and central part of North America (sites AR, G, and S in Montana; sites AFB in Nebraska, SC in Kansas, and BW near Mobile Bay in Alabama; Fig. 1) are identified as individual layers, without overlying or underlying tephra layers, so the supportive evidence of homotaxial succession is not available for these sites (Fig. 11). In most instances, however, other independent evidence is available to support correlation, in addition to the chemical composition of the tephra layers, including independent age control obtained from the U-Pb date at Ash Fall State Park in Nebraska (AFB in Figs. 1 and 13C), and fission-track dates for the sites in Montana (AR, G, and S in Figs. 1 and 13C; Table 5).

Because the three samples in Montana (AR, G, and S) and the one in Nebraska (AFB; Fig. 1), were analyzed by LA-ICP-MS, but not INAA, we cannot relate the two sets of analyses quantitatively because we do not have conversion factors derived from both types of analyses done on the same samples.

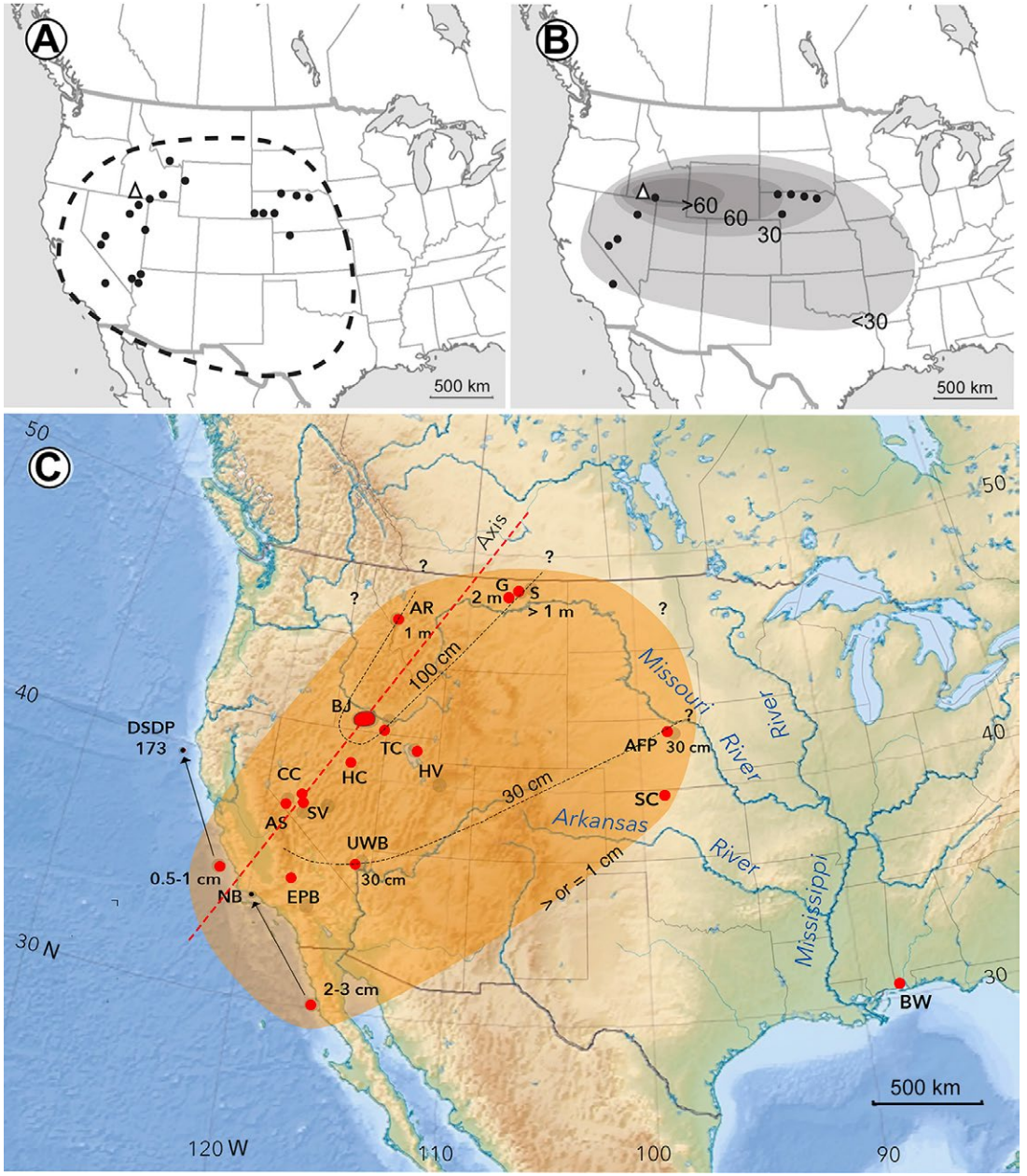

Figure 13. Maps of North America showing different versions of distributions of tephra layers from the Bruneau-Jarbidge volcanic center and distributions of the Ibex Hollow Tuff. (A) Map of the locations (circles) where tephra layers from the 12.7–10.5 Ma Bruneau-Jarbidge volcanic center (triangle) were identified along with inferred distributions of those tuffs (Perkins, 1998; Smith et al., 2018). (B) Map of locations (circles) where the 12.08 Ma Ibex Hollow Tuff was identified along with isopachs of tuff thickness (cm) (from Tucker et al., 2014). (C) Physiographic map of part of North America showing sites where the Ibex Hollow Tuff was identified in this study (red circles) along with a minimum area of fallout shown by the orange overlay (≥1 cm) and additional ~30 cm and 100 cm isopachs of ash-fall tephra. Question marks indicate that ash fall to the north and northeast is unknown but likely to be present. Outcroppings of tuff are visible in geobrowser satellite images beyond the sampled locations to the northeast; consequently, ash fall from the Ibex Hollow Tuff eruption extended in this direction. Abbreviations are the same as in Figure 1. BJ—Bruneau-Jarbidge volcanic source area of the Ibex Hollow Tuff. The dashed red line represents the inferred position of the fallout plume axis. Note the asymmetrical distribution about the axis, which suggests either that considerable windshear existed in the atmosphere, with low-level southeast-directed winds during the eruption of the Ibex Hollow Tuff, or that the initial deposit was symmetrical, with additional fallout to the north and northeast, but these sites have not been found yet, or that tephra from these sites has been removed by erosion—or a combination of both latter possibilities.

We know that they do not plot in exactly the same places in binary diagrams of one element against another, for some combinations of elements, but they do so for other combinations (Figs. 7–10; also see Item S5). The LA-ICP-MS analyses show greater scatter than the INAA analyses for most elements analyzed, possibly because the former analyses were conducted on individual shards, and the latter were conducted on bulk separates of glass shards that average the compositions of perhaps as many as several thousand shards.

Despite small variations in composition, the three sites in Montana and the one in Nebraska (AR, G, S, and AFB; Fig. 1) match most closely to the Ibex Hollow Tuff, rather than to the other chemically similar tephra layers within the Trapper Creek section (Fig. 2; Tables 6A and 6B). In addition to the greater scatter present in the LA-ICP-MS data, some of the differences in composition between the samples at the three sites in Montana and the rest of the samples correlated here with the Ibex Hollow Tuff may be due to variations within the magma chamber existing prior to eruption. The thick lobe deposited in Montana may represent the earlier, most highly differentiated top of the magma chamber (Fig. 13C), similar to what was proposed for the Tsankawi ash by Westgate et al. (2018). Additional work is needed to identify the source unit of the Ibex Hollow Tuff at the source area, the Bruneau-Jarbidge volcanic center, and to look for possible compositional gradients, both vertically and laterally, within the ash-flow and Plinian facies of this unit, work that was beyond the temporal and logistical scope of the present study.

Areal Distribution

Perkins et al. (1998) mapped the ash-fall distribution of all tuffs from the Bruneau-Jarbidge volcanic center (Fig. 13A). Subsequently, Tucker et al. (2014) mapped the distribution of the Ibex Hollow Tuff (Fig. 13B). Both of these maps indicate that ash-fall dispersal was predominantly to the east and southeast, a direction more-or-less consistent with pervasive westerly winds. Our data indicate a more southwest to northeast (~N30°E) dispersal of the Ibex Hollow Tuff (Fig. 13C), also a common wind direction currently observed. Outcrops of fall tephra of the Ibex Hollow Tuff as much as 2 m thick in northern Montana, more than 1000 km from the eruption source, support the interpretation that the fallout lobe axis was oriented northeast from the Bruneau-Jarbidge source area (Fig. 13C). Outcrops of this tephra, visible in geobrowser imagery, are unconfirmed continuations of the 1–2-m-thick Glentana and Scobey outcrops in Montana, suggesting that the Ibex Hollow Tuff eruption deposited tephra farther to the northeast than shown on Figure 13C. We propose that the Ibex Hollow Tuff may have been dispersed much farther north, across the Canadian Shield, Greenland, and other parts of the Northern Hemisphere. This is based on the fact that the areal distribution and thickness of the Ibex Hollow Tuff (as much as 1 and 2 m thick) are much greater at 1000 km distance from the source than, for example, that of the 7.6 ka Mount Mazama ash, which erupted from Crater Lake, Oregon, in the western United States, for the same distance. As much as ~176 km^3 of ash and pumice may have been produced during the Mazama eruption (Buckland et al., 2020), a volume much smaller than the minimum of ~800 km^3 that we estimate for the Ibex Hollow Tuff. Despite this, the Mazama ash has been identified in ice cores in Greenland (Zdanowicz et al., 1999), and thus the Ibex Hollow Tuff should have been transported at least as far as the Mazama ash, and probably much farther and with greater thickness. Moreover, the much smaller eruption of Mount St. Helens in Washington State in 1981, small with respect to both areal distribution and volume (Sarna-Wojcicki et al., 1981), was detected by satellite throughout the Northern Hemisphere and thus had at least a hemispheric impact (Stratospheric Aerosol and Gas Experiment [SAGE] satellite optical depth data; Kent [1983]), despite the fact that measurable ash fall was not detected beyond a distance of ~1000 km from the eruption site. The presence of the Ibex Hollow Tuff in the few cores that extend into the Miocene in the Arctic and North Atlantic Oceans, however, has not been, to our knowledge, researched or observed (e.g., Stein, 2008).

As stated above, we correlate the tephra at Ambrose Road (AR), Glentana (G), and Scobey (S) in Montana and at the Ash Fall State Park (AFB) in Nebraska (Figs. 1, 11, and 13C) with the Ibex Hollow Tuff based on similarity of glass shard compositions, presence of rod-shaped shards, and similar fission-track and U-Pb ages to those of the Ibex Hollow Tuff at its type locality, as well as a thickness distribution that trends to the northwest. Our interpretation is that the somewhat lower TiO_2 concentration in the glass shards at the Glentana and Scobey sites may represent the earliest, most highly differentiated material from the top of the magma chamber, whereas the more proximal tephra is an integrated composite of the entire Plinian eruption column and ash-flow elutriate. This explanation is similar to one proposed by Westgate et al. (2018) for geochemical differences between proximal Tsankawi Pumice in the Jemez Mountains of New Mexico and the distal Duncairn tephra, 1500 km to the north in Saskatchewan, Canada.

Volume of Ash Fall

The widespread distribution of Ibex Hollow Tuff indicates that it may have been produced by one of the larger and more explosive volcanic eruptions from the Snake River Plain–Yellowstone set of volcanic source areas, tephra from which has been deposited over North America. The minimum tephra fall-out area is ~2.7 million km^2 (Figs. 1 and 13C), which encompasses the area within the sites where the tephra layer is identified (inside the 1 cm or >1 cm isopach on Fig. 13C). The massive plume of airborne tephra obviously was not detained at the U.S.–Canadian border but must have continued farther northeast, as indicated by patchy white outcrops visible on geobrowser images extending well into Canada, and by its great thickness (1–2 m) in northwestern Montana, near the border. In comparison, the areal distributions of ash from the ca. 0.63 Ma Lava Creek B and the ca. 2.10 Ma Huckleberry Ridge supereruptions are 3.0 and 3.4 million km^2, respectively (Fig. 1), and the areal distributions for these younger eruptions can perhaps be better estimated due to better preservation and exposure.

There is insufficient thickness data available to provide a realistic estimate of the total volume of ash produced by the Ibex Hollow Tuff eruption. Perkins et al. (1995) compared the Ibex Hollow Tuff at Trapper Creek with the Cougar Point Tuff VIII ignimbrite and suggested these were equivalent in volume. Although the 11.852 ± 0.0007 Ma age of the Cougar Point Tuff VII ignimbrite (Finn et al., 2016; recalculated to ca. 12.00 Ma using Min et al., 2000; Kuiper et al., 2008) is close to the 12.08 ± 0.03 Ma age of the Ibex Hollow Tuff, the glass compositions of the Cougar Point Tuff VII and Ibex Hollow Tuff are different (Perkins et al., 1995; this report). There is no proximal ignimbrite that has been correlated with the Ibex Hollow Tuff, which, in turn, also prevents us from obtaining an accurate total volume for the eruption. A minimum volume for the Ibex Hollow Tuff fall ash was obtained using the currently known minimum areal distribution and thickness information for the 1 or >1, 30, and 100 cm isopachs. Using a simple step-pyramidal stack of the three isopach layers, we obtained a minimum volume of ~813 km^3. Considering the great thickness of the ash at the northeastern margins of the distribution, and the apparent asymmetric distribution of the ash about its northeasterly trending axis of on-the-ground deposits (Fig. 13C), more ash must have been deposited to the north and northeast of the axis. A volume twice the minimum volume we calculated here may be expected for the Plinian phase of the Ibex Hollow Tuff eruption. To that figure must be added the as-yet-unknown volume of the near-source deposits of the Ibex Hollow Tuff at the Bruneau-Jarbidge volcanic field.

Environmental Impacts

The effect of the Ibex Hollow Tuff eruption on the environment and ecology of a large part of North America must have been significant. This is particularly apparent at Ashfall Fossil Beds State Park, Nebraska, where animals ranging from birds to rhinoceroses succumbed to illness that was caused presumably by inhalation of ash particles and filling of watering sites with ash (Fig. 3; Tucker et al., 2014). Conditions such as those at Ashfall Fossil Beds State Park must have been pervasive across North America as documented in NALMA faunal changes at ca. 12 Ma from the Pacific Ocean to the Great Plains (Tedford et al., 2004).

The eruption of the Ibex Hollow Tuff coincides in time with a paleotemperature change from relatively warm to cool temperatures in DSDP core 173 (Barron and Keller, 1983). It is at present unknown whether a short-lived cooling effect, such as that which may have resulted from the Ibex Hollow Tuff eruption, could have been the cause for the longer-term cooling recorded in the biostratigraphy at about this time. Certainly, persistence of dust veils repeatedly entrained into the atmosphere after the eruption from this widespread and thick tephra deposit may have contributed to a regional cooling effect lasting for some time after the eruption, as suggested by the presence of the 50-m-thick, reworked ash interval in the drill hole at site BW near Mobile Bay, Alabama (Figs. 1 and 13C). Frequent incremental cooling following the Miocene climatic optimum, from ca. 14.5 to ca. 9 Ma, with a short warming period between ca. 10.7 and ca. 10 Ma, has been documented by Holbourn et al. (2013). Furthermore, Heusser et al. (2022) documented a cooling period from 13 to 7.6 Ma based on analysis of fossil flora. This period also coincided with, and was punctuated by, numerous large-volume volcanic eruptions from the Snake River Plain–Yellowstone volcanic fields (Perkins and Nash, 2002; Bonnichsen et al., 2008) as well as the Southern Nevada volcanic field (Christiansen et al., 1977; Sawyer et al., 1994). These eruptions could have accentuated the cooling effect, not only by the initial Plinian injection of ash into the atmosphere, but even more so by the persistent dust veils derived from Northern Hemisphere land areas that were repeatedly entrained into the atmosphere by winds, as well as by the higher reflectivity (albedo) of on-the-ground ash cover.

The Ibex Hollow Tuff tephra covered all of the central to southern part of the San Joaquin Valley (the present farming breadbasket of the United States) with an estimated ~1–3 cm of ash and parts of the northwestern Great Plains with 30 cm to as much as 2 m of tephra. It is difficult to predict the effects of such an event if it were to occur today, other than to say that it would be disastrous, certainly within the area of heavy ash fallout, and probably in adjacent areas as well. Based on the long-term record of such supereruptions within the conterminous United States, it is likely that such an eruption occurs roughly once every 0.6 m.y., a reassuringly long period that easily encompasses all of the development of human culture and civilization measured within the last ~45,000 yr or so. A sobering thought, however, is that the most recent of these mega-eruptions, that of the Lava Creek B ash bed, occurred ~0.6 m.y. ago.

Regardless of the possible environmental effects from such an eruption and the duration of these effects on climate, however, the Ibex Hollow Tuff will prove to be a most useful chronostratigraphic marker bed for future studies in both the marine and terrestrial environments. We can now correlate this time horizon across much of the North American continent and adjacent ocean areas, and we can determine, for example, how marine diatoms in the Pacific Ocean responded to the same event that killed off Miocene rhinoceroses and many other kinds of animals within the conterminous United States.

CONCLUSIONS

The Ibex Hollow Tuff is a high-silica rhyolite tephra with a minor mineral component consisting mostly of plagioclase, quartz, sanidine, and Fe-Ti oxides. Its age is precisely determined at 12.08 ± 0.03 Ma by $^{40}Ar/^{39}Ar$ (Perkins et al., 1998; corrected to new standards as given in Min et al., 2000; Kuiper et al., 2008), which is broadly consistent with glass fission-track age determinations, a U/Pb zircon date, and the even broader age brackets from the marine and terrestrial biostratigraphic data, as well as magnetostratigraphy. We can confidently identify the Ibex Hollow Tuff via glass shard composition, but trace elements are required when other supporting data such as homotaxial stratigraphic sequence or other lines of evidence are not available. The relative precisions of INAA and LA-ICP-MS still need to be evaluated and calibrated one to the other on the same set or sets of samples, and solution ICP-MS could be

tested together with these as well to evaluate these methods with regard to comparability and precision. The data set presented here indicates that INAA analyses are more precise than LA-ICP-MS analyses (Figs. 8–10), probably because the former were conducted on a glass separate of many glass shards that average out small-scale heterogeneities, but the latter were conducted as individual spot analyses on small areas within individual glass shards, and thus they are vulnerable to small-scale heterogeneity in the glass or, alternatively, variations in the effectiveness of volatilization of small areas using the laser.

The Ibex Hollow Tuff coincides with large-scale changes in North American fauna and in global temperature. While it is uncertain that the Ibex Hollow Tuff eruption alone contributed to the long-term climate cooling, the Ibex Hollow Tuff is exceptionally valuable as a widespread chronostratigraphic marker bed in late Miocene paleoclimate studies. The evidence of environmental change is very clear from the Konservat-Lagerstätte (abundant, diverse, and well-preserved fossil death assemblage) at Ashfall Fossil Beds State Park in Nebraska (Fig. 3). Because this site is over 1000 km from the Bruneau-Jarbidge volcanic center, and because of the extraordinary thickness and volume of ash deposited on the North American continent as well as over the adjacent ocean areas (as seen, for example, at the Boswell site near the mouth of the Mississippi River near the Gulf of Mexico, at DSDP Site 173, and at the Naples Beach site in southern California), the environmental impact must have encompassed the entire North American continent and adjacent ocean areas, and perhaps the entire Northern Hemisphere as well, as we infer from effects observed for much smaller eruptions such as that of Mount Mazama, ca. 7 ka, and Mount St. Helens in 1980.

The minimum measured spatial distribution of Ibex Hollow Tuff ash is similar, although somewhat smaller, than those of the much younger Huckleberry Ridge and Lava Creek B mega-eruptions. We suspect that the Ibex Hollow Tuff was initially dispersed over a far larger area than is presently known, but erosion or concealment by burial and the lack of additional regional studies have not revealed its full areal distribution.

SUGGESTED FUTURE WORK

Future work that was beyond the logistical and temporal scope of this study could attempt to correlate the Ibex Hollow Tuff at Trapper Creek, Idaho, and its distal sites, with its caldera- proximal ignimbrite and fallout deposits at the Bruneau-Jarbidge volcanic center, to better determine the proximal eruption volume of the Ibex Hollow Tuff and determine its overall chemical and petrological characteristics. A documentation of progressive compositional change during the eruption of the Ibex Hollow Tuff with stratigraphic position at the source volcanic field, Bruneau-Jarbidge volcanic field, such as is suspected here, would provide additional certainty to tephrochronological correlations and would provide information on the course of magma evolution for this eruption. A related study would be to discover new sites where the Ibex Hollow Tuff is present, both macroscopic and cryptotephra, in Upper Miocene sediments to the north and northeast of its presently known distribution in North America, the North Atlantic Ocean, the Arctic Ocean, and perhaps as far as northern Eurasia. A more precise estimate of the volume of this eruption could be obtained by field work to establish the ash-fall thickness of this unit more accurately, both within the area of fallout as determined in this study, as well as possible new sites beyond the area of our study.

Other research that would contribute to the advancement of tephrochronologic studies could be from improved comparisons between the INAA, LA-ICP-MS, solution ICP-MS, and X-ray fluorescence (XRF) analytical methods on samples that were obtained in this study, and additional samples of the Ibex Hollow Tuff from sites that may be found in the future. Improvement in LA-ICP-MS methods will be particularly important in the analysis of individual shards of cryptotephra.

APPENDIX

Stratigraphy of Distal Sites at Which the Ibex Hollow Tuff Has Been Identified

Hansel Valley, Northeastern Utah (HV, Fig. 1)

Thick (2100 m) Neogene tuffaceous fluvial and lacustrine sediments in northwestern Utah include voluminous ash-fall and reworked tephra within the Miocene Salt Lake Formation (Miller and Schneyer, 1994), including sample M89TH-23 from Hansel Valley, Utah (Figs. 1, 11, and 13C). The tephra layer is medium to light gray, moderately indurated, and contains, at most, small amounts of biotite, feldspar, pyroxene, magnetite, and hornblende. Most glass shards in this bed are clear but often have brown rims; less common are brown glass shards. Both the major- and minor-element glass shard compositions of the Hansel Valley sample correlate well with the Ibex Hollow Tuff at its type locality (Figs. 6A, 6B, and 7–10; Tables 2, 3, and 4).

Ambrose Road, Western Montana (AR, Fig. 1)

A 1-m-thick tephra bed is exposed in a road cut along Ambrose Creek in the Bitterroot Valley of Montana (AR, Figs. 1, 11, 12A, and 13C). Bedded and indurated brown silt, sand, and gravel occur above and below the tephra. This tephra (UT2282 and UT2283) is correlated to the Ibex Hollow Tuff based on major-, minor-, and trace-element concentrations (Figs. 6C, 6D, and 7–10; Tables 2, 3, and 4; Item S2). Glass fission-track ages of 11.56 ± 1.01 Ma and 11.51 ± 0.57 Ma (1σ) (Table 5) overlap the 12.08 ± 0.03 Ma $^{40}Ar/^{39}Ar$ age of Ibex Hollow Tuff at 2σ and support correlation to the latter tephra bed. These ages, however, also overlap some of the ages of tephra beds in the Trapper Creek section that overlie the Ibex Hollow Tuff. Analyses of this sample by LA-ICP-MA support correlation to the Ibex Hollow Tuff (Figs. 6C and 6D; Table 4), although scatter in the data from this method is somewhat greater than that by INAA.

Glentana, Northeastern Montana (G, Fig. 1)

At Glentana, near the Canadian border (Figs. 1, 11, 12B, and 13C), a 2-m-thick, massive tephra bed (UT2289) is covered by 50 cm of bedded and rippled tephra, which, in turn, is overlain by brown, quartzite-rich gravel of the Flaxville Formation. Several exposures of this tephra can be seen in Figure 12B. Collier and Thom (1918) first described this section, noting 5 m of tuff, which they designated as "CT-1," below a cemented sandstone and above 6 m of semiconsolidated coarse gravel.

The major-element composition of glass shards in the tephra at Glentana is very similar to the Ibex Hollow Tuff, although the TiO_2 concentration is lower (Table 2). A glass fission-track age of 11.39 ± 1.22 Ma (1σ) (Table 5) overlaps the age of the Ibex Hollow Tuff at 2σ (but also overlaps several of the younger tephra layers in the Trapper Creek section).

The Glentana tephra has high major- and minor-element similarity coefficients with the 10.94 Ma Cougar Point Tuff XIII (0.96) and the 11.80 Ma Cougar Point Tuff XI tuff (0.96). However, the REE composition of the Glentana sample (Figs. 6C and 6D) is more similar to the Ibex Hollow Tuff, with the Cougar Point Tuff XI having a greater Eu anomaly and the Cougar Point Tuff XIII having higher concentrations of REEs (Table 4; Figs. 6C and 6D).

Scobey, Northeastern Montana (G, Fig. 1)

A >7 m thickness of rhyolitic tephra is exposed within the upper part of the Flaxville Formation near Scobey (Figs. 1, 11, and 13C). Massive tephra, >1 m thick, crops out at the base of the section and is covered by 4 m of reworked tephra with prominent horizontal beds and abundant ripple structures. A 2-m-thick bed of silty tephra forms the uppermost unit and is capped by >2 m of quartzite-rich gravel and sand of the Flaxville Formation. This tephra deposit is visible in geobrowser satellite imagery in northeastern Montana and southwestern Saskatchewan, Canada, as white outcrops along creeks and as white mottling of ploughed fields.

As expected, given its proximity to the Glentana site (Fig. 1), the Scobey sample (UT2286) is very similar in the major- and minor-element compositions of its glass shards to the Glentana tephra sample (UT2289; Table 3). Trace-element concentrations measured by LA-ICP-MS (Figs. 6C and 6D; Table 4) support correlation to the Ibex Hollow Tuff, despite the somewhat greater scatter in these data. A glass fission-track age of 11.45 ± 1.37 Ma supports correlation with the Ibex Hollow Tuff. Again, however, the fission-track age overlaps with several of the other Trapper Creek tephra layers.

Ashfall Fossil Beds State Park, Northern Nebraska (AFB, Fig. 1)

A 2.5–3-m-thick bed of fine-grained tephra is present at Ashfall Fossil Beds State Park, Nebraska (Figs. 1, 3, 11, and 13C). The lowermost 30 cm interval is tephra-fall, with the overlying tephra reworked by wind and water into the low-lying parts of the landscape that existed at the time of eruption (Voorhies and Thomasson, 1979). This well-known site has a remarkably well-preserved fossil death assemblage (Konservat-Lagerstätte) of fully articulated skeletons of rhinos, horses, camels, deer, and other animals (Fig. 3; Voorhies and Thomasson, 1979; Voorhies, 1985; Tucker et al., 2014; Smith et al., 2018).

Except for minor leaching of alkali elements, the major-, minor-, and trace-element glass composition of the tephra at Ashfall Fossil Beds (samples Orchard N-1 and UT2425) is essentially the same, within errors of analysis, as the Ibex Hollow Tuff at its type locality (Tables 2, 4, and 6). Smith et al. (2018) obtained a U-Pb date from zircons of 11.86 ± 0.13 Ma at the base of the Ashfall Fossil Beds deposit, which is statistically identical to the original 11.80 ± 0.03 Ma $^{40}Ar/^{39}Ar$ age of the Ibex Hollow Tuff, and which overlaps the corrected 12.08 ± 0.03 Ma date at 2σ. This age also overlaps that of two tephra layers that overlie the Ibex Hollow Tuff at Trapper Creek: Cougar Point Tuff IX and Ibex Peak 8 (Fig. 2). Based on the glass shard compositions (Figs. 6C, 6D, and 7–10), their morphology (Fig. 4), and the U-Pb date, we correlate the tephra layer at this deposit with the Ibex Hollow Tuff at Trapper Creek.

Smith County, Northern Kansas (SC, Fig. 1)

An ash bed (sample GL-SCS-KMI; Table 2) interbedded with sandstones and siltstones of the Ogallala Formation of northern Kansas (Greg A. Ludvigson, 2021, written commun.; Ludvigson et al., 2009; see also Figs. 1, 11, 12C, and 13C) is correlated with the Ibex Hollow Tuff based on its major- and minor-element glass shard compositions (Fig. 7; Table 2). The Ogallala Formation of Kansas is known to include fossils ranging from Barstovian to Hemphillian, which is consistent with correlation to the Ibex Hollow Tuff (Ludvigson et al., 2009), although fossils have not been found at this particular locality. Only EMA analyses have been run on this sample. This ash has the rod-shaped shards typical of the Ibex Hollow Tuff (Fig. 4C).

Boswell Drill Site, Gulf of Mexico (BW, Fig. 1)

Samples of disseminated to abundant glass shards were obtained from drill cuttings taken at multiple depths in the First Energy Corporation well (W.B. Boswell 8–13 No. 1) in coastal Alabama, near the Gulf of Mexico (Figs. 1, 11, and 13C). Sediments present in this well are estuarine sands of the Pensacola Formation, probably the Escambia Sand Member of Miocene age, as based on microfossil biostratigraphy (Smith, 1991).

The samples from the Boswell site are: BOSWELL 1840, BOSWELL 1870, BOSEWELL 1810–1930 ALL, and BOSWELL SELECT. The sample numbers represent depth in the well, in feet below the surface (Smith, 1991). Volcanic glass shards are present between 1810 and 1990 ft (551–607 m), but they are most abundant between 1840 and 1870 ft (561–570 m). The shards are dominantly large, thin, slightly curved, bubble-wall and bubble-wall junction types with rare rod-shaped shards, which are (both) shown in Figures 4A and 4B.

Glass shard concentrations in the well suggest that there are no sharp contacts below and above the ashy interval, and that the shard distribution with depth is most consistent with fluvial reworking and deposition into a marine basin of a large volume of tephra by the ancestral Missouri-Mississippi River system, over a considerable—but indeterminate—time period (Figs. 1, 11, and 13C), rather than direct ash fall into the Gulf of Mexico. Similar glass shard distributions have been observed in cuttings from an oil industry drill core in subbottom sediments of the northwestern Gulf of Mexico, where a 16 m interval of ashy sediments was identified as the Lava Creek B ash bed (ca. 0.63 Ma; Ostergren, 1991).

The glass shard compositions from the Boswell site are all very similar regardless of their depth in the well (Table 2; Item S3), indicating that the shards were derived from one eruption. Major-, minor-, and trace-element similarity coefficients comparing the Boswell samples to the Ibex Hollow Tuff type locality are high (Figs. 6A, 6B, and 7–10; Tables 2 and 3). We correlate the tephra in the Boswell site with the Ibex Hollow Tuff on the basis of glass shard composition (major, minor, and trace elements) and glass shard morphology (Figs. 1, 12, and 13C).

Huntington Creek, Northeastern Nevada (HC, Fig. 1)

Perkins et al. (1998) described the tephra beds at Huntington Creek (Figs. 1, 11, and 13C) as part of the Humboldt Formation (restricted) of Smith and Ketner (1976). According to the latter authors, the Humboldt Formation consists of fluviatile and lacustrine sediments with vertebrate fauna indicating a late Miocene age for the Humboldt Formation. Perkins et al. (1998), however, did not publish the geochemical data from their sample htc93–461, which they correlated with the Ibex Hollow Tuff.

We present here the EMA data from sample htc93–461 of Perkins et al. (1998), which show a high similarity to the Ibex Hollow Tuff (Barbara P. Nash, University of Utah, 2020, data from written commun.; see also Fig. 7; Table 2). According to Perkins et al. (1998), at Huntington Creek, the ca. 11.97 ± 0.10 Ma Logan Ranch ash bed (sample htc93–462) overlies the Ibex Hollow Tuff, and the ca. 12.38 Ma White Basin ash bed and Cougar Point Tuff V ash underlie the Ibex Hollow Tuff (Fig. 11). Based on paleontology, glass shard composition, and stratigraphic sequence, we concur with the correlation made by Perkins et al. (1998), correlating sample htc93–461 with the Ibex Hollow Tuff.

Stewart Valley, West-Central Nevada (SV, Fig. 1)

Perkins et al. (1998) collected tephra from an 800-m-thick section within the Stewart Valley Group (Figs. 1, 11, and 13C). The section includes fluvial, lacustrine, and tuffaceous sediments with abundant fossils of invertebrate and vertebrate fauna, insects, and flora of Miocene age (Schorn et al., 1989). At this locality, Perkins et al. (1998) correlated tephra beds ranging from ca. 16 to 11.7 Ma, including the Ibex Hollow Tuff. The geochemical data, however, were not published.

Here, we present the glass shard composition from Stewart Valley (sample sv92–54) that Perkins et al. (1998) correlated with the Ibex Hollow Tuff (Barbara P. Nash, University of Utah, 2020, data from written commun.; see also Fig. 7; Table 2; Item S4). The major- and minor-element compositions of the glass shards from the Stewart Valley sample are very similar to the Ibex Hollow Tuff type locality (Table 2). Perkins et al. (1998) showed that the Ibex Hollow Tuff is overlain by the Rainier Mesa Tuff (11.87 ± 0.05 Ma) and underlain by the White Basin ash bed and the Cougar Point Tuff V ash bed (Fig. 11). Based on the biostratigraphy, glass shard compositions (Fig. 7; Table 2), and relative stratigraphic positions of the tephra layers (Fig. 11), we again concur with Perkins et al. (1998) regarding correlation of the Stewart Valley sample sv92–54 with the Ibex Hollow Tuff.

Cobble Cuesta, West-Central Nevada (CC, Fig. 1)

The Cobble Cuesta sample (2379–17JB) is from Gabbs Valley in west-central Nevada (Figs. 1, 11, and 13C). The sample is from unnamed Upper Miocene sedimentary rocks of Cobble Cuesta, consisting of 850 m within an anticlinal section consisting of fluvial, deltaic, and lacustrine strata, including at least 15 discrete tephra layers and tuffaceous intervals (Stewart et al., 1999). Sample 2379–17JB corresponds to "tephra layer C-3" of Stewart et al. (1999), which is ~30 m above the base of their measured section 1.

This sample correlates well—for the most part—with the Ibex Hollow Tuff on the basis of major-, minor-, and trace-element compositions of the glass shards (Figs. 6A, 6B, and 7–10; Tables 2 and 3; Item S3). The Mn concentration, however, is significantly higher and the Rb concentration is significantly lower for the Cobble Cuesta sample compared to the Ibex Hollow Tuff type locality and the Ibex Hollow Tuff at other locations. The high Mn and lower Rb may be an effect of postdepositional chemical exchange in the glass. In the case of Mn, the higher concentration may be a result of postdepositional solution and precipitation of Mn from the soil or surrounding sediments into vesicles of the glass shards. Concentrations of other elements analyzed are

indistinguishable from the Ibex Hollow Tuff type locality. In the case of Rb, there may have been progressive leaching of Rb and replacement by water as a consequence of repeated wetting and drying of the sediment in situ.

Their ash B is located ~75 m stratigraphically above tephra layer C-3 (Ibex Hollow Tuff) in section 1 of Stewart et al. (1999), and it correlates with the 11.93 ± 0.10 Ma Overnight ash bed of Perkins et al. (1998) (see Table A1). Ash A of Stewart et al. (1999) is ~220 m below ash B in their section 4. Ash A (sample 13384–7J) correlates with the 12.98 ± 0.04 Ma Grant Claim ash bed (sample tc89–20) of Perkins et al. (1995) at Trapper Creek, which is stratigraphically below the Ibex Hollow Tuff (Fig. 11; Table A1). Although ash C-3 (Ibex Hollow Tuff) is not present in section 4, Stewart et al. (1999) projected ash A as stratigraphically lower than tephra layer C-3 (Ibex Hollow Tuff). Thus, based on the geochemical composition of the volcanic glass shards and stratigraphic sequence of the tephra layers (Fig. 11; Table A1), we correlate ash C-3 at Cobble Cuesta with the Ibex Hollow Tuff.

Aldrich Station, Western Nevada (AS, Fig. 1)

At Aldrich Station, western Nevada (Figs. 1, 11, 12D, and 13C), early to middle Miocene andesite and rhyolite lava flows unconformably underlie late Miocene andesites, rhyolites, and sedimentary deposits, including a number of tephra layers (Fig. 12D; Eastwood, 1969). Eastwood

TABLE A1. RESULTS OF ELECTRON-MICROPROBE ANALYSIS OF VOLCANIC GLASS SHARDS FROM TEPHRA LAYERS FOUND AT THE COBBLE CUESTA, UPPER WHITE BASIN, AND DEEP SEA DRILLING SITE 173 LOCATIONS IN ADDITION TO THE IBEX HOLLOW TUFF

Field/lab number	Locality*	Concentration of oxides (wt%)									SC†
		SiO_2	Al_2O_3	Fe_2O_3	MgO	MnO	CaO	TiO_2	Na_2O	K_2O	
Rainier Mesa Tuff (11.87 ± 0.03 Ma)											
UWB-13	UWB	77.20	12.89	0.52	0.03	0.07	0.36	0.09	3.89	4.94	1.0000
DPB-14	NB	78.22	12.97	0.61	0.05	0.06	0.38	0.09	3.13	4.49	0.9561
Overnight ash bed (11.95–11.87 Ma)											
UWB-14	UWB	77.13	13.02	0.54	0.04	0.08	0.33	0.08	3.92	4.87	1.0000
2379-14J	CC	77.21	12.60	0.53	0.06	0.06	0.36	0.09	3.33	5.77	
wb93-320	UWB	77.61	12.55	0.56	0.04	0.08	0.34	0.07	2.95	5.80	0.9535
Unnamed tuff (12.23–12.08 Ma)											
UWB-19	UWB	77.19	12.13	1.71	0.04	0.03	0.57	0.19	3.66	4.48	
White Basin tuff (12.227 ± 0.03 Ma)											
UWB-20	UWB	77.19	12.13	1.71	0.04	0.03	0.57	0.19	3.66	4.48	1.0000
TC89-19b	TC	76.72	12.00	1.64	0.09	0.02	0.55	0.25	1.89	6.84	0.9802
Pictograph tuff (ca. 12.49 Ma)											
DSDP 173-23-1 (148–150 cm)	DSDP	76.42	12.25	1.88	0.06	0.05	0.68	0.21	3.13	5.32	1.0000
TC89-15	TC	76.8	12.03	1.71	0.08	0.02	0.58	0.23	1.48	7.07	0.9305
DSDP 173-23-1 (145–147 cm)	DSDP	76.66	12.18	1.87	0.05	0.04	0.66	0.21	3.10	5.22	0.9813
DSDP 173-23-1 (148–150 cm) T85	DSDP	76.31	12.20	1.96	0.07	0.03	0.64	0.21	3.16	5.41	0.9790
Cougar Point Tuff III (12.838 ± 0.03 Ma)											
UWB-21	UWB	77.19	12.13	1.71	0.04	0.03	0.57	0.19	3.66	4.48	1.0000
TC89-12	TC	76.23	12.2	1.55	0.06	0.03	0.54	0.18	1.93	7.28	0.9566
Unnamed ash bed (ca. 12.8 Ma)											
UWB-23	UWB	76.62	12.38	1.57	0.01	0.04	0.44	0.07	3.64	5.23	1.0000
DSDP 173-24-4 (60–62 cm)	DSDP	76.67	12.41	1.58	0.00	0.04	0.46	0.08	3.64	5.11	0.9644
Grant Claim ash bed (12.96 ± 0.04 Ma)											
13384-7J	CC	77.39	11.75	1.73	0.05	0.03	0.58	0.18	2.26	6.01	1.0000
TC89-20a	TC	76.36	11.95	1.77	0.04	0.03	0.56	0.18	1.69	7.40	0.9826

Notes: See Figures 1, 2, 11, and 13C for localities of samples.

*Sample locations are from Figure 1: Cobble Cuesta (CC), Deep Sea Drilling Project Site 173 (DSDP), Naples Beach (NB), Trapper Creek (TC), Upper White River Basin (UWB).

†Similarity coefficient (SC) of Borchardt et al. (1972) was used to quantitatively compare each tephra sample to its presumed correlative at other sites. 1.0000 represents a perfect match. All similarity coefficients were calculated using concentrations of Si, Al, Fe, Ca, and Ti oxides.

(1969) identified 15 Upper Miocene tephra layers within three superposed formations (Figs. 11, 12D, and A1). Perkins et al. (1998) analyzed splits of Eastwood's samples provided by the USGS Tephrochronology Project along with additional samples they collected at Aldrich Station. Perkins et al. (1998) identified 14 different tephra layers, five of which Eastwood (1969) did not previously sample. Knott et al. (2022) presented major-, minor, and trace-element data for tephra layers present in the marine Monterey Formation, which correlate to tephra layers of Eastwood (1969) at Aldrich Station, as well as to many other sites in the western and central United States.

At Aldrich Station, samples BE-16 and BE-16A of Eastwood (1969) (Fig. 12D), two samples collected laterally within the same tephra bed, correlate well with the Ibex Hollow Tuff. The major-, minor-, and trace-element compositions of the glass shards from BE-16 and BE-16A are essentially the same, within the errors of analysis, as the Ibex Hollow Tuff type locality samples (Figs. 6A, 6B, and 7–10; Tables 2 and 3). The presence of the underlying 12.22 Ma Cougar Point Tuff V ash bed (as92–16 of Perkins et al., 1998) and overlying 11.87 Ma Rainier Mesa Tuff (BE-62 of Knott et al., 2022) confirms the correlation of BE-16 and BE-16a to the Ibex Hollow Tuff (Figs. 11 and A1).

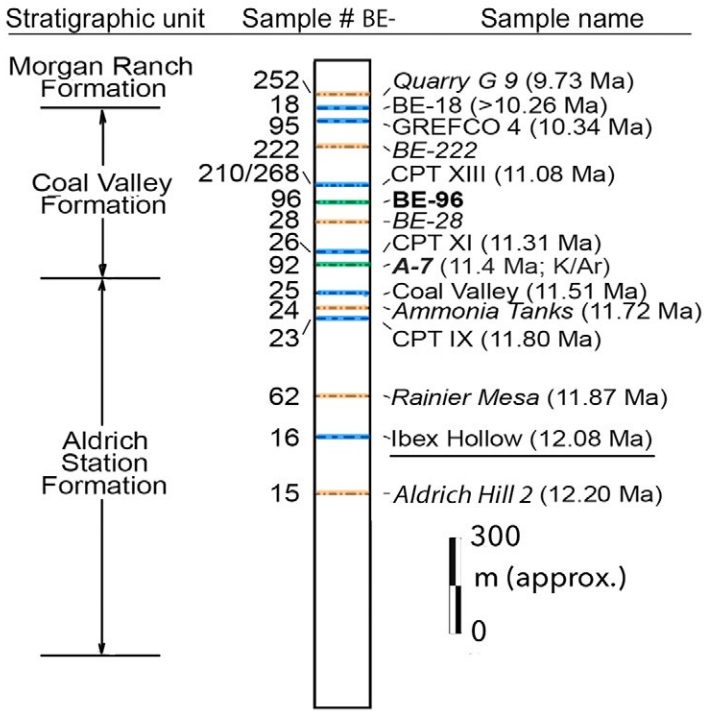

Figure A1. Composite tephrostratigraphy at Aldrich Station, Nevada (see Figs. 1 and 13C for location), showing the stratigraphic position of the Ibex Hollow Tuff (underlined) relative to other tephra layers in this section. Blue–silver-gray to bluish-gray—tephra layers erupted from Snake River Plain volcanic sources, with names shown in regular type; orange—chalky white pumiceous shards, derived mostly from the Southern Nevada volcanic field, with names shown in italic type; green—chalky, light-brown pumiceous shards, with names shown in bold type, erupted from the Mono Basin area east of the central Sierra Nevada. CPT—Cougar Point Tuff. Figure is modified from Knott et al. (2022) and previously from Eastwood (1969).

Upper White Basin, Southeastern Nevada (UWB, Fig. 1)

James Yount and Charles E. Meyer collected samples from 23 tephra layers from the red sandstone member of the Horse Spring Formation (Bohannon, 1984) in the Upper White River Basin (Figs. 1, 11, and 13C; C.E. Meyer and J. Yount, U.S. Geological Survey, written commun., 1991). Samples were numbered from top (low numbers; younger beds) to bottom (high numbers; older beds). Sample UWB-17 is an ~30-cm-thick, light-gray, pure, glassy, ash-fall tephra layer ~94 m below the top and ~156 m above the base of the red sandstone member.

Major-, minor-, and trace-element compositions of the glass shards indicate that UWB-17 correlates to the Ibex Hollow Tuff at its type locality (Figs. 6A, 6B, and 7–10; Tables 2 and 3). This correlation is supported by correlation of other tephra layers present in the section (Fig. 11; Table A1): Units overlying sample UWB-17 (correlative with Ibex Hollow Tuff) are the ca. 11.93 ± 0.10 Ma Overnight ash bed of Perkins et al. (1998; sample UWB-14) and the 11.87 ± 0.05 Ma Rainier Mesa Tuff (sample UWB-13; Fig. 11); units underlying UWB-17 are the unnamed tuff (UWB-19), the 12.17 ± 0.10 Ma White Basin tuff, and the ca. 12.84 ± 0.03 Ma Cougar Point Tuff III. Underlying the Cougar Point Tuff III, there is another unnamed tuff (sample UWB-23), which also underlies the Ibex Hollow Tuff in Deep Sea Drilling Project (DSDP) core 173 (sample DSDP-173–21–4; Fig. 11; Table A1).

Correlation of these tephra layers is consistent with the zircon fission-track and $^{40}Ar/^{39}Ar$ dates of between 12.8 Ma and 11 Ma for the red sandstone member of Bohannon (1984). Perkins et al. (1998) also sampled tephra ranging in age from 15.5 to 11.5 Ma from the red sandstone member; however, the relations of their sample sites relative to those collected by Yount and Meyer are unclear because the two collection areas were in different parts of the basin. Perkins et al. (1998) did not find the Ibex Hollow Tuff in the White River Basin section. They did, however, identify the ca. 11.95 ± 0.04 Ma Ibex Peak 8 and the ca. 12.22 ± 0.10 Ma Aldrich Hill 1 ash bed in addition to the tephra layers in Table A1 and Figures 11 and A1. Perkins and Nash (2002) indicated the presence of the Ibex Hollow Tuff in the Upper White Basin section on their correlation chart. No data for the Ibex Hollow Tuff in the Upper White Basin, however, were given in Perkins et al. (1998) or Perkins and Nash (2002).

El Paso Basin, California, Southeastern California (EPB, Fig. 1)

Perkins et al. (1998) correlated sample epb94–580 at the contact between Members 1 and 2 of the Dove Springs Formation (Whistler and Burbank, 1992; Whistler et al., 2009) in the El Paso Basin (Figs. 1, 11, and 13C) with the Ibex Hollow Tuff. Here, we present the EMA data for sample epb94–580, which has a high similarity coefficient with the Ibex Hollow Tuff at the Trapper Creek type locality (Table 2; Barbara Nash, University of Utah, 2020, EMA data from written commun.).

The geochemical correlation to the Ibex Hollow Tuff (Fig. 7; Table 2) is supported by the presence here of the overlying ca. 11.95 Ma Ibex Peak 8 and the underlying 12.22 Ma Cougar Point Tuff V ash (Fig. 11; Perkins et al., 1998; Whistler et al., 2009). In addition to the tephrostratigraphic relations, correlation to the Ibex Hollow Tuff is consistent with both paleomagnetic and paleontologic data. Whistler et al. (2009) showed the Ibex Hollow Tuff (their Ash 2) as being within a reverse polarity interval, and within the 12.049–11.657 Ma chron C5r.3r of Ogg (2012). Within the Dove Canyon Formation, the Ibex Hollow Tuff separates the Clarendonian subintervals Cl1 from Cl2 in the NALMA stages. Tedford et al. (2004) assigned an age of 12 Ma to the Cl1/Cl2 subinterval contact, in close agreement with the 12.08 ± 0.03 Ma $^{40}Ar/^{39}Ar$ age of the Ibex Hollow Tuff.

Deep Sea Drilling Program (DSDP) Hole 173, Eastern Pacific Ocean (DSDP 173, Fig. 1)

Samples of tephra were obtained from the DSDP core repository at La Jolla, California, and analyzed by both EMA (Table 2) and INAA (Table 3). The DSDP Hole 173 site (39.12861°N, 125.4500°W; Figs. 1, 11, and 13C) is located on the continental slope above the Delgada submarine fan at a water depth of 2927 m (von Huene et al., 1973). DSDP Site 173 was translated ~270 km northwest by motion of the Pacific plate relative to the North American plate since the late Miocene, according to data in McQuarrie and Wernicke (2005). We show the inferred location of this site at ca. 12 Ma and the modern coring site for DSDP Hole 173 in our figures (Figs. 1, 11, and 13C). The much younger ca. 1.45 Ma Rio Dell ash bed has been previously identified at a shallower depth in this core (Sarna-Wojcicki et al., 1987).

Two samples of volcanic ash were obtained from a depth of 186.27 m below the ocean water–sediment interface (samples DSDP 173–21–4 [27–28 cm] and DSDP 173–21–4 [32–35 cm]). The core number is 21, and the core section is 4. The distance in centimeters refers to a point in the core section. The distance shown by the sample numbers (e.g., 27–28 cm) represents the sampling interval, not bed thickness. The ash was likely deformed and smeared out over this interval

of core during the drilling operation. Von Huene et al. (1973) described the ashes as 0.5 cm and 1 cm thick, respectively, in a pale-olive, nannofossil-rich diatomite.

Both samples of tephra layer DSDP 173–21–4 have the same composition and correlate very well with the Ibex Hollow Tuff based on EMA and INAA analyses (Figs. 6A, 6B, and 7–10; Tables 2 and 3). Biostratigraphic analysis indicates that the sediments are within the 12.3–10 Ma *Denticulopsis hustedtii–Denticulopsis lauta* subzone c (Barron and Keller, 1983).

Two other samples (DSDP 123–23–1 [145–148 cm] and DSDP 123–23–1 [148–150 cm]) were collected from a 1.5-cm-thick, bioturbated ash at 206.45 m stratigraphically below the Ibex Hollow Tuff in core DSDP 173–23–1 (Fig. 11). Diatom biostratigraphy places these samples in North Pacific diatom zone *D. hustedtii–D. lauta* subzone b, with an estimated age of 12.6 Ma (Barron and Keller, 1983). The glass shard composition of these samples is very similar, indicating both samples are from the same ash and were deformed and smeared out during drilling. The glass shard composition is similar to several tephra beds of the Snake River Plain–Yellowstone hotspot trend; however, using the diatom data, the DSP-173–23–1 ash correlates best with the 12.49 ± 0.10 Ma Pictograph tuff of Perkins et al. (1998) (see also Fig. 11; Table A1).

Another ash bed in core 173–24–4, described only as "thin" (von Huene et al., 1973), below the ash beds mentioned above, was recovered from 219.6 m (sample DSDP 173–24–4) and was also analyzed by us (Fig. 11). This ash lies near the base of the *D. hustedtii–D. lauta* zone, with an estimated age of 12.87 Ma (Barron and Keller, 1983). The glass shard composition of this ash is very similar to the unnamed ash bed in the Upper White Basin (sample UWB-23; Fig. 11; Table A1). At Upper White Basin, sample UWB-23 underlies the 12.84 Ma Cougar Point Tuff III ash bed (Fig. 11), which is consistent with the 12.87 Ma diatom-based age determined for the depth of DSDP 173–24–4. The low Fe_2O_3, CaO, and TiO_2 concentrations of this ash bed (samples DSDP 173–24–4 and UWB-23) are consistent with tephra erupted from the Southern Nevada volcanic field, rather than that of the Snake River Plain–Yellowstone hotspot trend of volcanic sources.

Naples Beach (Dos Pueblos Beach), Southwestern California (NB, Fig. 1)

Sample DPB-12 is a tephra layer found within the middle part of a coastal exposure of the marine Monterey Formation at Naples Beach (Dos Pueblos Beach), ~36 km west of Santa Barbara, California, along a southwest-facing part of the California coast (Figs. 1, 11, and 13C). As part of the Transverse Ranges west of the San Andreas fault, and thus within the Pacific plate, the Naples Beach location was translated 270 km northwest and rotated 45° since the Miocene, according to data of McQuarrie and Wernicke (2005) (see also Figs. 1, 12E, and 13C). The Monterey Formation here has been studied by many geologists and paleontologists over the years (e.g., Barron, 1976; Isaacs, 1981; Follmi et al., 2005; Hornafius, 1994; Knott et al., 2022). The Monterey Formation consists mostly of soft, friable, diatomaceous shale interspersed with sparse indurated phosphatic limestone beds and thin tephra beds. The beds here strike ~N80°W and dip ~60° to the south. Twenty-one tephra samples (DPB-4 to DPB-25) were collected northwest to southeast (up section) along the shoreline from Dos Pueblos Creek over an ~0.5 km distance.

Sample DPB-12 is ~41 m up section from the mouth of Dos Pueblos Creek. This tephra bed (DPB-12 bed) is 15 cm thick, but it thins laterally over a few decimeters to as little as 2–3 cm (Fig. 12E). The thickening of the bed does not appear to be depositional, but it may be a result of shearing along bedding planes or liquefaction. The major-, minor-, and trace-element composition of the glass shards from sample DPB-12 matches well with the Ibex Hollow Tuff (Figs. 6A, 6B, and 7–10; Tables 2 and 3). Correlation to the Ibex Hollow Tuff is supported by correlation of the overlying 11.95 ± 0.04 Ma Ibex Peak 8 ash (sample DPB-13) and the stratigraphically higher 11.87 ± 0.05 Ma Rainier Mesa Tuff (DPB-14; Fig. 13E; Table A1), as well as correlation of the 12.16 ± 0.10 Ma Aldrich Hill 2 ash below the Ibex Hollow Tuff (Figs. 11 and 12B). In addition, sample DPB-12 is within the 12.3–10 Ma *D. hustedtii–D. lauta* subzone c (Knott et al., 2022).

ACKNOWLEDGMENTS

We dedicate this article to the group of people that first established a significant part of this excellent, well-dated, and well-documented tephrochronological and tephrostratigraphic spatial-temporal framework for the Upper Miocene section of the western United States, which was published in three landmark journal articles from 1995 to 2002: Michael E. Perkins, Francis H. Brown (deceased), Barbara P. Nash, Robert J. Fleck, William McIntosh, and S.K. Williams (Perkins et al., 1995, 1998; Perkins and Nash, 2002).

We thank William Eastwood and the University of California–Berkeley for splits of samples from the Aldrich Station section, west-central Nevada; the former Ocean Drilling Program sample repository in La Jolla, California, for marine core samples; and Mike Perkins for help, advice, and for sharing many samples and data from the Trapper Creek and Ibex Hollow sections. We thank Barbara P. Nash for providing unpublished EMA data for the Ibex Hollow Tuff from three sites in the western United States. We thank the late Frank H. Brown for information and advice on sample sites, advice on analytical and evaluation methods, and his continuous encouragement in furthering research in tephrochronology. We are grateful to the University of Nebraska State Museum for permission to use their photograph of the fossil rhinoceroses at Ashfall Fossil Beds State Park. We thank Lewis Caulk, Paul Russell, Jose Rivera, Kate Lormand, John Diaz, Janet Slate, Robert Fehr, Andrew Brownstone, Drew Ericson, Regina Broussard, Mike Haemer, and James P. Walker for their laboratory work in processing and separating volcanic glass of tephra samples, and for analysis of these samples by EMA and XRF over a period of about five decades.

Work for this study and support were provided by the U.S. Geological Survey (USGS) and the Tephrochronology Laboratory and Project in Menlo Park, California, specifically from the National Mapping Program, the Volcanic Hazards Program, the Earthquake Hazards Program, and other specific projects, both within the USGS and from other organizations, during the period 1976–2005. Funding to J.A. Westgate was provided by the Natural Sciences and Engineering Research Council of Canada and the University of Toronto. Additional funding to J.R. Knott was provided by the National Science Foundation (EAR-1516593) and California State University–Fullerton. We thank Kathryn Watts, USGS, for her constructive review of the manuscript; we thank three anonymous reviewers, who helped to improve the manuscript; we thank Joel Saylor, assistant editor of *Geosphere*, for his review and suggestions, which improved the manuscript; and we thank Managing Editor Gina Harlow and Editorial Assistant Jordan Osborne for help in the final editing and publication process. Any use of trade, firm, or product names is for descriptive purposes only and does not imply endorsement by the U.S. Government.

REFERENCES CITED

Bacon, C.R., 1983, Eruptive history of Mount Mazama and Crater Lake, Cascade Range, USA: Journal of Volcanology and Geothermal Research, v. 18, p. 57–115, https://doi.org/10.1016/0377-0273(83)90004-5.

Bacon, C.R., and Druitt, T.H., 1988, Compositional evolution of the zoned calcalkaline magma chamber of Mount Mazama, Crater Lake, Oregon: Contributions to Mineralogy and Petrology, v. 98, p. 224–256, https://doi.org/10.1007/BF00402114.

Barron, J.A., 1976, Marine Diatom and Silicoflagellate Biostratigraphy and Paleoecology [Ph.D. dissertation]: Los Angeles, California, University of California–Los Angeles, 289 p.

Barron, J.A., and Isaacs, C.M., 2001, Updated chronostratigraphic framework for the California Miocene, *in* Isaacs, C.M., and Rullkotter, J., eds., The Monterey Formation: From Rocks to Molecules: New York, Columbia University Press, p. 393–395.

Barron, J.A., and Keller, G., 1983, Paleotemperature oscillations in the middle and late Miocene of the northeastern Pacific: Micropaleontology, v. 29, no. 2, p. 150–181, https://doi.org/10.2307/1485565.

Bohannon, R.G., 1984, Nonmarine Sedimentary Rocks of Tertiary Age in the Lake Mead Region, Southwestern Nevada and Northwestern Arizona: U.S. Geological Survey Professional Paper 1259, 72 p., https://doi.org/10.3133/pp1259.

Bonnichsen, B., 1982, Chemical Composition of the Cougar Point Tuff and Rhyolite Lava Flows from the Bruneau-Jarbidge Eruptive Center, Owyhee County, Idaho: Idaho Bureau of Mines and Geology Technical Report 82–1, 26 p.

Bonnichsen, B., and Citron, G.P., 1982, The Cougar Point Tuff, southwestern Idaho, *in* Bonnichsen, B., and Breckenridge, R.M., eds., Cenozoic Geology of Idaho: Idaho Bureau of Mines and Geology Bulletin 26, p. 255–281.

Bonnichsen, B., Leeman, W.P., Honjo, N., McIntosh, W.C., and Godchaux, M.M., 2008, Miocene silicic volcanism in southwest Idaho: Geochronology, geochemistry, and evolution of the central Snake River Plain: Bulletin of Volcanology, v. 70, p. 315–342, https://doi.org/10.1007/s00445-007-0141-6.

Borchardt, G.A., Aruscavage, P.J., and Millard, H.T., 1972, Correlation of the Bishop Ash Pleistocene marker bed, using instrumental neutron activation analysis: Journal of Sedimentary Petrology, v. 42, no. 2, p. 301–306, https://doi.org/10.1306/74D72527-2B21-11D7-8648000102C1865D.

Boynton, W.V., 1992, Cosmochemistry of the rare earth elements: Meteorite studies, *in* Henderson, P., ed., Rare Earth Element Geochemistry: Amsterdam, Netherlands, Elsevier, Developments in Geochemistry Volume 2, p. 63–114, https://doi.org/10.1016/B978-0-444-42148-7.50008-3.

Buckland, H.M., Cashman, K.V., Engwell, S.L., and Rust, A.C., 2020, Sources of uncertainty in the Mazama isopachs and the implications for interpreting distal tephra deposits from large

magnitude eruptions: Bulletin of Volcanology, v. 82, 23, https://doi.org/10.1007/s00445-020-1362-1.
Budahn, J.R., and Wandless, G.A., 2002, Instrumental neutron activation by long count, *in* Taggart, J.E., Jr., ed., Analytical Methods for Chemical Analysis of Geologic and Other Materials: U.S. Geological Survey Open-File Report 02–0223, p. X1–X13.
Christiansen, R.L., 2001, The Quaternary and Pliocene Yellowstone Plateau Volcanic Field of Wyoming, Idaho, and Montana: U.S. Geological Survey Professional Paper 729-G, 156 p., https://doi.org/10.3133/pp729G.
Christiansen, R.L., and Blank, H.R., 1972, Volcanic Stratigraphy of the Quaternary Rhyolite Plateau in Yellowstone National Park: U.S. Geological Survey Professional Paper 729-B, 18 p., https://doi.org/10.3133/pp729B.
Christiansen, R.L., Lipman, P.W., Carr, W.J., Byers, F.M., Jr., Orkild, P.P., and Sargent, K.A., 1977, Timber Mountain–Oasis Valley caldera complex of southern Nevada: Geological Society of America Bulletin, v. 88, p. 943–959, https://doi.org/10.1130/0016-7606(1977)88<943:TMVCCO>2.0.CO;2.
Collier, A.J., and Thom, W.T., Jr., 1918, The Flaxville Gravel and its Relation to Other Terrace Gravels of the Northern Great Plains: U.S. Geological Survey Professional Paper 108, p. 179–184, https://doi.org/10.3133/pp108J.
Eastwood, W.C., 1969, Trace Element Correlation of Tertiary Volcanic Ashes from Western Nevada [Master's thesis]: Berkeley, California, University of California, 89 p.
Ellis, B.S., Mark, D.F., Pritchard, C.J., and Wolff, J.A., 2012, Temporal dissection of the Huckleberry Ridge Tuff using the $^{40}Ar/^{39}Ar$ dating technique: Quaternary Geochronology, v. 9, p. 34–41, https://doi.org/10.1016/j.quageo.2012.01.006.
Finn, D.R., Coe, R.S., Brown, E., Branney, M., Reichow, M., Knott, T., Storey, M., and Bonnichsen, B., 2016, Distinguishing and correlating deposits from large ignimbrite eruptions using paleomagnetism: The Cougar Point Tuffs (mid-Miocene), southern Snake River Plain, Idaho, USA: Journal of Geophysical Research, v. 121, no. 9, p. 6293–6314, https://doi.org/10.1002/2016JB012984.
Follmi, K.B., de Kaenel, E., Stille, P., John, C.M., Adette, T., and Stelmann, P., 2005, Phosphogenesis and organic-carbon preservation in the Miocene Monterey Formation at Naples Beach, California—Monterey hypothesis revisited: Geological Society of America Bulletin, v. 117, p. 589–619, https://doi.org/10.1130/B25524.1.
Heusser, L.E., Barron, J.A., Blake, G.H., and Nichols, J., 2022, Miocene terrestrial paleoclimates inferred from pollen in the Monterey Formation, Naples Coastal Bluffs section, California, *in* Aiello, I., Barron, J., and Ravelo, C., eds., Understanding the Monterey Formation and Similar Biosiliceous Units across Space and Time: Geological Society of America Special Paper 556, p. 215–227, https://doi.org/10.1130/2022.2556(09).
Hildreth, W., and Wilson, C.J., 2007, Compositional zoning of the Bishop Tuff: Journal of Petrology, v. 48, no. 5, p. 951–999, https://doi.org/10.1093/petrology/egm007.
Holbourn, A., Kuhnt, W., Clemens, S., Prell, W., and Andersen, N., 2013, Middle to late Miocene stepwise climate cooling: Evidence from a high-resolution deep water isotope curve spanning 8 million years: Paleoceanography, v. 28, https://doi.org/10.1002/2013PA002538.
Hornafius, J.S., 1994, Correlation of volcanic ashes in the Monterey Formation between Naples Beach and Gaviota Beach, California, *in* Field Guide of the Monterey Formation between Santa Barbara and Gaviota, California: Bakersfield, California, Pacific Section, American Association of Petroleum Geologists, Guidebook 72, p. 45–58, https://doi.org/10.32375/1994-GB72.4.
Hurford, A.J., and Green, P.F., 1983, The zeta calibration of fission-track dating: Isotope Geoscience, v. 1, p. 285–317, https://doi.org/10.1016/S0009-2541(83)80026-6.
Huxley, T.H., 1862, Anniversary Address: Quarterly Journal of the Geological Society of London, v. 18, p. xl–liv (containing references to homotaxial succession), https://doi.org/10.1144/GSL.JGS.1862.018.01-02.07.
Isaacs, C.M., 1981, Lithostratigraphy of the Monterey Formation, Goleta to Point Conception, Santa Barbara Coast, California, *in* Isaacs, C.M., ed., Guide to the Monterey Formation in the California Coastal Area, Ventura to San Louis Obispo: Bakersfield, California, Pacific Section, American Association of Petroleum Geologists Special Publication 52, p. 9–24, https://doi.org/10.32375/1981-GB52.2.
Izett, G.A., and Wilcox, R.A., 1982, Map Showing Localities and Inferred Distribution of the Huckleberry Ridge, Mesa Falls and Lava Creek Ash Beds (Pearlette Family Ash Beds) of Pliocene and Pleistocene Age in Western United States and Canada: U.S. Geological Survey Miscellaneous Map I-1325, 1 sheet, scale 1:4,000,000.
Kent, G.S., 1983, SAGE measurements of Mount St. Helens volcanic aerosols: Atmospheric Effects and Potential Climatic Impact of the 1980 Eruption of Mt. St. Helens: NASA, Langley Research Center, conference paper, Oct. 1, 1982, document 19830003273, accession number 83N11543, https://ntrs.nasa.gov/citations/19830003273.
Knott, J.R., Sarna-Wojcicki, A.M., Barron, J., Wan, E., Heizler, L., and Martinez, P., 2022, Tephrochronology of the Miocene Monterey and Modelo Formations, California, *in* Aiello, I., Barron, J., and Ravelo, C., eds., Understanding the Monterey Formation and Similar Biosiliceous Units across Space and Time: Geological Society of America Special Paper 556, p. 187–214, https://doi.org/10.1130/2022.2556(08).
Knott, T.R., Branney, M.J., Reichow, M.K., Finn, D.R., Tapster, S., and Coe, R.S., 2020, Discovery of two new super-eruptions from the Yellowstone hotspot track (USA): Is the Yellowstone hotspot waning?: Geology, v. 48, p. 934–938, https://doi.org/10.1130/G47384.1.
Kuiper, K.F., Deino, A., Hilgen, F.J., Krijgsman, W., Renne, P.R., and Wijbrans, J.R., 2008, Synchronizing rock clocks of Earth history: Science, v. 320, p. 500–504, https://doi.org/10.1126/science.1154339.
Lanphere, M.A., Dalrymple, G.B., Fleck, R.J., and Pringle, M.S., 1991, Intercalibration of mineral standards for K-Ar and $^{40}Ar/^{39}Ar$ age measurements [abs.]: Eos (American Geophysical Union Transactions), v. 7, no. 43, p. 1658.
Lowe, D.J., 2011, Tephrochronology and its application: A review: Quaternary Geochronology, v. 6, p. 107–153, https://doi.org/10.1016/j.quageo.2010.08.003.
Ludvigson, G.A., Sawin, R.S., Franseen, E.K., Watney, W.L., West, R.R., and Smith, J.J., 2009, A Review of the Stratigraphy of the Ogallala Formation and Revisions of Neogene ("Tertiary") Nomenclature in Kansas: Kansas Geological Survey Current Research in Earth Sciences Bulletin 256, p. 1–9.
Mason, B.G., Pyle, D.M., and Oppenheimer, C., 2004, The size and frequency of the largest explosive eruptions on Earth: Bulletin of Volcanology, v. 66, p. 735–748, https://doi.org/10.1007/s00445-004-0355-9.
Matthews, N.E., Vazquez, J.A., and Calvert, A.T., 2015, Age of the Lava Creek supereruption and magma chamber assembly at Yellowstone based on $^{40}Ar/^{39}Ar$ and U-Pb dating of sanidine and zircon crystals: Geochemistry, Geophysics, Geosystems, v. 16, no. 8, p. 2508–2528, https://doi.org/10.1002/2015GC005881.
McManus, D.A., Burns, R.E., and 24 others (i.e., Shipboard Party), 1970, Initial Reports of the Deep Sea Drilling Project Volume 5: Washington, D.C., U.S. Government Printing Office, 827 p., https://doi.org/10.2973/dsdp.proc.5.1970.
McQuarrie, N., and Wernicke, B.P., 2005, An animated tectonic reconstruction of southwestern North America since 36 Ma: Geosphere, v. 1, p. 147–172, https://doi.org/10.1130/GES00016.1.
Miller, D.M., and Schneyer, J.D., 1994, Geologic Map of the Sunset Pass Quadrangle, Box Elder County, Utah: Utah Geological and Mineral Survey Map 154, 14 p., scale 1:24,000.
Min, K., Mundil, R., Renne, P.R., and Ludwig, K.R., 2000, A test for systematic errors in $^{40}Ar/^{39}Ar$ geochronology through comparison with U-Pb analysis of a 1.1 Ga rhyolite: Geochimica et Cosmochimica Acta, v. 64, no. 1, p. 73–98, https://doi.org/10.1016/S0016-7037(99)00204-5.
Morgan, L.A., and McIntosh, W.C., 2005, Timing and development of the Heise volcanic field, Snake River Plain, Idaho, western USA: Geological Society of America Bulletin, v. 117, p. 288–306, https://doi.org/10.1130/B25519.1.
Ogg, J.G., 2012, Geomagnetic polarity time scale, *in* Gradstein, R.M., Ogg, J.G., Schmitz, M.D., and Ogg, G.M., eds., The Geologic Time Scale 2012: Oxford, UK, Elsevier, p. 85–113, https://doi.org/10.1016/B978-0-444-59425-9.00005-6.
Ostergren, C.L., 1991, Tephrochronology of Core E67–126A, Northwestern Gulf of Mexico [M.S. thesis]: San Jose, California, San Jose State University, 209 p.
Perkins, M.E., 1998, Tephrochronologic and Volcanologic Studies of Silicic Fallout Tuffs in Miocene Basins of the Northern Basin and Range Province [Ph.D. thesis]: Salt Lake City, Utah, University of Utah, 206 p.
Perkins, M.E., and Nash, B.P., 2002, Explosive silicic volcanism of the Yellowstone hotspot: The ash fall record: Geological Society of America Bulletin, v. 114, p. 367–381, https://doi.org/10.1130/0016-7606(2002)114<0367:ESVOTY>2.0.CO;2.
Perkins, M.E., Nash, W.P., Brown, F.H., and Fleck, R.J., 1995, Fallout tuffs of Trapper Creek, Idaho—A record of Miocene explosive volcanism in the Snake River Plain volcanic province: Geological Society of America Bulletin, v. 107, p. 1484–1506, https://doi.org/10.1130/0016-7606(1995)107<1484:FTOTCI>2.3.CO;2.
Perkins, M.E., Brown, F.H., Nash, W.P., Mcintosh, W., and Williams, S.K., 1998, Sequence, age, and source of silicic fallout tuffs in middle to late Miocene basins of the northern Basin and Range Province: Geological Society of America Bulletin, v. 110, p. 344–360, https://doi.org/10.1130/0016-7606(1998)110<0344:SAASOS>2.3.CO;2.

Pierce, K.L., and Morgan, L.A., 1992, The track of the Yellowstone hot spot: Volcanism, faulting, and uplift, *in* Link, P.K., Kuntz, M.A., and Platt, L.B., eds., Regional Geology of Eastern and Western Wyoming: Geological Society of America Memoir 179, p. 1–54, https://doi.org/10.1130/MEM179-p1.

Sampson, S.D., and Alexander, E.C., Jr., 1987, Calibration of the interlaboratory $^{40}Ar/^{39}Ar$ dating standard, MMhb-1: Chemical Geology, v. 66, p. 27–34, https://doi.org/10.1016/0168-9622(87)90025-X.

Sandhu, A.S., and Westgate, J.A., 1995, The correlation between reduction in fission-track diameter and areal track density in volcanic glass shards and its application in dating tephra beds: Earth and Planetary Science Letters, v. 131, p. 289–299, https://doi.org/10.1016/0012-821X(95)00022-5.

Sandhu, A.S., Westgate, J.A., and Alloway, B.V., 1993, Optimizing the isothermal plateau fission-track dating method for volcanic glass shards: Nuclear Tracks and Radiation Measurements, v. 21, no. 4, p. 479–488, https://doi.org/10.1016/1359-0189(93)90187-E.

Sarna-Wojcicki, A.M., 2000, Tephrochronology, *in* Noller, J.S., Sowers, J.M., and Lettis, W.R., eds., Quaternary Geochronology: Methods and Applications: Washington, D.C., American Geophysical Union Reference Shelf Volume 4, p. 357–378, https://doi.org10.1029/RF004p0357.

Sarna-Wojcicki, A.M., Shipley, S., Waitt, R.B., Jr., Dzurisin, D., and Wood, S.H., 1981, Areal distribution, thickness, mass, volume, and grain size of airfall ash from the six major eruptions of 1980, *in* Lipman, P.W., and Mullineaux, D.R., eds., The 1980 Eruptions of Mount St. Helens, Washington: U.S. Geological Survey Professional Paper 1250, p. 577–600, https://doi.org/10.3133/pp1250.

Sarna-Wojcicki, A.M., Morrison, S.D., Meyer, C.E., and Hillhouse, J.W., 1987, Correlation of Upper Cenozoic tephra layers between sediments of the western United States and eastern Pacific Ocean and comparison with biostratigraphic and magnetostratigraphic data: Geological Society of America Bulletin, v. 98, p. 207–223, https://doi.org/10.1130/0016-7606(1987)98<207:COUCTL>2.0.CO;2.

Sarna-Wojcicki, A.M., Reheis, M.C., Pringle, M.S., Fleck, R.J., Burbank, D., Meyer, C.E., Slate, J.L., Wan, E., Budahn, J.R., Troxel, B., and Walker, J.P., 2005, Tephra Layers of Blind Spring Valley and Related Upper Pliocene and Pleistocene Tephra Layers, California, Nevada, and Utah: Isotopic Ages, Correlation, and Magnetostratigraphy: U.S. Geological Survey Professional Paper 1701, 63 p., https://pubs.usgs.gov/pp/pp1701.

Sawyer, D.A., Fleck, R.J., Lanphere, M.A., Warren, R.G., Broxton, D.E., and Hudson, M.R., 1994, Episodic caldera volcanism in the Miocene Southwestern Nevada volcanic field: Revised stratigraphic framework, $^{40}Ar/^{39}Ar$ geochronology, and implications for magmatism and extension: Geological Society of America Bulletin, v. 106, p. 1304–1318, https://doi.org/10.1130/0016-7606(1994)106<1304:ECVITM>2.3.CO;2.

Schmieder, M., Kennedy, T., Jourdan, F., Buchner, E., and Reimold, W.U., 2018, A high-precision $^{40}Ar/^{39}Ar$ age for the Nördlinger Ries impact crater, Germany, and implications for the accurate dating of terrestrial impact events: Geochimica et Cosmochimica Acta, v. 220, p. 146–157, https://doi.org/10.1016/j.gca.2017.09.036.

Schorn, H.E., Scudder, H.I., Savage, D.E., and Firby, J.R., 1989, General stratigraphy, and paleontology of the Miocene continental sequence in Steward Valley, Mineral County, Nevada, U.S.A., *in* Liu, Gengwu, Tsuchi, Ryuchi, and Lin, Qibin, eds., Proceedings of International Symposium of Pacific Neogene Continental and Marine Events, National Working Group of China for IGCP-246: Nanjing, China, Nanjing University Press, p. 157–173.

Smith, C.C., 1991, Foraminiferal Biostratigraphic Framework, Paleoenvironments, Rates of Sedimentation, and Geologic History of the Subsurface Miocene of Southern Alabama and Adjacent State and Federal Waters: Geological Survey of Alabama, Stratigraphic and Paleontology Division Bulletin 138, 223 p.

Smith, J.F., and Ketner, K.B., 1976, Stratigraphy of Post-Paleozoic Rocks and Summary of Resources in the Carlin–Pinon Range Area, Nevada, with a Section on Aeromagnetic Survey: U.S. Geological Survey Professional Paper 867-B, 32 p., https://doi.org/10.3133/pp867B.

Smith, J.J., Turner, E., Moller, A., Joeckel, R.M., and Otto, R.E., 2018, First U-Pb zircon ages for late Miocene Ashfall Konservat-Lagerstätte and Grove Lake ashes from eastern Great Plains, U.S.A.: PLoS One, v. 13, p. 1–19, https://doi.org/10.1371/journal.pone.0207103.

Stein, R., 2008, Arctic Ocean Sediments: Processes, Proxies, and Paleoenvironment: Amsterdam, Netherlands, Elsevier, 592 p.

Stewart, J.H., Sarna-Wojcicki, A.M., Meyer, C.E., and Wan, E., 1999, Stratigraphy, Tephrochronology, and Structural Setting of Miocene Sedimentary Rocks in the Cobble Cuesta Area, West-Central Nevada: U.S. Geological Survey Open-File Report 99-352, 21 p., scale 1:24,000, https://doi.org/10.3133/ofr99352.

Tedford, R.H., Albright, L.B., Barnosky, A.D., Ferrusquia-Villafranca, Ismael, Hunt, R.M., Storer, J., Swisher, C.C., Voohries, M.R., Webb, D.S., and Whistler, D.P., 2004, Mammalian biochronology of the Arikareean through Hemphillian interval (late Oligocene through early Pliocene Epochs), *in* Woodburne, M.W., ed., Late Cretaceous and Cenozoic Mammals of North America, Biostratigraphy and Geochronology: New York, Columbia University Press, p. 169–231, https://doi.org/10.7312/wood13040-008.

Tucker, S.T., Otto, R.E., Joeckel, R.M., and Voorhies, M.R., 2014, The geology and paleontology of Ashfall Fossil Beds, a late Miocene (Clarendonian) mass-death assemblage, Antelope County and adjacent Knox County, Nebraska, USA, *in* Korus, J.T., ed., Geologic Field Trips along the Boundary between the Central Lowlands and Great Plains: 2014 Meeting of the GSA North-Central Section: Geological Society of America Field Guide 36, p. 1–22, https://doi.org/10.1130/2014.0036(01).

University of Nebraska, 2023, About Ashfall, Ashfall Animals: Lincoln, Nebraska, University of Nebraska, State Museum, Ashfall Fossil Beds, Nebraska, https://ashfall.unl.edu/about-ashfall/ashfall-animals.html (last accessed May 2023).

von Huene, R., Kuhn, L.D., Duncan, J.R., Ingle, J.C., Kling, S.A., Musich, L.M., Piper, D.J.W., Pratt, R.M., Schrader, H.-J., Weser, O., and Wise, S.W., Jr., 1973, Site 173, *in* Musich, L.F., and Weser, O.E., eds., Deep Sea Drilling Project Initial Reports, Volume 18: Washington, D.C., U.S. Government Printing Office, p. 31–95, https://doi.org/10.2973/dsdp.proc.18.104.1973.

Voorhies, M.R., 1985, A Miocene rhinoceros herd buried in volcanic ash: National Geographic Society Research Reports, v. 19, p. 671–688.

Voorhies, M.R., and Thomasson, J.R., 1979, Fossil grass anthoecia within Miocene rhinoceros skeletons: Diet in an extinct species: Science, v. 206, p. 331–333, https://doi.org/10.1126/science.206.4416.331.

Wagner, G.A., and Van den Haute, P., 1992, Fission-Track Dating: Stuttgart, Germany, Kluwer, 285 p.

Walkup, L.C., Sarna-Wojcicki, A.M., Wan, E., Meyer, C., Budahn, J.R., Westgate, J., and Bray, C., 2023, Tephra geochemistry of the Ibex Hollow Tuff, a ca 12-Ma super-eruption: U.S. Geological Survey Data Release, https://doi.org/10.5066/P9KI7L9J.

Westerhold, T., Narwan, R., Drury A.J., Liebrand, D., Agnini, C., Anagnostou, E., Barnet, J.S.K., Bohaty, S.M., De Vleeschouwer, D., Florindo, F., Frederiches, T. Hodell, D.A., Holbourn, A.E., Kroon, D., Lauretano, V., Littler, K., Lourens, L.J., Lyle, M., Pälike, H, Röhl, U., Tain, J., Wilkens, R.H., Wilson, P.A., and Zachos, J.C., 2020, An astronomically dated record of Earth's climate and its predictability over the last 66 million years: Science, v. 369, p. 1383–1387, https://doi.org/10.1126/science.aba6853.

Westgate, J.A., 1989, Isothermal plateau fission-track ages of hydrated glass shards from silicic tephra beds: Earth and Planetary Science Letters, v. 95, p. 226–234, https://doi.org/10.1016/0012-821X(89)90099-X.

Westgate, J.A., 2015, Volcanic glass (fission track), *in* Rink, W.J., and Thompson, J.W., eds., Encyclopedia of Scientific Dating Methods: Dordrecht, Netherlands, Springer, p. 941–946, https://doi.org/10.1007/978-94-007-6304-3_60.

Westgate, J.A., Christiansen, E.A., and Boellstorff, J.D., 1977, Wascana Creek Ash (middle Pleistocene) in southern Saskatchewan: Characterization, source, fission track age, paleomagnetism and stratigraphic significance: Canadian Journal of Earth Sciences, v. 14, p. 357–374, https://doi.org/10.1139/e77-037.

Westgate, J.A., Pearce, N.J.G., Perkins, W.T., Shane, P.A., and Preece, S.J., 2011, Lead isotope ratios of volcanic glass by laser ablation inductively-coupled plasma mass spectrometry: Application to Miocene tephra beds in Montana, USA and adjacent areas: Quaternary International, v. 246, p. 82–96, https://doi.org/10.1016/j.quaint.2011.08.003.

Westgate, J.A., Wolde Gabriel, G., Halls, H.C., Bray, C.J., Barendregt, R.W., Pearce, N.J.G., Sarna-Wojcicki, A.M., Gorton, M.P., Kelley, R.E., and Schultz-Fellenz, E., 2018, Quaternary tephra from the Valles caldera in the volcanic field of the Jemez Mountains of New Mexico identified in western Canada: Quaternary Research, v. 91, no. 2, https://doi.org/10.1017/qua.2018.139.

Whistler, D.P., and Burbank, D.W., 1992, Miocene biostratigraphy and biochronology of the Dove Spring Formation, Mojave Desert, California, and characterization of the Clarendonian mammal age (late Miocene) in California: Geological Society of America Bulletin, v. 104, p. 644–658, https://doi.org/10.1130/0016-7606(1992)104<0644:MBABOT>2.3.CO;2.

Whistler, D.P., Tedford, R.H., Takeuchi, G.T., Wang, X., Tseng, Z.J., and Perkins, M.E., 2009, Revised Miocene biostratigraphy and biochronology of the Dove Spring Formation, Mojave Desert, California, *in* Albright, L.B., III, ed., Papers on Geology Vertebrate Paleontology and Biostratigraphy in Honor of Michael O. Woodburne: Flagstaff, Arizona, Museum of Northern Arizona Bulletin 65, p. 331–362.

Zdanowicz, C.M., Zielinski, G.A., and Germani, M.S., 1999, Mount Mazama eruption: Calendrical age verification and atmospheric impact assessed: Geology, v. 27, p. 621–624, https://doi.org/10.1130/0091-7613(1999)027<0621:MMECAV>2.3.CO;2.